ALEX(01)-TR-77-04

AD A053 70[illegible]

FILE COPY

# CONTINUATION OF THE IRANIAN LONG PERIOD ARRAY EVALUATION

## TECHNICAL REPORT NO. 1

## VELA NETWORK EVALUATION AND AUTOMATIC PROCESSING RESEARCH

Prepared by
Lynn A. Shoney and Alan C. Strauss

TEXAS INSTRUMENTS INCORPORATED
Equipment Group
Post Office Box 6015
Dallas, Texas 75222

Prepared for

AIR FORCE TECHNICAL APPLICATIONS CENTER
Alexandria, Virginia 22314

Sponsored by

ADVANCED RESEARCH PROJECTS AGENCY
Nuclear Monitoring Research Office
ARPA Program Code No. 7F10
ARPA Order No. 2551

30 December 1977

Acknowledgment: This research was supported by the Advanced Research Projects Agency, [illegible] under the technical direction of the Air Force Technical Applications Center under Contract Number F[illegible]

FOR FURTHER TRAN

g

ALEX(01)-TR-77-01

12

# CONTINUATION OF THE IRANIAN LONG PERIOD ARRAY EVALUATION

## TECHNICAL REPORT NO. 1

## VELA NETWORK EVALUATION AND AUTOMATIC PROCESSING RESEARCH

Prepared by
Lynn A. Shaner and Alan C. Strauss

TEXAS INSTRUMENTS INCORPORATED
Equipment Group
Post Office Box 6015
Dallas, Texas 75222

Prepared for

AIR FORCE TECHNICAL APPLICATIONS CENTER
Alexandria, Virginia 22314

Sponsored by

ADVANCED RESEARCH PROJECTS AGENCY
Nuclear Monitoring Research Office
ARPA Program Code No. 7F10
ARPA Order No. 2551

DDC
RECEIVED
JUN 23 1978
B

30 December 1977

Acknowledgment: This research was supported by the Advanced Research Projects Agency, Nuclear Monitoring Research Office, under Project VELA-UNIFORM, and accomplished under the technical direction of the Air Force Technical Applications Center under Contract Number F08606-77-C-0004.

ALEX(01)-TR-77-01

# CONTINUATION OF THE IRANIAN LONG PERIOD ARRAY EVALUATION

## TECHNICAL REPORT NO. 1

## VELA NETWORK EVALUATION AND AUTOMATIC PROCESSING RESEARCH

Prepared by
Lynn A. Shaner and Alan C. Strauss

TEXAS INSTRUMENTS INCORPORATED
Equipment Group
Post Office Box 6015
Dallas, Texas 75222

Prepared for

AIR FORCE TECHNICAL APPLICATIONS CENTER
Alexandria, Virginia 22314

Sponsored by

ADVANCED RESEARCH PROJECTS AGENCY
Nuclear Monitoring Research Office
ARPA Program Code No. 7F10
ARPA Order No. 2551

30 December 1977

Acknowledgment: This research was supported by the Advanced Research Projects Agency, Nuclear Monitoring Research Office, under Project VELA-UNIFORM, and accomplished under the technical direction of the Air Force Technical Applications Center under Contract Number F08606-77-C-0004.

78 06 08 011

UNCLASSIFIED

SECURITY CLASSIFICATION OF THIS PAGE (When Data Entered)

## REPORT DOCUMENTATION PAGE

READ INSTRUCTIONS BEFORE COMPLETING FORM

1. REPORT NUMBER

2. GOVT ACCESSION NO.

3. RECIPIENT'S CATALOG NUMBER

9

4. TITLE (and Subtitle)

6 CONTINUATION OF THE IRANIAN LONG-PERIOD ARRAY EVALUATION,

5. TYPE OF REPORT & PERIOD COVERED

Technical rept.,

6. PERFORMING ORG. REPORT NUMBER

14 TI-ALEX (01)-TR-77-01

7. AUTHOR(s)

10 Lynn A. Shaner [redacted] Alan C. Strauss

8. CONTRACT OR GRANT NUMBER(s)

15 F08606-77-C-0004, ARPA Order-2551

9. PERFORMING ORGANIZATION NAME AND ADDRESS

Texas Instruments Incorporated
Equipment Group
Dallas, Texas 75222

10. PROGRAM ELEMENT, PROJECT, TASK AREA & WORK UNIT NUMBERS

VELA T/7705/B/ETR

11. CONTROLLING OFFICE NAME AND ADDRESS

Advanced Research Projects Agency
Nuclear Monitoring Research Office
Arlington, Virginia 22209

12 138p.

12. REPORT DATE

11 30 Dec[redacted] [redacted]77

13. NUMBER OF PAGES

134

14. MONITORING AGENCY NAME & ADDRESS (if different from Controlling Office)

Air Force Technical Applications Center
VELA Seismological Center
Alexandria, Virginia 22314

15. SECURITY CLASS. (of this report)

UNCLASSIFIED

15a. DECLASSIFICATION/DOWNGRADING SCHEDULE

16. DISTRIBUTION STATEMENT (of this Report)

APPROVED FOR PUBLIC RELEASE, DISTRIBUTION UNLIMITED

17. DISTRIBUTION STATEMENT (of the abstract entered in Block 20, if different from Report)

18. SUPPLEMENTARY NOTES

ARPA Order No. 2551

19. KEY WORDS (Continue on reverse side if necessary and identify by block number)

data base
data quality
mixed events
coherence
Iranian Long-Period Array
noise field characteristics
frequency-wavenumber spectra
SNR beamforming gains
signal similarity
detection capability
discrimination capability

20. ABSTRACT (Continue on reverse side if necessary and identify by block number)

This report presents a continuation of the evaluation of long-period data recorded at the Iranian Long Period Array (ILPA). This evaluation was performed by Texas Instruments ~~Incorporated~~ at the Seismic Data Analysis Center in Alexandria, Virginia.

In the area of long-period noise analysis, this report discusses RMS noise levels and trends and average noise RMS amplitude spectra for both the (over)

DD FORM 1 JAN 73 1473 EDITION OF 1 NOV 65 IS OBSOLETE

UNCLASSIFIED

SECURITY CLASSIFICATION OF THIS PAGE (When Data Entered)

405076

CL

20. Abstract (continued)

individual sites and the beamformed data. The array noise data is also used to investigate the questions of noise coherence and propagating noise.

In the area of signal analysis, signal-to-noise ratio gains due to beamforming and site-to-site signal similarities are investigated. Using a processed data base of 613 events, regionalized detection capability estimates and earthquake-presumed explosion discrimination are presented. Finally, the report briefly presents a comparison of the array and the closest Seismic Research Observatory station.

Conclusions regarding the above areas of investigation and plans for future work necessary to complete the ILPA evaluation are also presented.

1473B

# ABSTRACT

This report presents a continuation of the evaluation of long-period data recorded at the Iranian Long Period Array (ILPA). This evaluation was performed by Texas Instruments Incorporated at the Seismic Data Analysis Center in Alexandria, Virginia.

In the area of long-period noise analysis, this report discusses RMS noise levels and trends and average noise RMS amplitude spectra for both the individual sites and the beamformed data. The array noise data is also used to investigate the questions of noise coherence and propagating noise.

In the area of signal analysis, signal-to-noise ratio gains due to beamforming and site-to-site signal similarities are investigated. Using a processed data base of 613 events, regionalized detection capability estimates and earthquake-presumed explosion discrimination are presented. Finally, the report briefly presents a comparison of the array and the closest Seismic Research Observatory station.

Conclusions regarding the above areas of investigation and plans for future work necessary to complete the ILPA evaluation are also presented.

# TABLE OF CONTENTS

# TABLE OF CONTENTS
(continued)

# LIST OF FIGURES

# LIST OF FIGURES
(continued)

## LIST OF FIGURES
(continued)

# LIST OF TABLES

## LIST OF TABLES
(continued)

# SECTION I
# INTRODUCTION

## A. DISCUSSION

The Iranian Long-Period Array (ILPA) is located near Teheran, Iran. This array, which became operational on 1 May 1976, is a seismic recording installation comprised of a central recording station and an array of seven remote sites.

This report presents the results of a continuation of the evaluation of this installation. In the preliminary ILPA evaluation (Strauss, 1976), attention was focused on data quality and sources of data errors, beamforming gains in signal-to-noise ratio, first estimates of detection capability, and $M_s$-$m_b$ relationships. Due to the limited time available between reception of ILPA data and the end of the contract period, no noise analysis was performed. Since no recognized presumed nuclear explosions occurred during May, 1976 (from which time frame the data base was drawn), it was not possible to comment on the ILPA discrimination capability.

In this continuation of the ILPA evaluation, emphasis was placed on improving and refining the work started under the preliminary evaluation. With sufficient data now available, it was also possible to investigate the nature of the noise field at ILPA, regionalize the ILPA detection capability estimates, and consider the ILPA discrimination capability.

## B. THE SYSTEM

The instrumentation and operation of the Iranian Long-Period Array have been described in detail in the operation and maintenance manual for the ILPA seismic system and in the report on the preliminary evaluation of ILPA (Strauss, 1976). Therefore, it is only necessary here to briefly describe the system.

Each remote site of the seven-element array has a three-component broadband seismometer (KS 36000) located in a 100-meter deep borehole to reduce wind-generated noise. Each seismometer is a force-balance type which produces an output proportional to earth accelerations over the frequency range 0.02 - 1.0 Hz. The instrumentation at each remote site also includes a data acquisition subsystem, a telemetry subsystem, and a power subsystem. The data recorded at each site are transmitted directly to the central recording station, with one exception. Since site 6 does not have line-of-sight with the central recording station, the data from site 6 are relayed through site 5 to the central recording station. The locations of the remote sites are listed in Table I-1 and shown in Figure I-1.

The central recording station processes and records data received from the seven remote sites. The instrumentation housed in the central recording station includes the station processor, the visual recording system, the magnetic digital tape recording system, and the timing, telemetry, and power systems. The visual recording system converts the digital signals from the remote sites back to analog form for display on drum recorders and develocorders. The digital magnetic tape recording system records three components of long-period motion from each of the seven remote sites. This system is also used for the tasks of providing data for beamforming and display and of editing data to other tapes.

The output of the ILPA data recording system available to this evaluation task is the digital magnetic tape recorded in the satellite tape format. This is a second digital magnetic tape recording system which records three components of long-period motion from each of the remote sites and

## TABLE I-1

## REMOTE SITE COORDINATES

| Site | Location |  | Distance From Reference Site (km) |  |
|---|---|---|---|---|
|  | Latitude (°N) | Longitude (°E) | North | East |
| 1 (ref) | 35°24'58.3" | 50°41'19.5" | 0.0 | 0.0 |
| 2 | 35°39'46.1" | 50°53'51.5" | 27.277 | 19.035 |
| 3 | 35°28'34.0" | 51°01'25.5" | 6.217 | 30.377 |
| 4 | 35°14'19.3" | 50°54'04.2" | -19.536 | 19.162 |
| 5 | 35°12'46.2" | 50°34'52.0" | -22.415 | -9.830 |
| 6 | 35°28'25.2" | 50°25'32.2" | 5.815 | -23.775 |
| 7 | 35°42'10.1" | 50°36'32.0" | 31.700 | -6.951 |

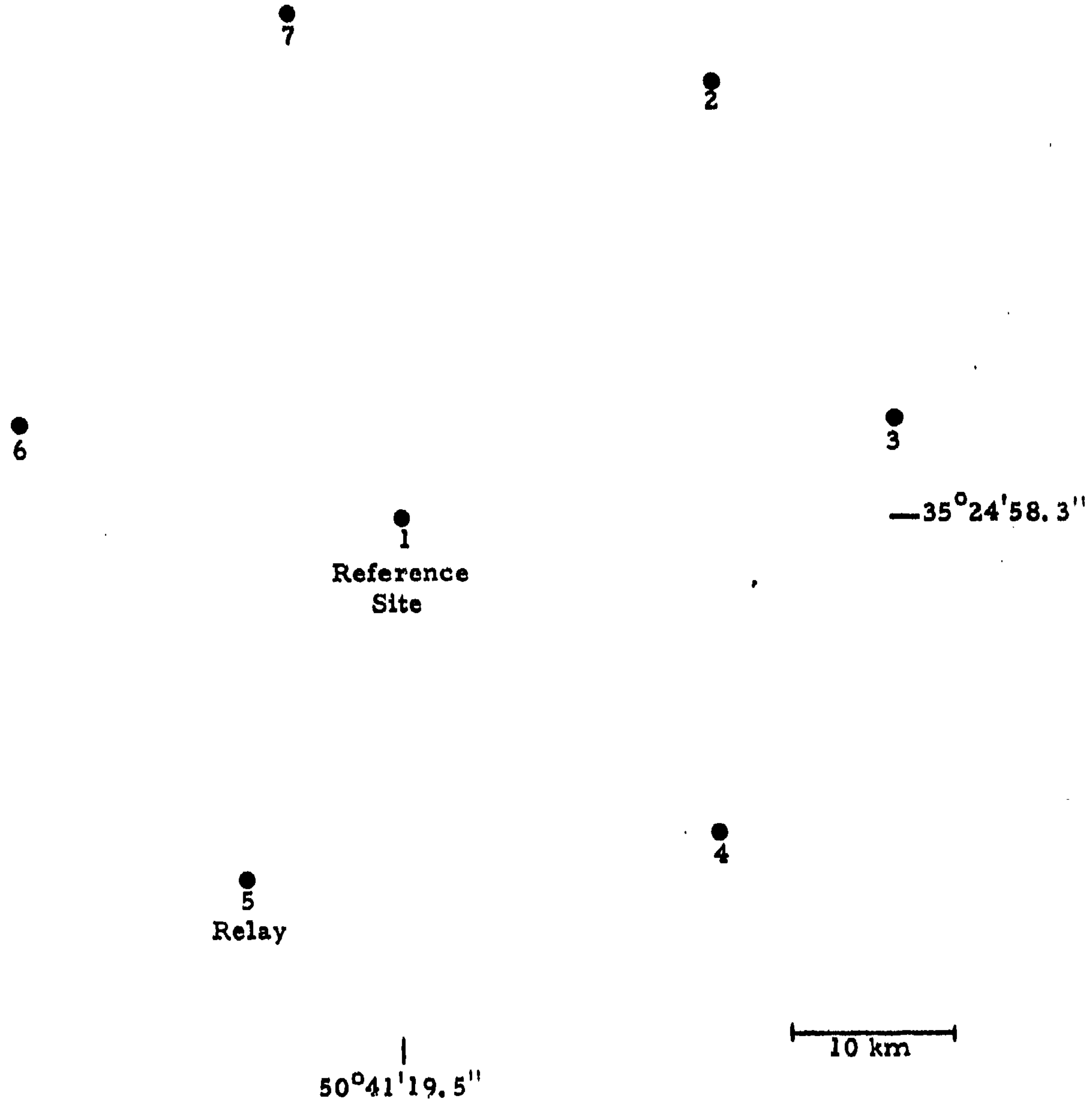

FIGURE I-1

ILPA SITE LOCATIONS

one component of short-period vertical motion (presently, from site 7) continuously. This tape is 800 BPI, 9-track, recorded using two's complement binary arithmetic. The data are quantized at 20.951 computer counts per millimicron (0.0477 m$\mu$/cc) of ground motion for long-period and 16.393 computer counts per millimicron (0.061 m$\mu$/cc) of ground motion for short-period. The data sampling rate is one sample per second of long-period data and twenty samples per second for short-period data.

## C. EVALUATION GOALS

The specific goals of this evaluation are:

- To determine data quality, sources of data errors, and reliability for each remote site and for the array as a whole.
- To investigate the long-period noise field characteristics at each remote site and for the array as a whole.
- To investigate the signal-to-noise ratio gains due to beamforming.
- To investigate site-to-site signal similarity.
- To determine estimates of the array detection capability on a regionalized basis.
- To consider the discrimination capability of the array on a regionalized basis.
- To compare the performance of ILPA with an SRO single-site station located approximately 700 km east of ILPA.

The method of reaching these evaluation goals is as follows. First, a suitable suite of seismic events and noise samples is created from available event lists. The procedure for selecting these events is described in Section II. This section also describes the manner in which the data were processed and presents some estimates of data quality and array reliability based on data processing experience. The investigation of the local noise field characteristics of the array is presented in Section III. The noise field is characterized by RMS noise level, monthly RMS noise level trends, peak noise amplitudes, and spectral content. The multiplicity of data provided by seven sites also permits investigating the question of propagating noise by means of frequency-wavenumber spectra. Section IV presents estimates of signal-to-noise ratio gains due to beamforming and site-to-site signal similarities. Section V presents estimates of the detection capability of the array in terms of the entire area of interest and in terms of specified sub-regions within this area of interest. In the course of estimating the array detection capability, the effect of mixed events and system malfunctions on these estimates is considered. Section VI discusses the question of discriminating between earthquakes and presumed nuclear explosions. The means of discriminating used in this section is the $M_s - m_b$ relationship. The final major area of this evaluation is found in Section VII, which assesses the performance of the array relative to a nearby single-site station. Section VIII summarizes the findings of this evaluation and suggests future avenues of investigation. Section IX lists the references cited in this report. Finally, Appendix A describes the data base used in this evaluation.

# SECTION II

# THE DATA BASE

## A. FORMATION OF THE DATA BASE

The data base used in this continued evaluation of the Iranian Long-Period Array is essentially a subset of the data base used in the Seismic Research Observatories evaluation (Strauss, 1977). This data base was formed by first selecting all events with Eurasian epicenters as listed by the Norwegian Seismic Array (NORSAR) bulletin. (This was the only available event list at the time the data base was formed.) The time frame selected was from 22 December 1975 to 30 September 1976, when the NORSAR bulletin ceased to be issued. This yielded a list of 2697 events.

This list was far too large to be successfully dealt with and was therefore reduced. First, the events were grouped by seismic regions as defined by Flinn and Engdahl (Flinn and Engdahl, 1965). Those regions containing fewer than 80 events were dropped from the event list. Next, the remaining seismic regions were broken into their geographic sub-regions, again as defined by Flinn and Engdahl. Those sub-regions which contained only a few events and which were separated from the main body of event-containing sub-regions in the region were then rejected and their contained events deleted from the event list. The remaining regions (shown in Figure II-1) were used in this evaluation. The regions have been renumbered but have the same boundaries as those of Flinn and Engdahl, with the exception of their region 19, which was sub-divided to form regions 1 and 2 of Figure II-1. The subregions composing each region are listed in Table II-1.

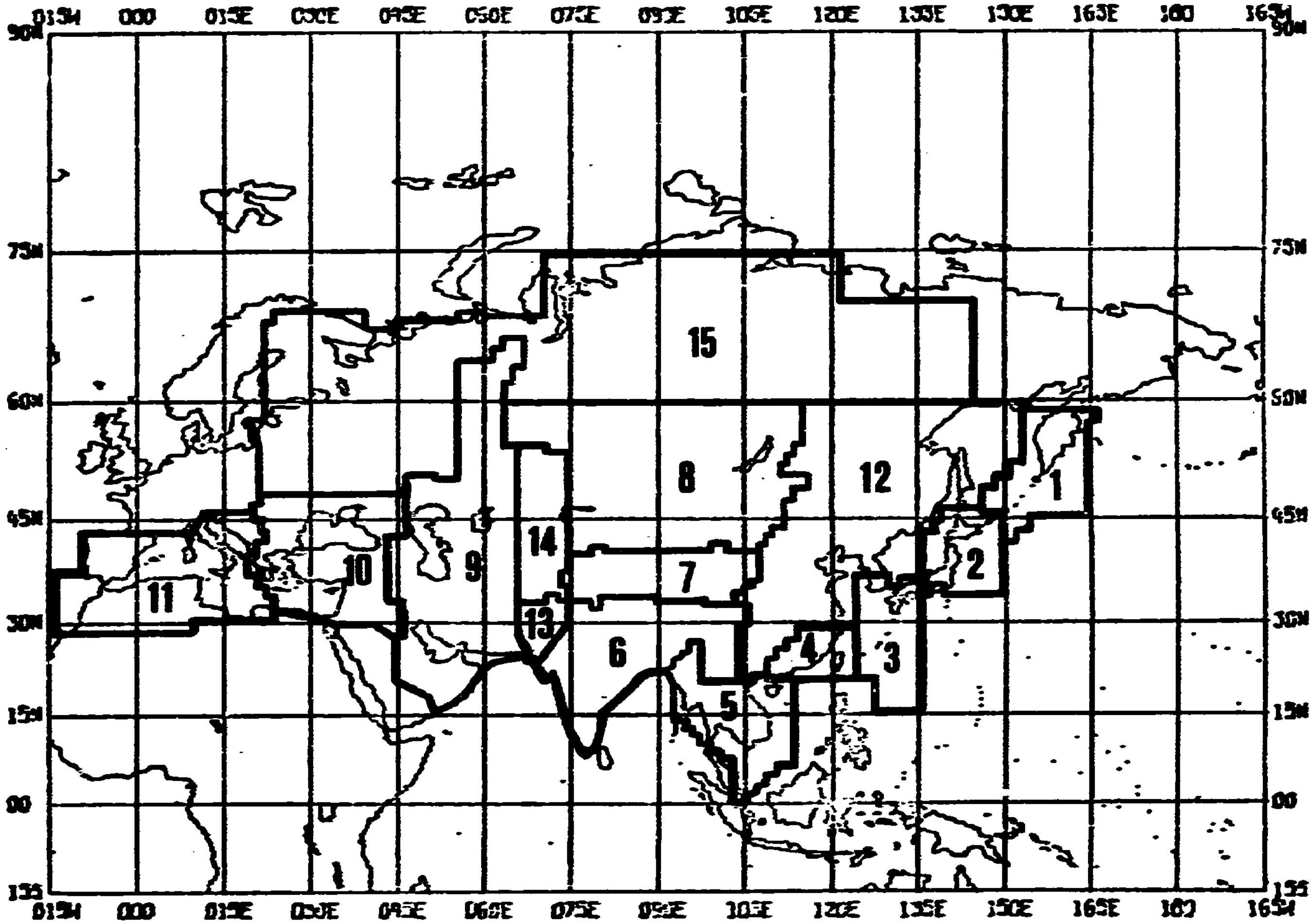

MILLER MODIFIED MERCATOR PROJECTION
MAP SCALE: 0.03429 INCHES/DEGREE LONGITUDE

FIGURE II-1

REGION BOUNDARIES

## TABLE II-1

## DATA BASE REGIONALIZATION

| Region # As Used in This Report | Flinn & Engdahl's Region # | General Area | Flinn & Engdahl's Geographic Subregions |
|---|---|---|---|
| 1 | 19 | Kuriles-Kamchatka | 217, 218, 219, 221, 222, 225 |
| 2 | 19 | N. Japan | 224, 227, 228, 229, 230 |
| 3 | 20 | S. Japan | 232, 233, 234, 235, 237, 238 |
| 4 | 21 | S.E. China | 242, 243, 244, 245, 246, 247 |
| 5 | 25 | Burma | 294, 296, 297, 298 |
| 6 | 26 | N. India | 302, 303, 304, 305, 306, 307, 308, 309, 310, 311, 313, 315, 317, 318, 319 |
| 7 | 27 | Tibet | 320, 321, 322, 323, 324, 325 |
| 8 | 28 | Central Asia | 326, 327, 328, 329, 330, 331, 332, 334 |
| 9 | 29 | Iran-Ural Mountains | 335, 336, 337, 338, 339, 340, 342, 343, 344, 345, 346, 347, 348, 349, 350, 351, 353, 354 |
| 10 | 30 | Greece-Turkey | 357, 358, 359, 360, 361, 362, 363, 364, 365, 366, 368, 369, 370, 371, 373, 375 |
| 11 | 31 | W. Mediterranean | 381, 382, 383, 390, 391, 392, 398, 399, 400 |
| 12 | 41 | E. China | 657, 658, 660, 661, 662, 663, 664, 665, 666 |
| 13 | 47 | S. Pakistan | 709, 710, 711, 712 |
| 14 | 48 | N. Pakistan-Afghanistan | 713, 714, 715, 716, 717, 718, 719, 720 |
| 15 | 49 | N. Russia-Siberia | 724, 726 |

At this point, the data base contained approximately 2300 events. To bring this down to a manageable size, events were systematically deleted (every other event, two out of every three events, as needed) from those regions containing more than 120 events until they each contained approximately 120 events. This reduced the data base to 1472 events.

The ILPA data base was created from this data base by selecting all events for which the array was nominally operational. This resulted in a data base of 497 events occurring between 1 May 1976 and 30 September 1976. Finally, this data base was increased to 613 events by selecting events from the above-defined regions as listed by the National Earthquake Information Service (NEIS) event bulletin from 1 October to 20 December 1976. The event parameters of this data base are presented in Appendix A.

In the preliminary ILPA evaluation, the data base consisted of 281 events from May 1976. For the current data base, these events were subjected to the same regionalizing procedure as the new events, reducing the total for May 1976 from 281 to 213. The 67 events of the old data base which were not included in the new data base were rejected because their epicenters were not in regions used in this evaluation. These 67 events will be used in the discussion of data quality and array reliability however, since these matters are independent of region.

Formation of the noise data base will be discussed in detail in the section on noise analysis (Section III). In brief, the noise data base was formed by searching the NORSAR and NEIS event bulletins for daily time intervals of at least one hour in duration during which no seismic signals would be expected to arrive at the array. Noise edits were then created by selecting data segments 4096 seconds in length sampled at a rate of one sample per two seconds from these intervals.

## B. DATA PROCESSING METHOD

The computer processing of seismic signals and noise samples can be divided into two functional stages - the basic processing stage and the analysis processing stage.

The basic processing stage is outlined in Figure II-2. The desired time segments of signal or noise are first edited from the merge tapes created by Teledyne/Geotech. (These merge tapes each contain three consecutive days of ILPA data recorded at 1600 BPI.) The output from the edit program consists of trace mean information for each component of each site, quality control information, and a permanent hold tape of the edited data. The quality control information consists of messages indicating the presence of parity errors, timing errors, clipped data, and spiked data. Also printed out is a summary of segment powers, which can be used to determine bad sites. (Bad sites are those sites which are dead, contain uncorrectable spikes, or display abnormally high or low power levels.) At this point, the analyst uses the quality control information to guide him in selecting the array sites to be input to the beamforming program.

The next major program of the basic processing stage performs trace mean removal, rotation of the data from thoir recorded vertical, north, east (V, N, E) configuration to a vertical, transverse, radial (V, T, R) configuration, and beamforming of the good sites. Rotation of the data separates the surface waves recorded on the horizontal components, theoretically resulting in two components of Rayleigh-wave motion (V and R) and one component of Love-wave motion (T). Noise samples retain their V, N, E configuration. Both the edit and beamforming programs operate on one 128-point data segment at a time, continuing until the desired data length has been processed.

The beamforming program operates by computing arrival time delays at each site relative to a reference site (site 1) using fixed velocities of 4.0 km/sec for Love waves and 3.5 km/sec for Rayleigh waves.

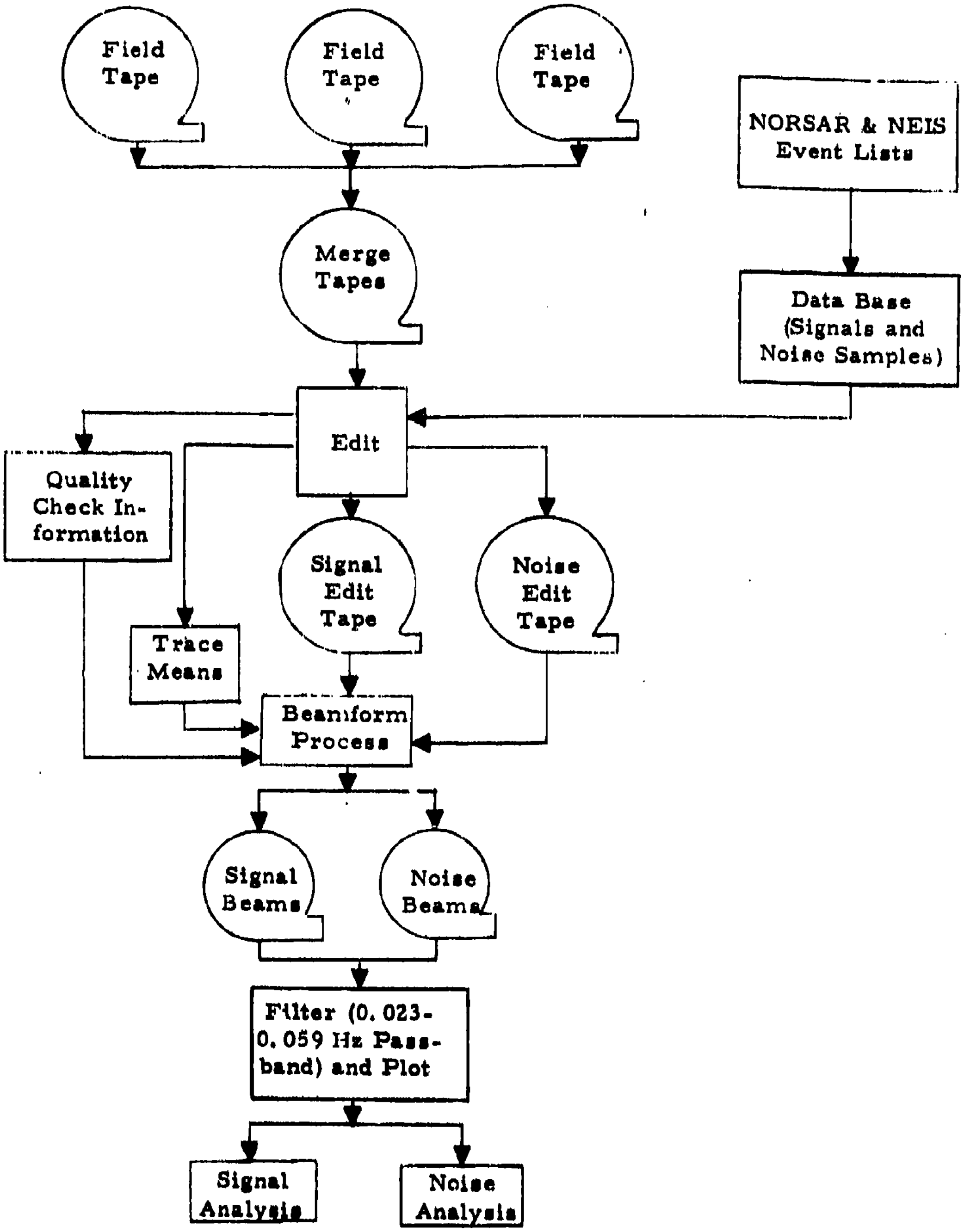

FIGURE II-2

DATA PROCESSING METHOD

The data from each site are then time-aligned using these time delays, summed, and scaled. This process produces a signal-to-noise ratio improvement by suppressing random noise by a factor approximately equal to the square root of the number of sites used. This program outputs three components of motion from a reference site (usually site 1) and three beams (V, T, R) to a permanent hold tape with appropriate annotation.

The final program of the basic processing stage performs bandpass filtering (0.023 - 0.059 Hz passband) of the reference site and beam traces and outputs plots suitable for analysis.

The various programs used in the analysis processing stage will be described in the sections on noise analysis and signal analysis.

## C. ARRAY RELIABILITY

The first point to be considered in any assessment of array reliability is the percentage of time for which the array is nominally operational. Table II-2 shows that this factor varies greatly from month to month. (These percentages represent the percentage of each month for which data was received at the Seismic Data Analysis Center in Alexandria, Virginia.) In the first thirteen months of operation, ILPA suffered from three major problems. Between 22 June 1976 and 6 August 1976, the array was down due to a malfunction of the air conditioner compressor, which allowed temperatures to rise above the operational limits of the CRS hardware. The second down period, from 18 September to 1 November 1976, was due to problems with the satellite-format tape recorders. (From the authors' point of view, the array is down when no data is available at the Seismic Data Analysis Center in Alexandria, Virginia, regardless of whether the remainder of the sensor - transmitter - recorder system comprising the array is operational. Thus, the array is considered to be down when the

## TABLE II-2

## PERCENTAGE OF TIME ILPA IS OPERATIONAL

| | | |
|---|---|---|
| May | 1976 | 100% |
| June | 1976 | 77% |
| July | 1976 | 3% |
| Aug. | 1976 | 87% |
| Sept. | 1976 | 50% |
| Oct. | 1976 | 0% |
| Nov. | 1976 | 100% |
| Dec. | 1976 | 68% |
| Jan. | 1977 | 0% |
| Feb. | 1977 | 79% |
| Mar. | 1977 | 87% |
| Apr. | 1977 | 100% |
| May | 1977 | 81% |
| | | Average = 64% |

satellite-format tape recorders are down.) The third down period, from 20 December 1976 to 2 February 1977, was due to problems with the thermal electric generators and the satellite-format tape recorders.

Overall, in the thirteen month period shown in Table II-2, the average up time percentage was only 64%. However, as hardware problems of the types described above are found and corrected, one can expect this value to increase. An indication that this is the case may be found in Table II-2, where the average up time for the last four months is 87%.

Even when the array functions as designed and tapes in the satellite format are received at the Seismic Data Analysis Center, two factors may prevent the analyst from processing a desired time frame. First, no data is recorded during the interval between the time one tape is filled and the next is mounted on the tape drive. (The average time gap between tapes is ten minutes.) Second, a tape is occasionally received which is unreadable due to such factors as poor tape quality or dust and dirt on the tape. When either of these occurs, the analyst cannot examine the time frame in which he is interested.

Out of 680 events examined (613 of the current data base plus 67 additional events from the data base of last year), 87 could not be processed due to gaps in the recorded data or unreadable data. Thus, it appears that even if the array is nominally operational 100 percent of the time, the analyst can expect to be unable to process approximately 12 percent of the data. However, it should be noted that 45 of the 87 events not processed were lost to unreadable tapes, a problem which should not be too difficult to rectify. Correction of this problem would bring the loss rate down to approximately 6 percent.

Even after an event has been successfully processed, system malfunctions can prevent the analyst from determining whether the data shows the desired signal, seismic noise, or a mixed event. These system malfunctions take the form of spikes, glitches, and data drop-outs. These system malfunctions degraded 28 of the 680 events examined last year and this year for a loss rate of 4 percent.

The overall ILPA reliability estimate is determined from the above causes of loss of data. This estimate is expressed as:

Reliability = Probability (array is operational) * Probability (data is recorded and readable) * Probability (no malfunctions).

The worst-case reliability assumes no improvements in the up-time or quality of data recording. This estimate is:

Reliability = (0.64) * (0.88) * (0.96) = 0.54.

If one assumes the improvement in operational reliability suggested by the last four months shown in Table II-2 is permanent, the array reliability becomes:

Reliability = (0.87) * (0.88) * (0.96) = 0.73.

Finally, there is no reason why all recorded data should not be readable. If proper tape handling procedures in recording and shipment are observed, the array reliability can be estimated as:

Reliability = (0.87) * (0.94) * (0.96) = 0.79.

This is the best-case estimate.

## D. SITE REJECTION STATISTICS

Another indication of the performance quality of ILPA is the number of sites considered to be acceptable for inclusion in beamforming. A site is rejected from the beamforming process if any of the following occurs on one or more site components:

- The component is dead
- The data contain uncorrectable spikes or clipped data
- The data contain power surges raising the 128-point processing segment powers more than ten times the power of the preceding and following segments
- The data contain 128-point processing segments with zero power (data drop-outs)
- The data contain 128-point processing segment powers consistently higher than the segment powers of corresponding components at other sites.

The decision as to whether to accept or reject a site is made using the edit printout, which lists segment powers for each component of each site of the array.

Of the 680 events in the combined data bases of last year and this year, unreadable or missing data prevented the processing of 87 events. The number of times each site was rejected from beamforming for the 593 processed events is summarized in Table II-3. (Note that site 1 did not become operational until 5 May 1976 and site 3 did not become operational until 8 September 1976.) The data of Table II-3 show that site 6 had the highest rejection rate. In almost all cases, the reason for rejecting this site was transmission errors occurring during the relaying of data from site 6 through site 5 to the central recording station. These transmission errors were fairly uniformly distributed throughout the time period covered by the data base. The transmission errors manifested themselves in the data as power surges, spikes, and data drop-outs.

Table II-4 presents the reasons for rejection of each site. Single segment power surges and entire component power surges are presented jointly as 'POWER SURGES'. The heading 'DEAD COMPONENT'

## TABLE II-3

## SUMMARY OF SITE REJECTION STATISTICS

| Site | Total Number of Times Site was Available | Number of Times Site was Rejected | Precent Re-jected (%) |
|---|---|---|---|
| 1 | 573 | 65 | 11.3 |
| 2 | 593 | 79 | 13.3 |
| 3 | 129 | 21 | 16.3 |
| 4 | 593 | 170 | 28.7 |
| 5 | 593 | 108 | 18.2 |
| 6 | 593 | 234 | 39.5 |
| 7 | 593 | 60 | 10.1 |

## TABLE II-4

## REASON FOR SITE DELETION

| Site / Reason | Percentage of Total Number of Rejections | | | | | | |
|---|---|---|---|---|---|---|---|
| | 1 | 2 | 3 | 4 | 5 | 6 | 7 |
| Power Surge | 76% | 36% | 50% | 94% | 34% | 49% | 36% |
| Dead Component | 11% | 57% | 50% | 5% | 61% | 39% | 49% |
| Spikes/Clipped Data | 13% | 7% | 0% | 1% | 5% | 12% | 15% |

includes data drop-outs and dead components. Following site 6, site 4 had the highest rejection rate. Table II-4 indicates that the primary reason for rejecting this site was power surges. Sites 3 and 5 had the next highest rejection rates. For these sites, power surges and dead components caused about the same number of rejections. Sites 1, 2, and 7 had the lowest rejection rates. Power surges accounted for the majority of rejections of site 1. At sites 2 and 7, dead components accounted for slightly more rejections than did power surges. In all cases, spikes and clipped data accounted for only a small number of site rejections.

## E. PROBABILITY OF MIXED EVENTS

The manner in which the data base for the evaluation of the Iranian Long Period Array was selected produces a data base which is essentially a random sampling of Eurasian seismic events. Since no effort was made to exclude obviously mixed events, the mixed event statistics derived from analysis of this data base should accurately reflect the frequency of occurrence of mixed events. (A mixed event is any event whose waveforms are masked or interfered with by the waveforms of a second event.)

Table II-5 presents the mixed event statistics and derived probability of mixing for four bodywave magnitude ($m_b$) ranges. These values are compiled for ranges in $m_b$ rather than for individual $m_b$ values to provide more robust statistics. (It seems reasonable to assume that there will be no major changes in the probability of mixing from one $m_b$ value to the next.). This table indicates that, as one might expect, the probability of mixing very gradually drops as the bodywave magnitude increases. This gradual decrease in the probability of mixing is due to beamforming the data, which suppresses off-azimuth signals so that events which are mixed on the reference site can sometimes be detected on the beam data.

## TABLE II-5

## ILPA BEAM DATA MIXED EVENT STATISTICS

| $m_b$ Range | Number of Mixed Events | Number of Non-Mixed Events | Probability of Mixed Event |
|---|---|---|---|
| 3.1-3.5 | 27 | 63 | 0.30 |
| 3.6-4.0 | 52 | 114 | 0.31 |
| 4.1-4.5 | 20 | 85 | 0.19 |
| 4.6-5.0 | 12 | 66 | 0.15 |

# SECTION III

# NOISE ANALYSIS

## A. DISCUSSION

The goal of this section is to determine the long-period noise field characteristics of the Iranian Long Period Array. Both single-site and beamformed data will be examined in order to estimate the effects of the beamforming process on the noise field. The major effort will be concentrated on the noise in the 0.023-0.059 Hz signal window. This window is used in the noise analysis to permit one to consider the effect of noise level on detection capability. Some information on the noise field at frequencies outside this window is presented by average noise amplitude spectra.

The analysis of the noise field is divided into two parts termed the basic noise analysis and the extended noise analysis. The basic noise analysis covers the points common to the analysis of the noise field at a single-site station such as one of the Seismic Research Observatories. These points are RMS noise amplitudes, RMS noise trends, spectral content of the noise, and peak noise amplitudes. The extended noise analysis covers those points which can only be investigated with array data. These points are multichannel noise coherence and propagating noise.

The noise sample data base was formed by searching the NORSAR event lists for daily time intervals of at least one hour in duration during which no seismic signals would be expected to arrive at the array. Data segments 4096 seconds in length were then selected from these intervals and processed as described in Section II. After processing, the data were plotted and visually examined for unreported signals and system malfunctions. If either of these was found, the noise sample was rejected unless the signal or malfunction occurred near the start or end of the sample. In this case, 2048 seconds of the noise sample were used.

The definition of seismic noise used in this report is most clearly stated by Enders A. Robinson (Robinson, 1967):

> "Any ground motion that is not caused by an explosion or an earthquake is usually regarded as ambient seismic noise. The predominant components of such seismic noise are surface-generated microseisms that originate from meteorlogical, hydrodynamic, or cultural sources. Such microseisms chiefly propagate along the surface of the earth as Rayleigh waves."

## B. BASIC NOISE ANALYSIS

The goals of the basic noise analysis were to estimate the long-period RMS noise levels, the peak 25-second noise amplitudes, and the spectral content of the noise for each of the three components of motion (vertical, north, and east) as recorded at each array site and for the beamformed noise sample. The overall evaluation time frame was from 1 May 1976 to 29 April 1977. This was used to study the reference site and beam noise. Thirty days of noise data were selected from within this time frame to study the noise at the individual sites.

After the preliminary processing and visual inspection, the noise samples were input to a program which performs the following functions:

- Compute RMS noise values uncorrected for instrument response in the 0.023-0.059 Hz passband.
- Measure zero-to-peak 25-second noise amplitudes.
- Compute the power spectrum for each component of motion of the noise sample and smooth to 128 frequencies.
- Compute RMS noise values corrected for instrument response in the 0.023-0.059 Hz passband.

The program output all measured and computed values on punched cards to facilitate data input to succeeding plot programs. The 25-second noise amplitudes were measured as the maximum 25-second noise amplitude of each component of motion of the noise sample.

The mean long-period RMS noise values in millimicrons as measured in the 0.023 - 0.059 Hz passband are presented in Table III-1. These values are uncorrected for instrument response. The individual RMS values were not plotted due to the relatively small number of samples used. In every case except one (site 1 north) the vertical component displays somewhat lower mean RMS noise values than do the horizontal components. There appears to be no correlation between the mean noise levels at the sites and the potential cultural noise sources described in the final report on the installation of ILPA (Texas Instruments, 1977). For example, an active manganese mine is described as being located 3 km from site 3, which has mean RMS noise values at about the median for the seven sites. It would appear that if the types of cultural activity in the area of the array produce long-period transient noise trains, these noise trains do not materially affect the mean RMS noise levels.

The long-period RMS noise values in millimicrons for the vertical, north, and east components of motion are plotted versus Julian day for the reference site (site 1) in Figure III-1 and for the beam in Figure III-2. In these figures, RMS noise values for consecutive days are connected by solid lines. Gaps of one or two days in length are due to bad noise samples. The three large gaps are due to array system failures, the causes of which were discussed in Section II. The monthly RMS noise level trends which were derived from these RMS noise values are shown in Figure III-3 for the reference site data and Figure III-4 for the beam data. Due to array down time, it is difficult to determine how the noise level varies with time. It appears that the noise levels rise in the winter months and decrease with

## TABLE III-1

## ILPA INDIVIDUAL SITE AVERAGE RMS NOISE AMPLITUDES IN mμ (UNCORRECTED FOR INSTRUMENT RESPONSE)

| Site Number | V | | N | | E | | No. of Samples |
|---|---|---|---|---|---|---|---|
| | Mean | S.D.* | Mean | S.D.* | Mean | S.D.* | |
| 1 | 9.13 | 2.32 | 8.76 | 1.98 | 10.03 | 2.92 | 30 |
| 2 | 7.40 | 1.80 | 12.75 | 6.17 | 10.98 | 4.20 | 18 |
| 3 | 8.08 | 3.59 | 9.68 | 3.16 | 9.47 | 3.60 | 7 |
| 4 | 7.43 | 1.44 | 13.20 | 8.83 | 12.97 | 8.69 | 14 |
| 5 | 6.53 | 1.42 | 8.33 | 1.42 | 9.54 | 2.52 | 24 |
| 6 | 7.97 | 2.73 | 9.00 | 2.29 | 10.17 | 3.63 | 15 |
| 7 | 8.45 | 2.32 | 9.32 | 2.42 | 13.56 | 5.20 | 32 |

* Standard Deviation

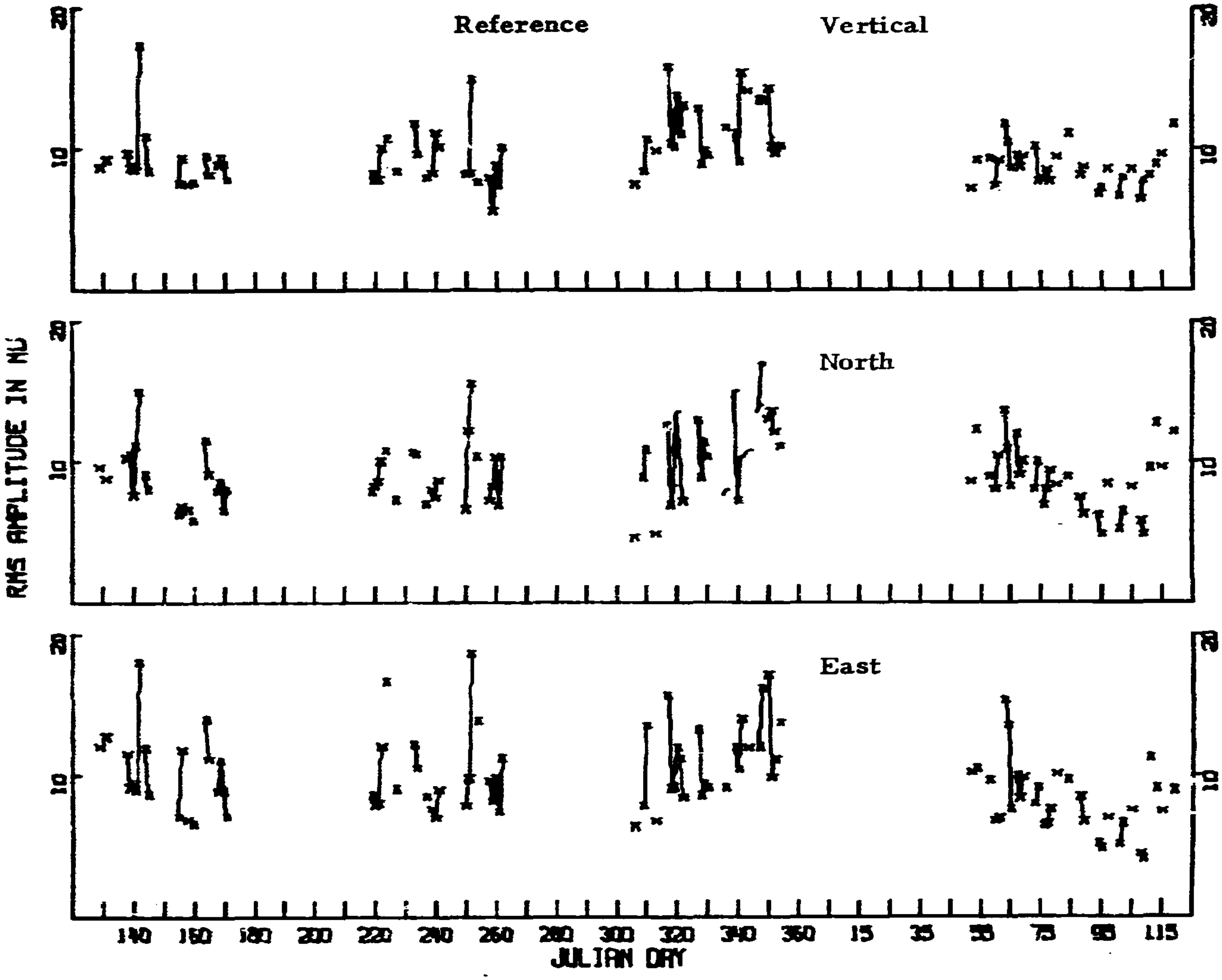

FIGURE III-1

REFERENCE SITE (SITE 1) RMS NOISE IN MILLIMICRONS

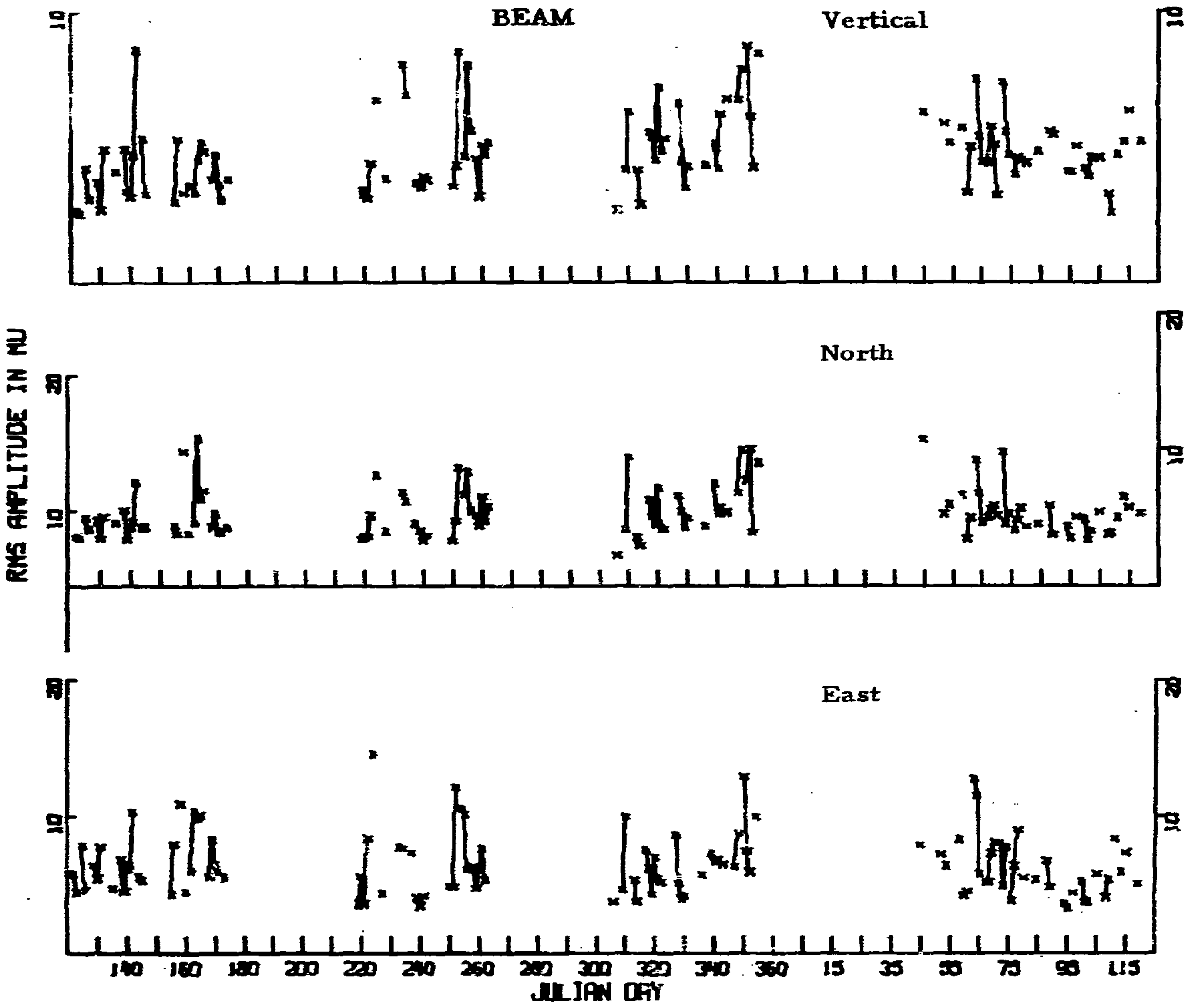

FIGURE III-2

BEAM RMS NOISE IN MILLIMICRONS

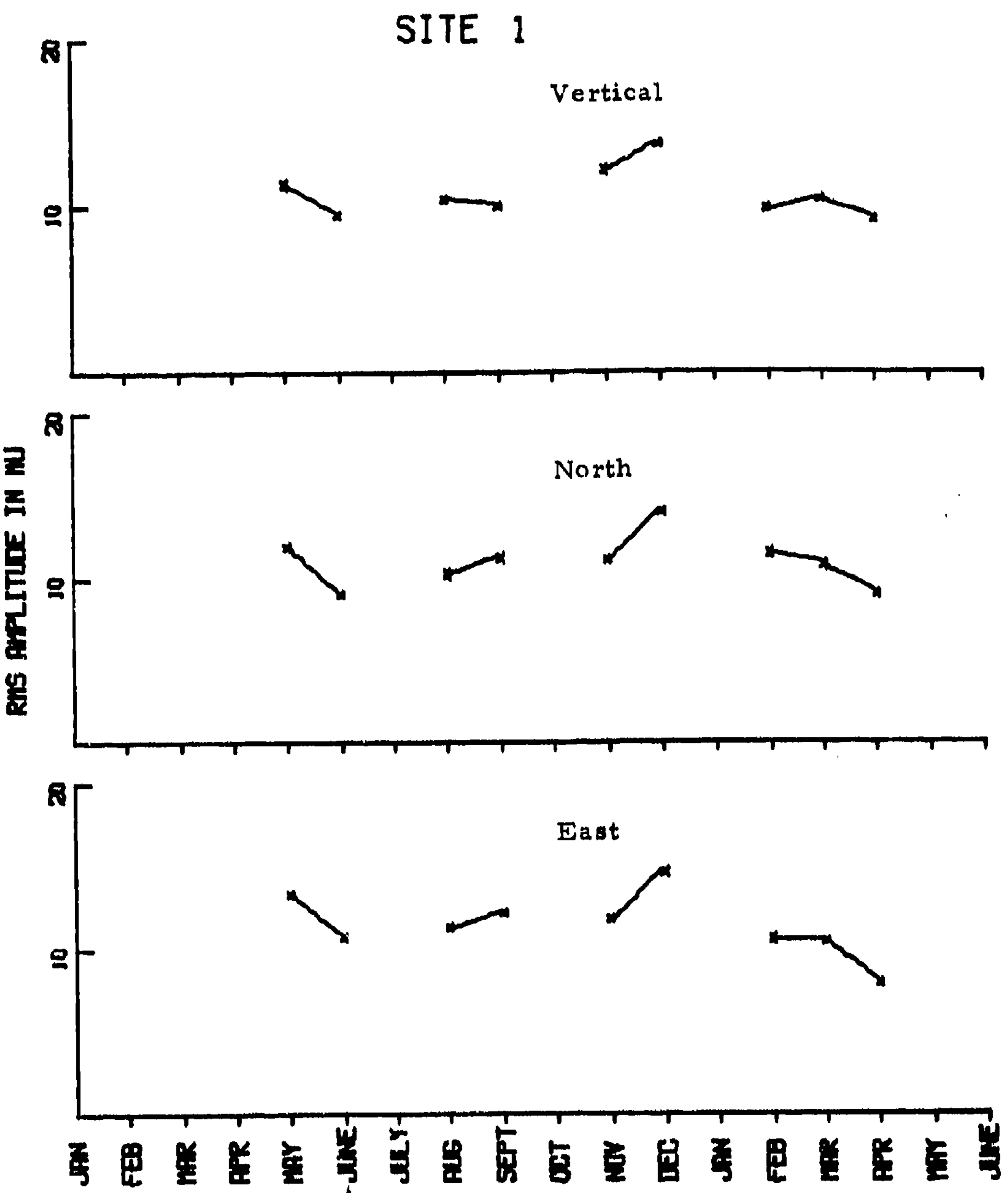

FIGURE III-3

REFERENCE SITE (SITE 1) RMS NOISE LEVEL TRENDS

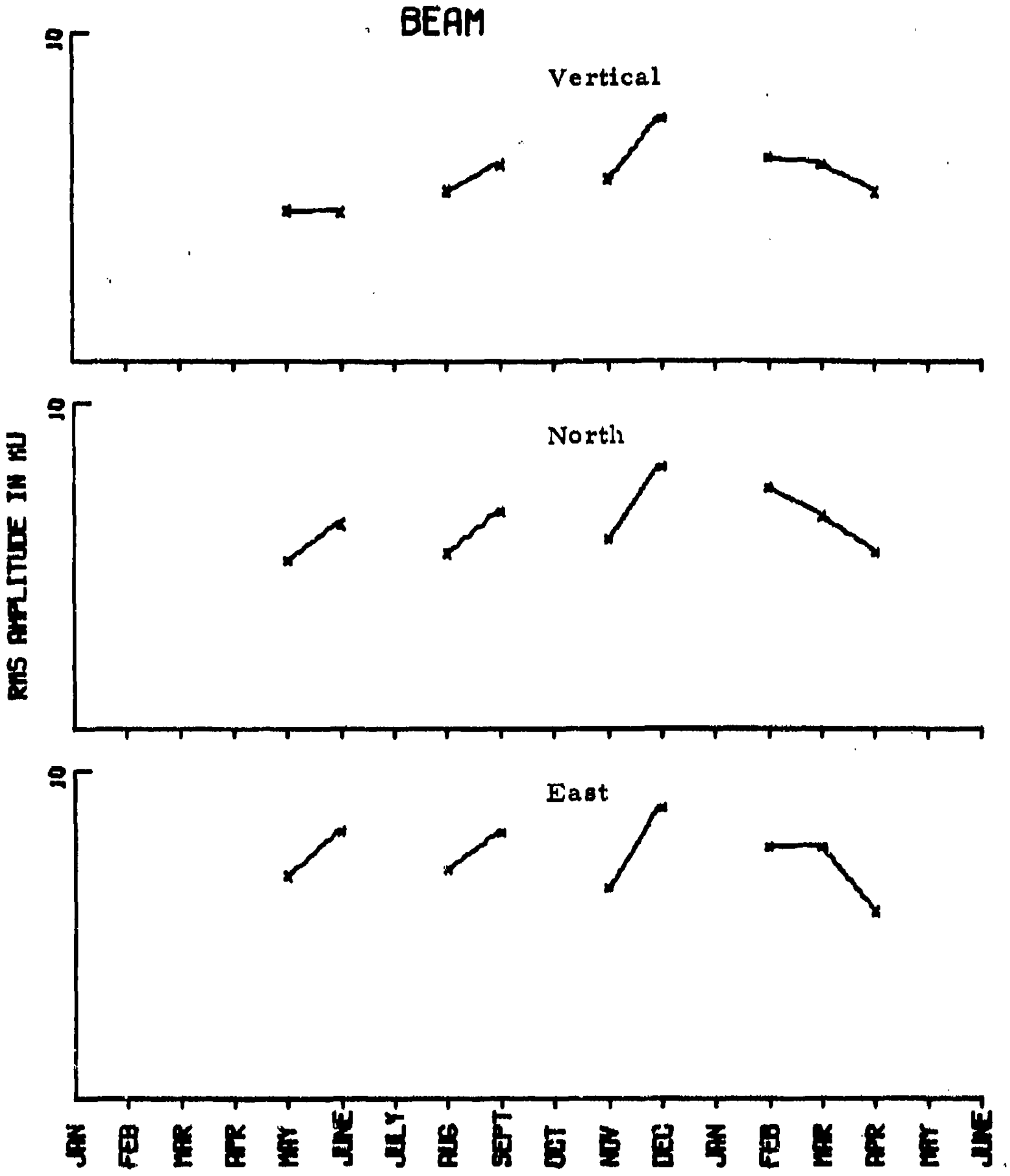

FIGURE III-4

BEAM RMS NOISE LEVEL TRENDS

the onset of spring. The only significant difference between the reference site data and beam data as portrayed by Figures III-1 to III-4 is the absolute noise level. Table III-2 compares the overall reference site and beam mean RMS noise levels. This table shows that beamforming reduces the RMS noise level in the 0.023 - 0.059 Hz passband by approximately 6.1 dB on the vertical component, 4.8 dB on the north component, and 3.6 dB on the east component.

Table III-3 presents the statistics for the 25-second noise amplitudes measured on each noise sample. The values used to compute these statistics were the largest 25-second noise amplitudes of each noise sample measured from zero-to-peak in millimicrons. The means and standard deviations in this table are for the base ten logarithms of these amplitudes. These values present another measure of noise suppression due to beamforming. The peak 25-second noise amplitudes are reduced by approximately 5.6 dB on the vertical component, 5.2 dB on the north component, and 5.0 dB on the east component due to beamforming. These values compare fairly well with the equivalent values for RMS noise suppression on the vertical and north components. The lower RMS noise suppression for the east component (3.6 dB) suggests that some range of frequencies on the east component in the 0.023 - 0.059 Hz passband contains noise energy which is to some extent correlated from site to site and which therefore is not as well suppressed by beamforming as noise at other frequencies.

Figure III-5 shows average RMS noise amplitude spectra for each of the remote sites of the array and for the beamformed noise data. These spectra are uncorrected for instrument response. They were computed by averaging the spectra measured from each noise sample and converting these average spectra to RMS amplitudes using Parseval's formula

$$\mathrm{RMS}_a^b = \sqrt{\Delta f \sum_{i=a}^{b} \mid A(f_i) \mid^2 * C(f_i)^2}$$

## TABLE III-2

## COMPARISON OF SINGLE-SITE AND BEAM RMS NOISE AMPLITUDES (UNCORRECTED FOR INSTRUMENT RESPONSE) (ALL VALUES ARE IN MILLIMICRONS)

| Type | V | | N | | E | | No. of Samples |
|---|---|---|---|---|---|---|---|
| | Mean | S.D.* | Mean | S.D.* | Mean | S.D.* | |
| Ref. Site | 9.58 | 2.19 | 9.34 | 2.56 | 9.86 | 2.98 | 97 |
| Beam | 4.77 | 1.44 | 5.36 | 1.82 | 6.51 | 2.31 | 113 |

* Standard Deviation

## TABLE III-3

## MAXIMUM 25-SECOND NOISE AMPLITUDES

$$\mathrm{LOG}_{10}\begin{bmatrix}\text{ZERO-PEAK*}\\ \text{AMPLITUDE}\end{bmatrix}$$

| | | Mean | Standard Deviation |
|---|---|---|---|
| Reference Site | V | 1.44 | 0.13 |
| | N | 1.45 | 0.14 |
| | E | 1.48 | 0.15 |
| Beam | V | 1.16 | 0.15 |
| | N | 1.19 | 0.14 |
| | E | 1.23 | 0.15 |

Suppression of 25-Second Noise Amplitudes by Beamforming:

V: 5.60 dB N: 5.20 dB E: 5.00 dB

* Zero-to-Peak amplitudes were measured in millimicrons.

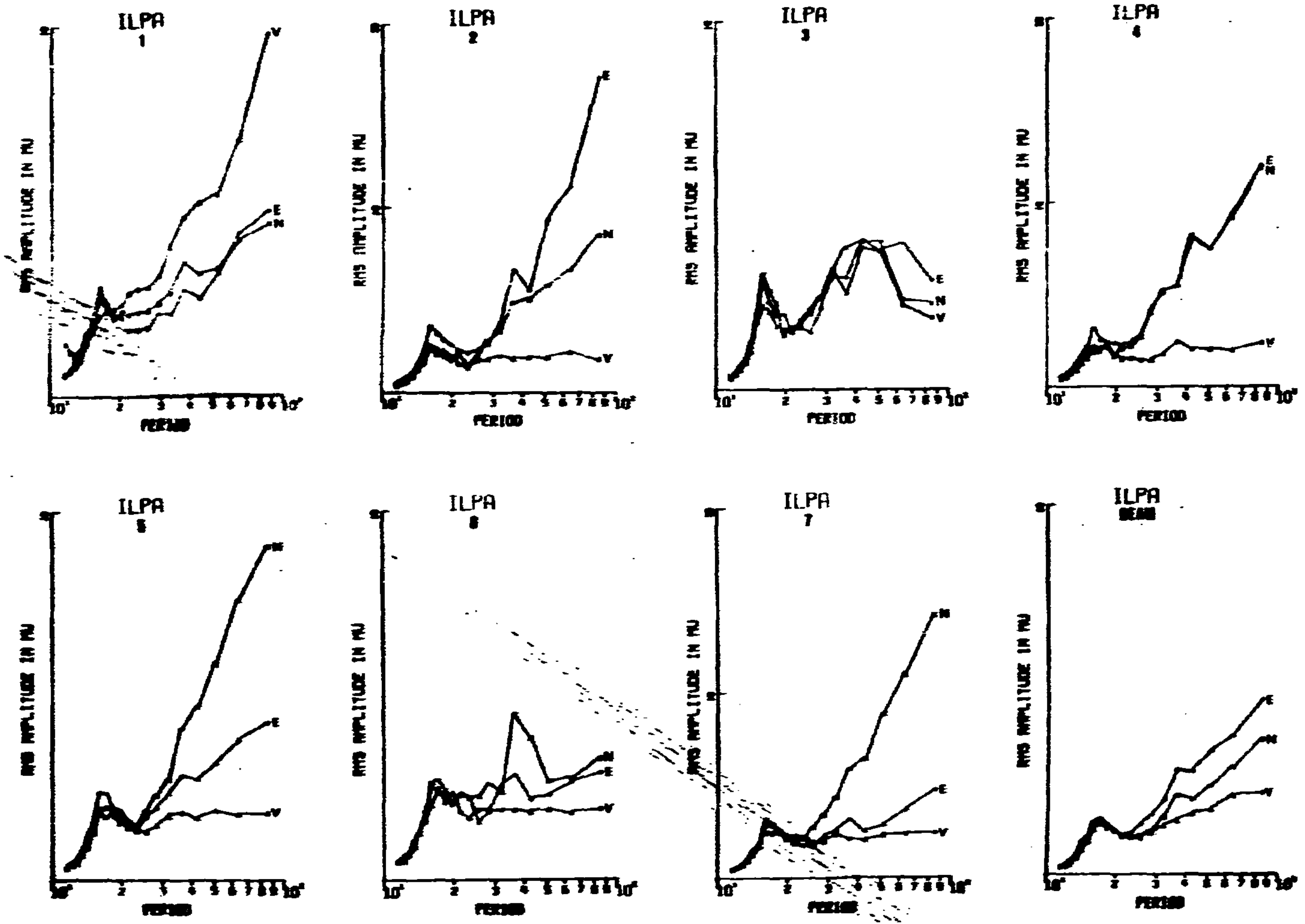

FIGURE III-5

AVERAGE RMS NOISE AMPLITUDE SPECTRA
INDIVIDUAL SITES AND BEAM

where $\Delta f$ = the elemental frequency interval ($\Delta f$=0.001953 Hz),

$|A(f_i)|^2$ = the discrete Fourier transform spectral density estimate at frequency $f_i$,

$C(f_i)$ = the instrument response correction at frequency $f_i$,

a = the initial frequency index, and

b = the final frequency index.

Since the RMS amplitude at each discrete frequency was desired, in this case a = b. Also, since no instrument response corrections were made, $C(f_i) = 1$ for all frequencies.

For all sites except site 1, the RMS noise amplitudes for periods greater than 25 seconds are higher on the horizontal components than on the vertical component. If the noise on the horizontal components at these periods contains a relatively large amount of coherent energy in comparison to the vertical, the difference between the reduction in noise due to beamforming for the vertical and horizontal components will be explained.

Figures III-6 and III-7 show the average RMS amplitude spectra of all noise samples for the reference site and beam data respectively. No instrument response corrections were applied to these data. The left-hand side of each figure shows the average RMS amplitude spectra for the three components of motion. The right-hand side of each figure shows the log RMS amplitude spectra. The vertical bars on these spectra represent plus-or-minus one standard deviation of the noise. These bars represent the day-to-day variability of the noise at each period. The following points should be noted from these figures:

- The smallest decreases in the amplitude spectra due to beamforming occur at the shorter periods. The most noticeable effect of beamforming at periods less than 25 seconds is to make the vertical and horizontal spectra nearly identical.

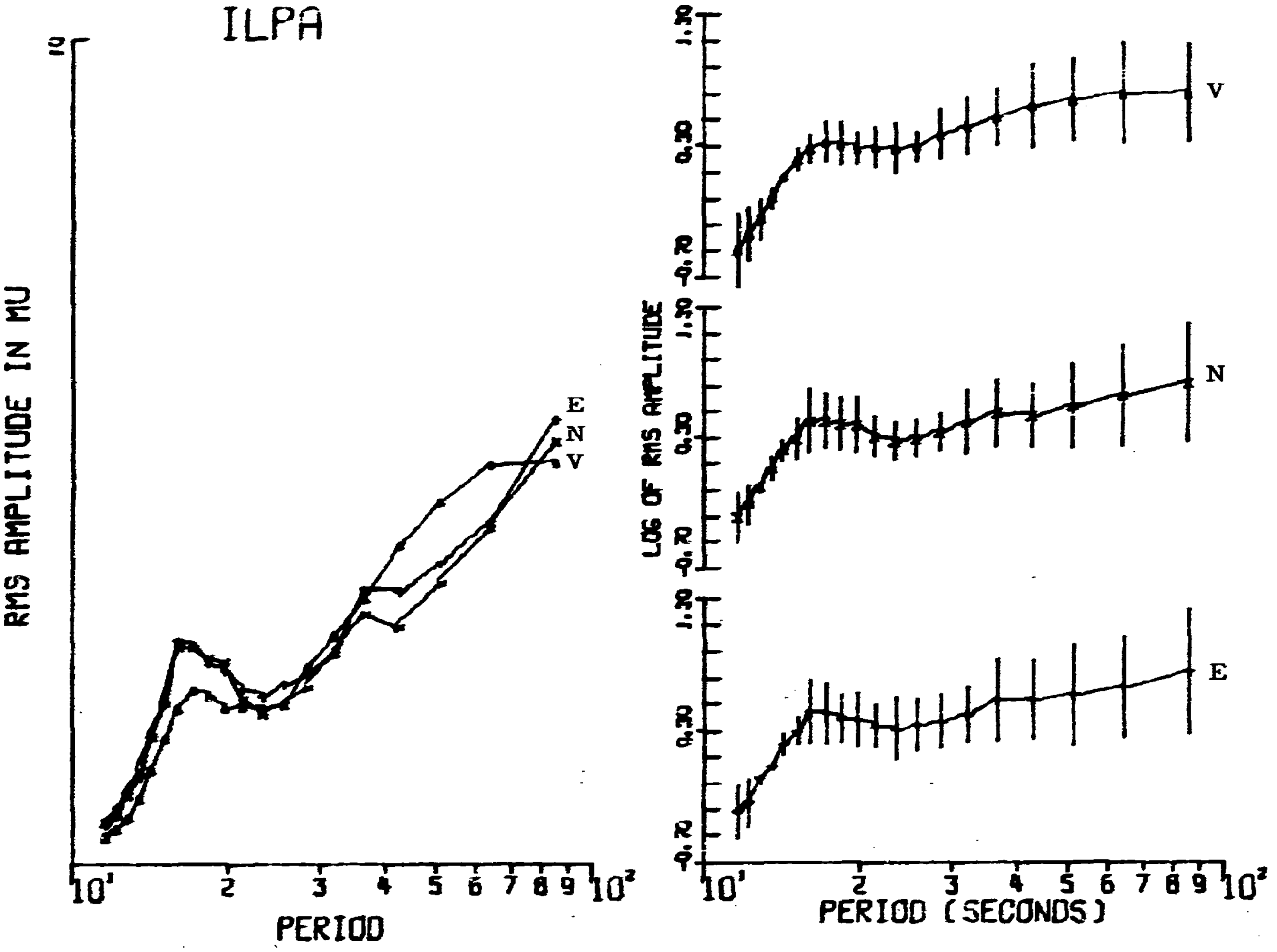

FIGURE III-6

AVERAGE RMS NOISE AMPLITUDE SPECTRA - REFERENCE (SITE 1) SITE
NO INSTRUMENT-RESPONSE CORRECTIONS APPLIED

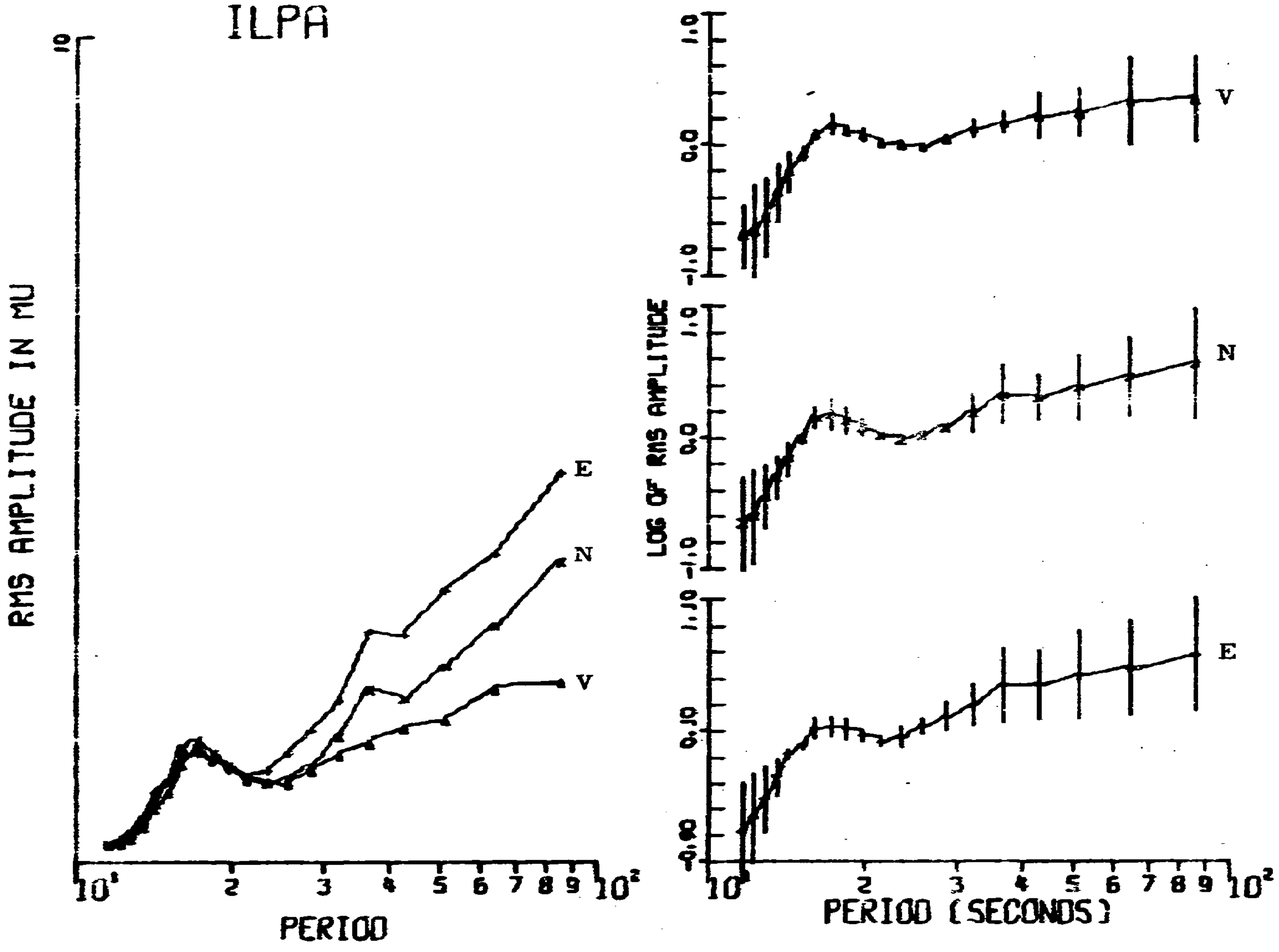

FIGURE III-7

AVERAGE RMS NOISE AMPLITUDE SPECTRA - BEAM
NO INSTRUMENT-RESPONSE CORRECTIONS APPLIED

- At periods greater than 25 seconds, beamforming lowers the vertical-component spectrum much more than the horizontal spectra. The east-component spectrum shows relatively little change due to beamforming.
- The reference site shows greatest day-to-day variation in the noise at periods greater than approximately 28 seconds.
- Beamforming greatly decreases the day-to-day variation in the noise at periods between 14 and 28 seconds.
- Beamforming has very little effect on the day-to-day variation in the noise at periods greater than 28 seconds.

A general conclusion which may be drawn from the preceding observations is that the signal-to-noise ratio may be greatly enhanced by changing the bandpass filter limits from 0.023 - 0.059 Hz (16.9 - 43.5 seconds period) to 0.033 - 0.050 Hz (20 - 30 seconds period). This will sharply curtail the effects of the noise at the microseismic peak and at periods beyond 30 seconds on the signal-to-noise ratio. Since the majority of the signal energy lies within the 0.033 - 0.050 Hz passband, the signal should not be materially affected by this change in filter limits.

## C. EXTENDED NOISE ANALYSIS

This subsection deals with the types of noise analysis which can only be performed with array data, i.e., coherence of the noise and directionality of the noise.

Two main programs were used to carry out this phase of the noise analysis. The first program computes crosspower spectral matrices from the time-domain noise data. This is performed in the following manner. The edited data in its recorded vertical, north, east configuration is entered into the program one 128-point (256 second) segment at a time. The program then removes the trace mean calculated in the edit program from the data segment and Fourier transforms the data segment. To provide greater frequency-to-frequency stability, a three-point Hanning function is applied to the transformed data. This Hanning function may be expressed as

$$T_i'(f) = +\frac{1}{4}T_{i-1}(f) + \frac{1}{2}T_i(f) + \frac{1}{4}T_{i+1}(f)$$

where $T_i(f)$ is the input transformed data at frequency f

$T_i'(f)$ is the output transformed data at frequency f

i = frequency index.

At this point, the crosspower spectral matrices are computed. One matrix is computed for each frequency within the specified passband for each component and site. The program calculates these crosspower spectral matrices $[\Phi]$ for the desired sites i, j from the complex transformed data $\vec{X}$ at each frequency f. Looping on the number of transformed segments (NSEG) stacks the matrix over the entire data trace. In equation form

$$\Phi_{ij}(f) = \sum_{n=1}^{NSEG} X_{in} X_{jn} \quad .$$

Each element of the matrix is scaled to account for the number of transform segments over which the matrix was accumulated and to convert from computer counts to millimicrons. The scale factor is:

$$SCALE = \frac{2\Delta t}{(NPTS)(NSEG)(Q)}$$

where: $\Delta t$ = the sampling interval

NPTS = the number of points in each segment

NSEG = the number of segments used, and

Q = the quantization in computer counts per millimicron.

Finally, the scaled crosspower spectral matrices are written on magnetic tape.

The second main program is used to analyze the array noise data by interrogating the crosspower spectral matrices. The analysis options provided by this program are: site power spectra, component average power spectra, multichannel coherencies, and conventional or high-resolution frequency-wavenumber spectra. The two options used in this evaluation are the multichannel coherence and high-resolution frequency-wavenumber spectra.

The multichannel coherence is calculated as follows. The elements of the crosspower spectral matrix corresponding to the reference site crosspowers with each site i to be used in the coherence calculation are placed in an array PHI dimensioned (2, 40). The real portion of the crosspower is in row 1 and the imaginary portion is in row 2. In the case where coherence is to be calculated between the reference site and some other data site, the reference site autopower is placed in a scalar PHI11 and the data site autopower in scalar PHI22. The coherence squared is then calculated as:

$$\mathrm{COH}^2 = \frac{\mathrm{PHI}(1,1)^2 + \mathrm{PHI}(2,1)^2}{\mathrm{PHI11} * \mathrm{PHI22}} .$$

For the more general case where a multichannel coherence is calculated, the remaining elements of the crosspower spectral matrix are placed in a matrix C. C is factored into a triangularized matrix S such that

$$C = (S^H)S$$

where H indicates the conjugate transpose of S. From this, an optimum filter set FIL is designed such that

$$(S^H)(S)(\mathrm{FIL}) = \mathrm{PHI} .$$

The multichannel coherence squared is then calculated as

$$\mathrm{COH}^2 = \frac{(\mathrm{PHI})(\mathrm{FIL})}{\mathrm{PHI11}} \quad .$$

Coherence is then a measure of the similarity of functions. For this evaluation of the Iranian Long-Period Array noise field characteristics, multichannel coherencies (measured as coherence squared) were computed from ten noise samples using sites 2, 4, 5, 6, and 7 to predict site 1. The results were averaged together to eliminate minor day-to-day variations. The average coherence squared values are plotted in Figures III-8 to III-10. The vertical dashed lines in each plot represent the bandpass filter limits (0.023 - 0.059 Hz) used in RMS noise computations and signal processing and analysis. In each figure, the coherence squared has a peak at approximately the same frequency (0.06 - 0.07 Hz) as the microseismic peak of the noise RMS amplitude spectra. Robinson (Robinson, 1967) notes that microseismic noise is correlated to various degrees both in time and in space. This would explain the presence of this peak in the coherence squared plots.

Within the signal bandpass filter limits of 0.023 - 0.059 Hz, a second peak appears on the plots of coherence squared at approximately 0.035 Hz. The peak on the plot of the vertical component coherence squared is lower than the peaks on either of the coherence squared plots for the horizontal components. The level of coherence in the signal passband is high enough that multi-channel filter processing may be effective. In general, the shape and coherence levels shown in these figures are quite similar to those determined from the inner-ring sites of the Norwegian Seismic Array (Laun, Shen, and Swindell, 1973).

The frequency-wavenumber spectra are calculated in the following manner. In order to beamsteer an array so that it enhances plane waves from a particular direction, time delays are applied to the data to

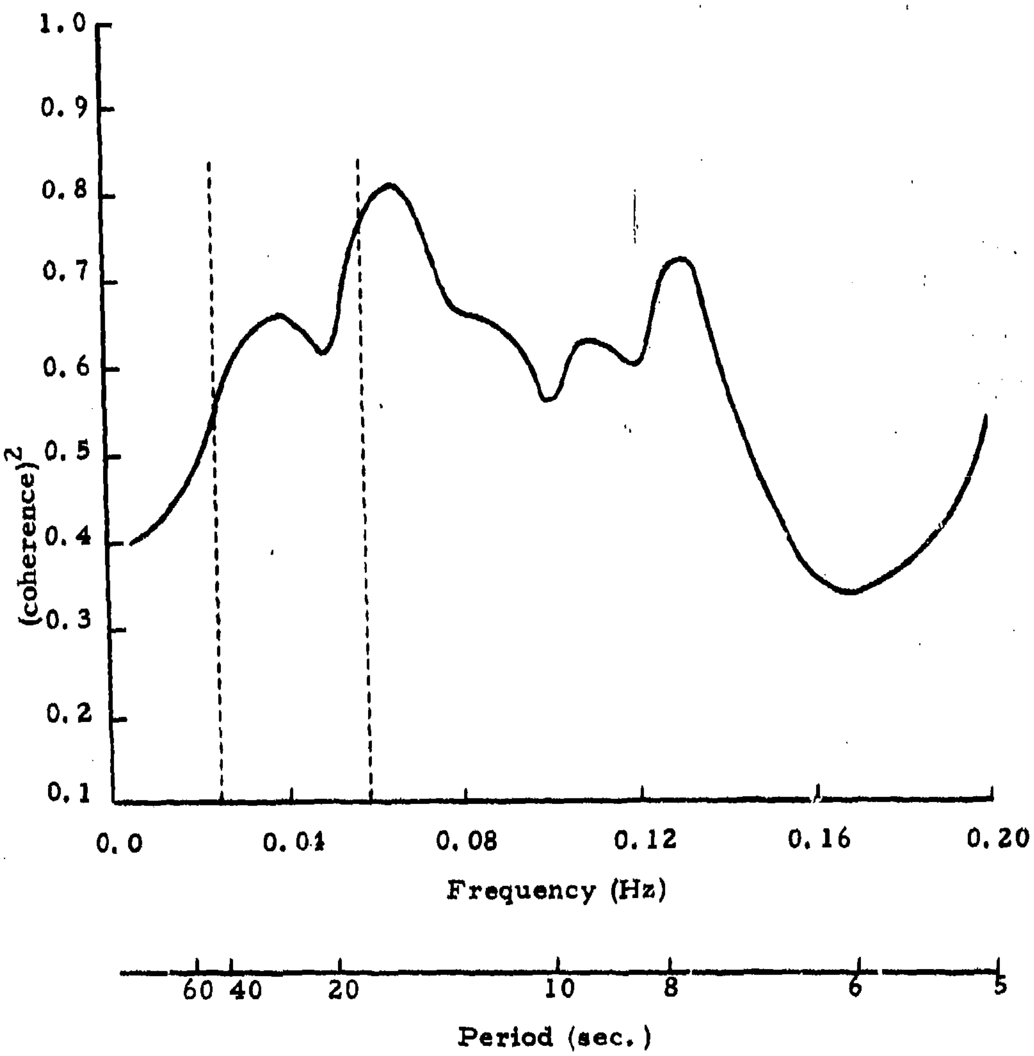

FIGURE III-8

VERTICAL COMPONENT AVERAGE MULTICHANNEL COHERENCE OF
10 ILPA NOISE SAMPLES
SITE 1 PREDICTED FROM SITES 2, 4, 5, 6, 7

The multichannel coherence squared is then calculated as

$$\mathrm{COH}^2 = \frac{(\mathrm{PHI})(\mathrm{FIL})}{\mathrm{PHI11}} \quad .$$

Coherence is then a measure of the similarity of functions. For this evaluation of the Iranian Long-Period Array noise field characteristics, multichannel coherencies (measured as coherence squared) were computed from ten noise samples using sites 2, 4, 5, 6, and 7 to predict site 1. The results were averaged together to eliminate minor day-to-day variations. The average coherence squared values are plotted in Figures III-8 to III-10. The vertical dashed lines in each plot represent the bandpass filter limits (0.023 - 0.059 Hz) used in RMS noise computations and signal processing and analysis. In each figure, the coherence squared has a peak at approximately the same frequency (0.06 - 0.07 Hz) as the microseismic peak of the noise RMS amplitude spectra. Robinson (Robinson, 1967) notes that microseismic noise is correlated to various degrees both in time and in space. This would explain the presence of this peak in the coherence squared plots.

Within the signal bandpass filter limits of 0.023 - 0.059 Hz, a second peak appears on the plots of coherence squared at approximately 0.035 Hz. The peak on the plot of the vertical component coherence squared is lower than the peaks on either of the coherence squared plots for the horizontal components. The level of coherence in the signal passband is high enough that multi-channel filter processing may be effective. In general, the shape and coherence levels shown in these figures are quite similar to those determined from the inner-ring sites of the Norwegian Seismic Array (Laun, Shen, and Swindell, 1973).

The frequency-wavenumber spectra are calculated in the following manner. In order to beamsteer an array so that it enhances plane waves from a particular direction, time delays are applied to the data to

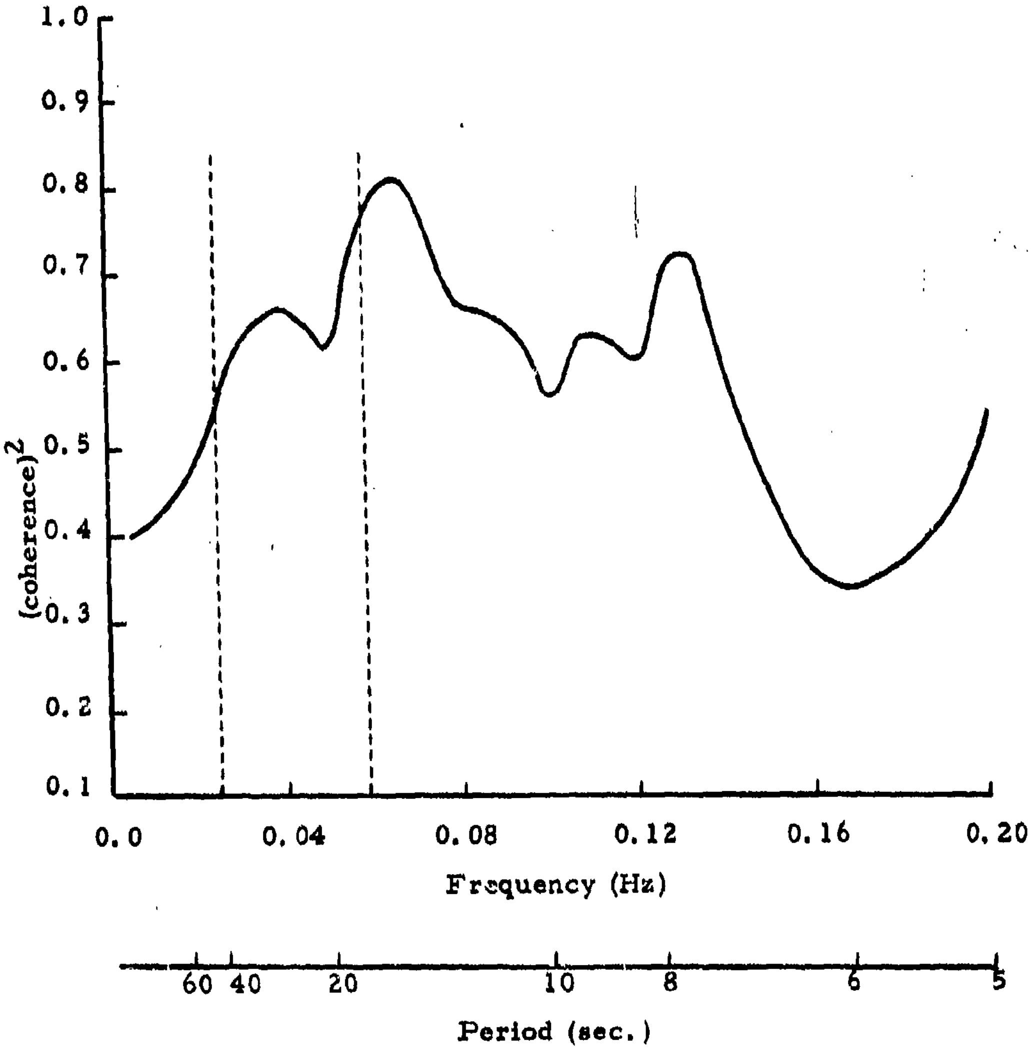

FIGURE III-8

VERTICAL COMPONENT AVERAGE MULTICHANNEL COHERENCE OF
10 ILPA NOISE SAMPLES
SITE 1 PREDICTED FROM SITES 2, 4, 5, 6, 7

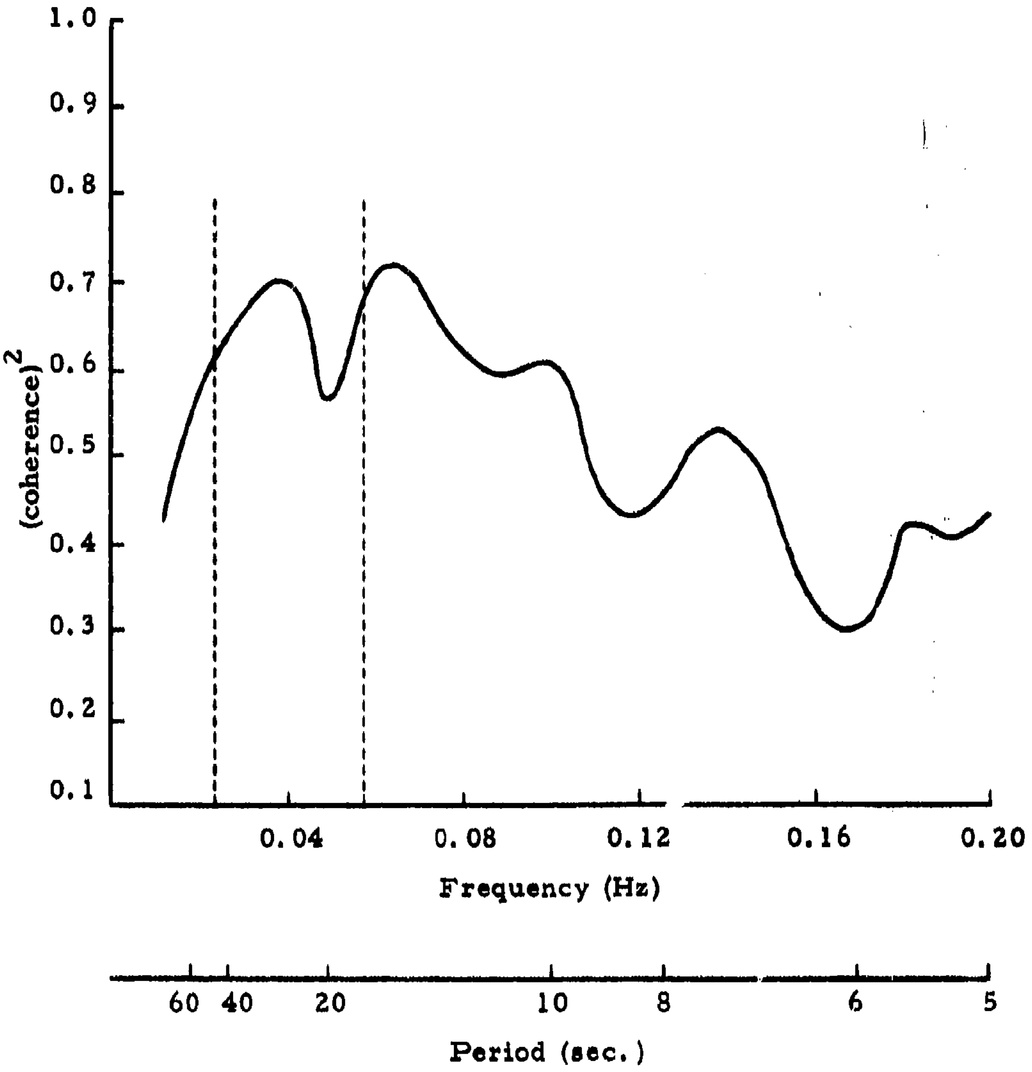

FIGURE III-9

NORTH COMPONENT AVERAGE MULTICHANNEL COHERENCE OF 10 ILPA NOISE SAMPLES SITE 1 PREDICTED FROM SITES 2, 4, 5, 6, 7

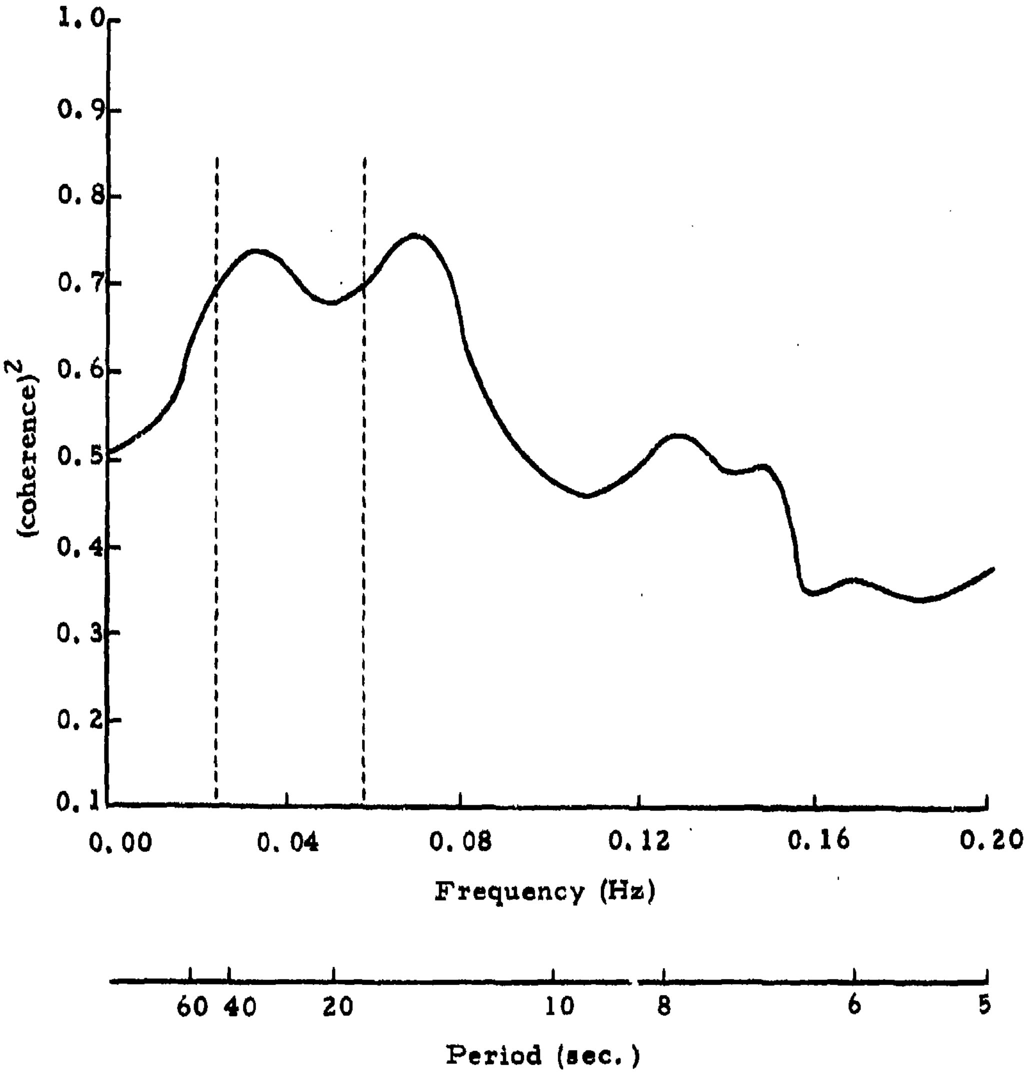

FIGURE III-10

EAST COMPONENT AVERAGE MULTICHANNEL COHERENCE OF 10 ILPA NOISE SAMPLES SITE 1 PREDICTED FROM SITES 2, 4, 5, 6, 7 time-align the arrival of wavefronts associated with that direction. The application of a time delay $\tau_i$ to the $i^{th}$ channel is equivalent to applying a convolution filter $\nu_i(\tau) = \delta(\tau - \tau_i)$ whose Fourier transform is $\exp(i2\pi\vec{k} \cdot \vec{X}_i)$, where $\vec{k}$ is the wavenumber space vector and $\vec{X}_i$ is the coordinate vector for site i. The beamsteer filter set for each wavenumber $\vec{k}$ is specified by the vector

$$\vec{V} = \begin{bmatrix} \exp(i2\pi\vec{k}\cdot\vec{X}_1) \\ \exp(i2\pi\vec{k}\cdot\vec{X}_2) \\ \bullet \\ \bullet \\ \bullet \\ \bullet \\ \exp(i2\pi\vec{k}\cdot\vec{X}_N) \end{bmatrix}$$

where N is the number of channels.

The power output of the filter set is then

$$CS(\vec{k}) = V^T \phi V$$

or

$$HRS(\vec{k}) = \frac{1}{V^T \phi^{-1} V}$$

where CS = conventional frequency-wavenumber spectra

HRS = high-resolution frequency-wavenumber spectra

$\phi$ = crosspower spectral matrix.

By incrementing the phase vector $\vec{V}$ by appropriate discrete values, the wavenumber spectra for each corresponding point in $\vec{k}$ space is computed. The spectra are next converted to dB units and for purposes of plotting the maximum value is assigned the symbol +A. Each power level below this maximum is assigned a symbol from A to Z, the dB decrement being user specified.

Figure III-11 shows a high-resolution frequency-wavenumber spectrum computed at a frequency of 0.03516 Hz using the vertical component data of event 1295. A signal was used for this figure to show how well the method can determine arrival azimuth and velocity. The azimuth of this event as computed from the epicenter coordinates is 38.2°. From the frequency-wavenumber spectrum of Figure III-11, the azimuth is 40.9°. The phase velocity measured from this figure is 3.6 km/sec., which appears to be a good Rayleigh wave phase velocity.

In order to investigate the question of propagating noise, high resolution frequency-wavenumber spectra were computed using each component of 91 noise samples. These spectra were computed at three frequencies: at 0.05859 Hz for the microseismic peak, at 0.04297 Hz for a representative signal-gate frequency, and at 0.01172 Hz for a point on the other side of the signal gate. The arrival azimuth and phase velocity of the peak value of each frequency-wavenumber spectrum were then measured. Table III-4 presents the number of occurrences by azimuth of the peak power of these frequency-wavenumber spectra. These values are tabulated without regard for the phase velocity associated with the measured azimuth.

The values in this table do not show any particular pattern as regards arrival azimuth. This would imply that there is no dominant source of propagating noise.

The next step in considering the question of propagating noise is to take into account the measured phase velocities. Propagating noise with phase velocities well below or above the beamforming velocities (4.0 km/sec. for Love, 3.5 km/sec. for Rayleigh) will be suppressed by the beamforming process. Therefore, those peaks in the frequency-wavenumber spectra which showed phase velocities below 3.2 km/sec. or above 4.5 km/sec. were removed from the results. The remainder were grouped by arrival azimuth.

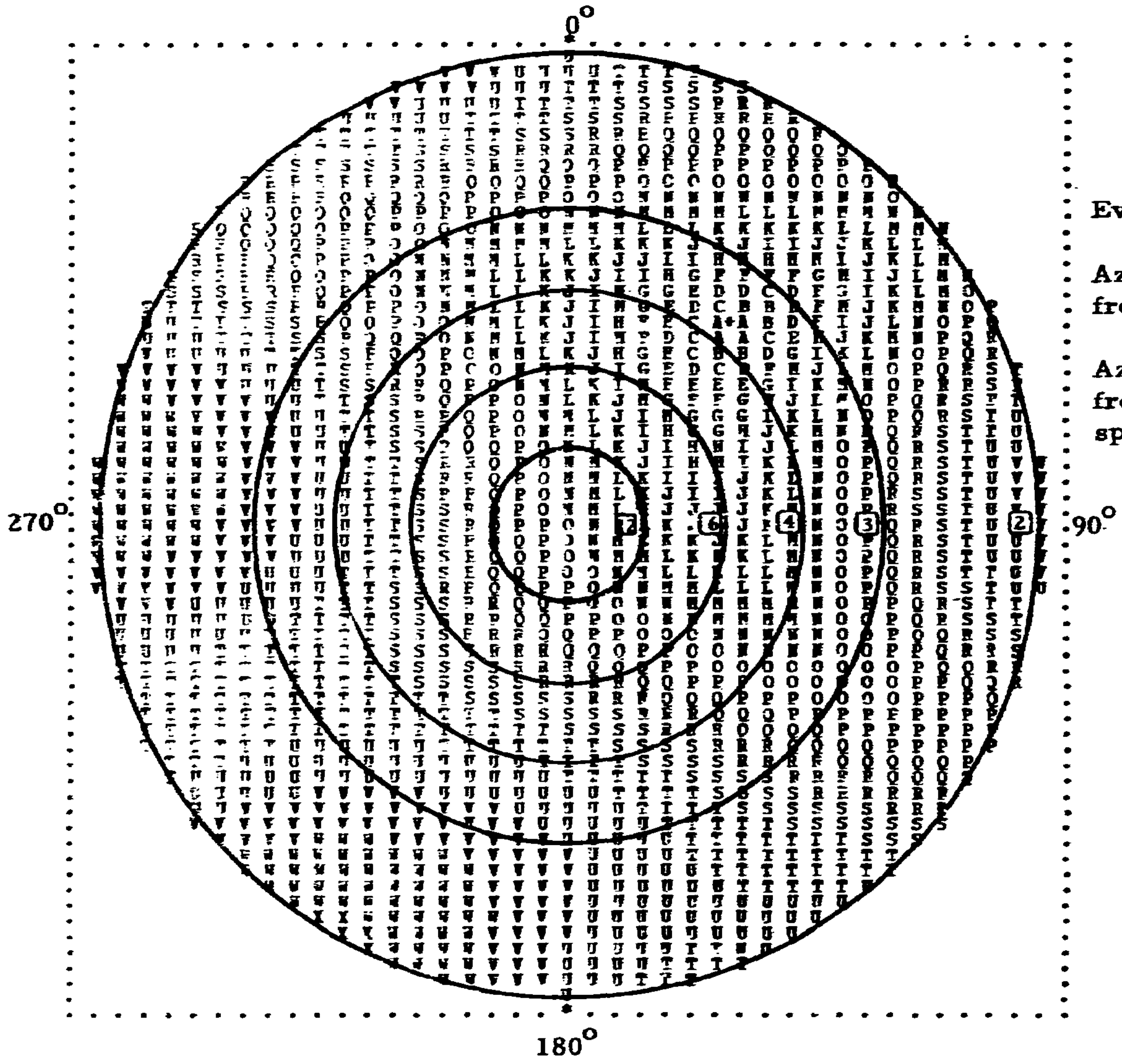

Event Number 1295

Azimuth = 38.2° computed from epicenter coordinates.

Azimuth = 40.9° measured from frequency-wavenumber spectrum.

FIGURE III-11

FREQUENCY-WAVENUMBER SPECTRUM FOR VERTICAL COMPONENT OF EVENT 1295 COMPUTED AT FREQUENCY = 0.03516 Hz

## TABLE III-4

## NUMBER OF OCCURRENCES OF PEAK POWER BY AZIMUTH

| | Number of Occurrences of Peak Power | | | | | | | | |
|---|---|---|---|---|---|---|---|---|---|
| | f = 0.01172 Hz | | | f = 004297 Hz | | | f = 0.05859 Hz | | |
| Component<br>Azimuth Range | V | N | E | V | N | E | V | N | E |
| 0-44 | 12 | 10 | 16 | 12 | 14 | 7 | 8 | 10 | 5 |
| 45-89 | 6 | 7 | 8 | 6 | 11 | 12 | 4 | 3 | 6 |
| 90-134 | 10 | 5 | 6 | 14 | 18 | 23 | 12 | 14 | 17 |
| 135-179 | 12 | 19 | 5 | 13 | 8 | 15 | 11 | 7 | 13 |
| 180-224 | 13 | 20 | 14 | 17 | 5 | 10 | 29 | 19 | 19 |
| 225-269 | 17 | 9 | 14 | 12 | 9 | 8 | 8 | 14 | 20 |
| 270-314 | 10 | 5 | 14 | 5 | 8 | 11 | 12 | 15 | 8 |
| 315-359 | 11 | 16 | 14 | 12 | 18 | 5 | 7 | 9 | 3 |

The results are shown in Figure III-12 for the frequency-wavenumber spectra computed at 0.01172 Hz, in Figure III-13 for the frequency-wavenumber spectra computed at 0.04297 Hz, and in Figure III-14 for the frequency-wavenumber spectra computed at 0.05859 Hz. The darkened area in each azimuth bin ($0^\circ$-$45^\circ$, $45^\circ$-$90^\circ$, and so on) represents the number of times propagating noise was observed arriving at the array in that azimuth range at signal velocities. Bearing in mind the above description of how these figures were created, the following points should be noted from the figures:

- Figure III-12. There appears to be very little 0.01172 Hz propagating noise arriving at the array at signal velocities. What little there is shows no dominant range of source azimuths.
- Figure III-13. Approximately half of the frequency-wavenumber spectra computed at 0.04297 Hz had peaks with phase velocities in the signal velocity range, indicating that propagating noise may well form a significant part of the noise field at signal frequencies. On the vertical and east components, the majority of propagating noise arrivals had arrival azimuths between $90^\circ$ and $225^\circ$, indicating noise sources lying to the south of the array, away from the general area of interest. On the north component, the majority of propagating noise arrivals had arrival azimuths between $315^\circ$ and $45^\circ$.
- Figure III-14. Approximately half of the frequency-wavenumber spectra computed at 0.05859 Hz had peaks with phase velocities in the signal velocity range, indicating that propagating noise forms a significant portion of the microseismic noise peak. On all three components, the great majority of the propagating noise arrivals had source azimuths to the south of the array, away from the general area of interest.

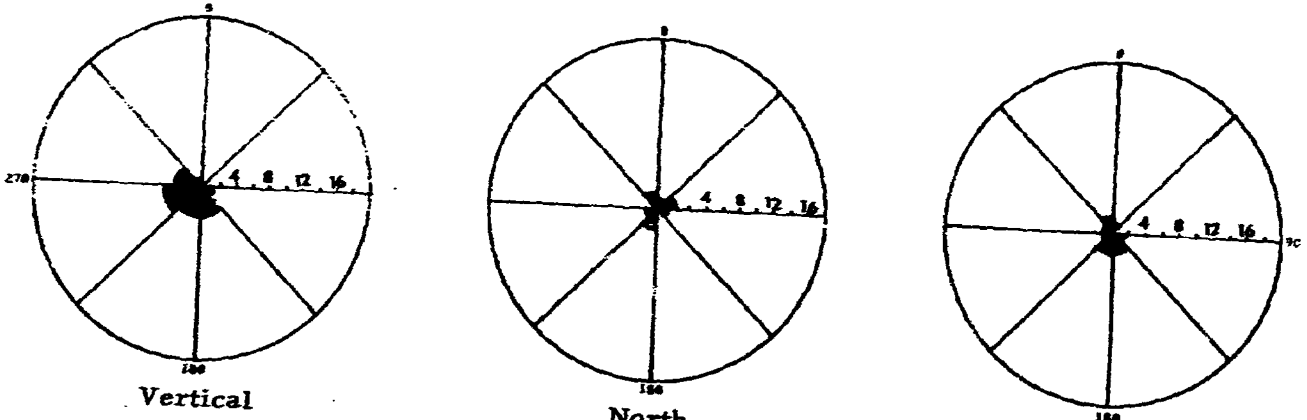

Vertical North East

FIGURE III-12

AZIMUTHAL DISTRIBUTION OF 0.01172 Hz PROPAGATING NOISE WITH PHASE VELOCITIES IN THE RANGE 3.2 - 4.5 KM/SEC.

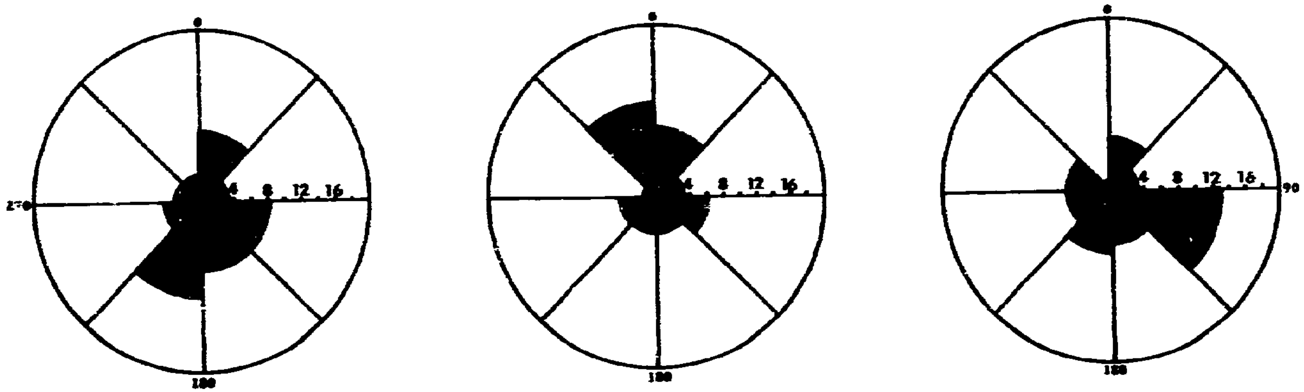

Vertical North East

FIGURE III-13

AZIMUTHAL DISTRIBUTION OF 0.04297 Hz PROPAGATING NOISE
WITH PHASE VELOCITIES IN THE RANGE 3.2 - 4.5 KM/SEC.

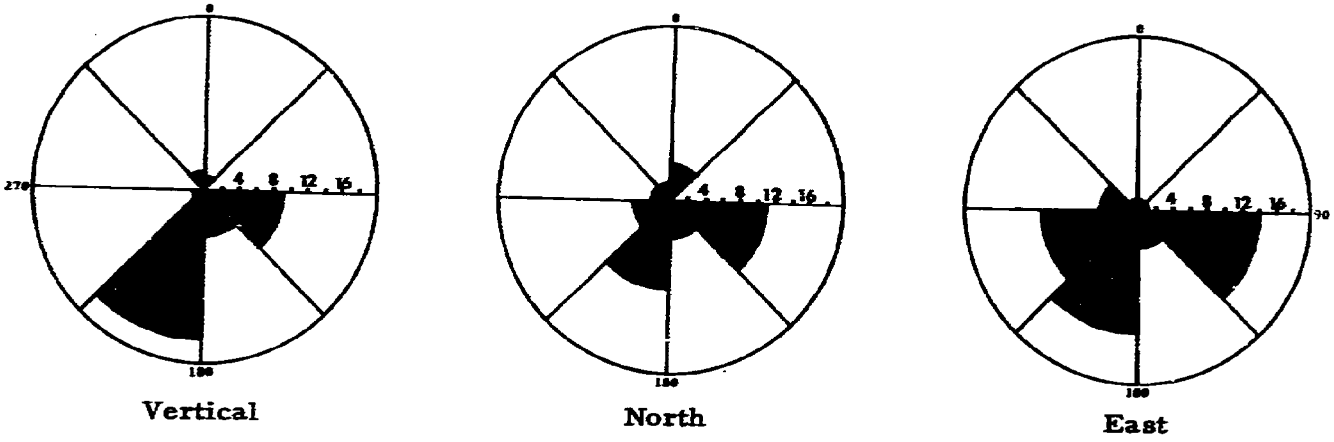

Vertical

North

East

FIGURE III-14

AZIMUTHAL DISTRIBUTION OF 0.05859 Hz PROPAGATING NOISE WITH PHASE VELOCITIES IN THE RANGE 3.2 - 4.5 KM/SEC.

# SECTION IV

# SIGNAL ANALYSIS

## A. DISCUSSION

This section will look at two aspects of signal analysis-gains in signal-to-noise ratio due to beamforming and site-to-site signal similarity. The first aspect is intended to indicate how much better than a single-site station at the same location the array will perform in terms of detection capability. To carry out this study, signal-to-noise ratios were computed for a suite of 100 events which were detected on both the reference site and beam data. The signal-to-noise ratio differences between the reference site data and beam data provide the array gain due to beamforming.

The site-to-site signal similarity computations are intended to describe how much alike a signal recorded at one site is to the same signal recorded at other sites. Local geologic differences from site to site and (unintended) differences in instrumentation can both affect the signal similarity. The less similar the signals are from site to site, the poorer the beamforming process will work, since the dissimilar portions of the signals will add randomly.

## B. SIGNAL-TO-NOISE RATIO GAINS DUE TO BEAMFORMING

When the data recorded at the individual sites of an array are formed into beams, the signal-to-noise ratio of each component is increased due to suppression of noise. In the ideal case, the noise is purely random and is suppressed by a factor approximately equal to the square root of the number of sites used in the beamforming process. In practice, the noise is composed of a random element and a propagating non-random element. This propagating element is suppressed to a lesser degree than the random element, the amount of suppression depending on how far off the beamforming azimuth its azimuth lies and how far from signal velocities is its velocity. Also, the beamforming process suppresses the signal to some extent. This is dependent on how accurate the computed time delays used to time-align the individual traces are and how similar the signals are from site to site. In particular, at some point close to the array, the plane-wave assumption used to compute these time delays must break down.

To obtain an estimate of the signal-to-noise ratio gains to be expected from the beamforming process, a suite of events was selected which were detected on both the reference site and beam traces and contained only noise in the time gate immediately preceding the signal arrival time. The signal-to-noise ratios for all components of the reference site and beam traces were then computed using the equation:

$$S/N\ (\text{dB}) = 20.\ {*}\text{LOG}_{10}\ \frac{\text{zero-peak amplitude}}{\text{RMS noise}}$$

where 'zero-to-peak amplitude' is the amplitude of the largest peak of the signal waveform and 'RMS noise' is measured in the time gate immediately preceding the signal arrival. The gain due to beamforming is then simply the difference between the beam signal-to-noise ratio and the reference site signal-to-noise ratio.

The results in Table IV-1 are grouped on the basis of epicentral distance. The values in the column headed 'optimum gain' were computed from the following equation:

$$\text{Optimum Gain (dB)} = 20.\ {*}\text{LOG}_{10} \sqrt{\text{number of sites}}$$

## TABLE IV-1

## SNR GAINS IN dB DUE TO BEAMFORMING

| Epicentral Distance | No. of Samples | Average No. of Sites | 'Optimum' SNR Gain | Measured SNR Gains | | |
|---|---|---|---|---|---|---|
| | | | | V | T | R |
| 0°-10° | 23 | 4.6 | 6.6 | 2.9 | 2.5 | 0.5 |
| 10°-20° | 23 | 5.4 | 7.4 | 7.8 | 4.8 | 4.6 |
| 20°-40° | 18 | 4.7 | 6.7 | 7.3 | 4.9 | 5.0 |
| 40°-80° | 36 | 5.0 | 7.0 | 6.0 | 4.0 | 3.2 |
| 10°-80° | 77 | 5.0 | 7.0 | 6.9 | 4.4 | 4.0 |

where 'average number of sites' is the average number of sites used in beamforming. This table shows that beamforming gains for all components of events with epicentral distances less than ten degrees are very low. One possible explanation of this is that the plane-wave assumption used in beamforming to compute time delays fails for events with epicenters less than ten degrees from the array. A second possible explanation is that the fixed velocities used in beamforming (3.5 km/sec for Rayleigh, and 4.0 km/sec for Love) are not appropriate for beamforming close events.

The mean gains for the other ranges of epicentral distances remain fairly constant. This implies that the plane-wave assumption holds for events with epicentral distances greater than ten degrees.

Comparing the mean gains in Table IV-1 with the corresponding optimum gains, the data show that in general the mean gains for the horizontal components are lower than the optimum gains. This implies that some of the noise is propagating, since, as was described earlier, propagating noise is suppressed by beamforming to a lesser degree than is random noise.

An interesting feature of the data in Table IV-1 is that the radial component gains are lower than the vertical component gains. In Table IV-2 the signal-to-noise ratio gains are separated into the signal-to-noise gain due to RMS noise suppression and the signal-to-noise ratio loss due to peak signal suppression. From the data in this table it appears that the difference in signal-to-noise ratio gain between the vertical and radial components is due roughly equally to both lower RMS noise suppression and greater signal suppression on the radial component. The lower RMS noise suppression on the radial component in conjunction with lower RMS noise suppression on the transverse component relative to the vertical component implies that there is more propagating noise on the horizontal components than on the vertical components and that this noise is propagating as both Love and Rayleigh waves.

## TABLE IV-2

## NOISE AND SIGNAL SUPPRESSION IN dB DUE TO BEAMFORMING

| Epicentral Distance | RMS Noise Suppression | | | Peak Signal Suppression | | |
|---|---|---|---|---|---|---|
| | V | T | R | V | T | R |
| 0°-10° | 6.5 | 5.0 | 5.0 | 3.5 | 2.5 | 4.5 |
| 10°-20° | 8.8 | 5.8 | 7.1 | 1.0 | 1.0 | 2.5 |
| 20°-40° | 7.5 | 6.0 | 6.5 | 0.2 | 1.1 | 1.5 |
| 40°-80° | 6.6 | 5.0 | 5.6 | 0.6 | 1.0 | 2.4 |
| 10°-80° | 7.5 | 5.4 | 6.2 | 0.6 | 1.0 | 2.2 |

## C. SITE-TO-SITE SIGNAL SIMILARITY

The program used to measure site-to-site signal similarity requires as its input the edited time-domain data in the recorded vertical, north, east configuration. The program computes beamsteer time delays for each propagation mode by the equation:

$$D_i = \frac{(X_r - X_i)\sin\theta + (Y_r - Y_i)\cos\theta}{V}$$

where: $D_i$ is the time delay for site i

$X_r$ and $Y_r$ are the X and Y coordinates of the reference site

$X_i$ and $Y_i$ are the X and Y coordinates of the data site i

$\theta$ is the beamsteer azimuth, and

V is the velocity of the propagation mode.

The time delay, or lag, is considered to be negative if the signal arrives at data site i before it arrives at the reference site and positive if it arrives at the data site i after it arrives at the reference site.

The data at the various sites next have their trace means removed and are rotated to the beamsteer azimuth. Following this, the reference site zero-lag autocorrelation values are computed from:

$$\phi_{rr}(0) = \frac{1}{N}\sum_{k=1}^{N} X_r(k)X_r(k)$$

where $X_r(k)$ represents the reference site time series of N points sampled at $\Delta t$ intervals. Correlation processing then continues for the data sites. The zero-lag autocorrelation $\phi_{ii}(0)$ is first computed. The cross-correlation functions $\phi_{ri}(\tau\Delta t)$ are next computed in the user-specified range for each lag $\tau$. The zero-lag center point of the range of lags for a site is the beamsteer lag for that site. The cross-correlation function for each site i at a lag $\tau$ is computed using

$$\Phi_{ri}(\tau\Delta t) = \frac{1}{N} \sum_{k=1}^{N} X_r(k)\, X_i(k+\tau\Delta t) \, .$$

After the autocorrelation values and cross-correlation functions are computed for each mode-component combination at each site, the cross-correlation matrix is searched for its maximum values and corresponding lags. For each combination the correlation coefficient is computed according to

$$CC_{ri} = \frac{\Phi_{ri}(\Delta)}{\left[\Phi_{rr}(0)\,\Phi_{ii}(0)\right]^{1/2}}$$

where $\Delta$ is the lag at which $\Phi_{ri}(\tau\Delta t)$ is a maximum and $CC_{ri}$ is the correlation coefficient for the reference site and data site i. Correlation coefficient means are computed after all sites are processed.

Site-to-site signal similarity was investigated for each component by generating correlation coefficients between the reference site and the remaining six sites for a suite of large events. The results of computing correlation coefficients for 22 events ranging in bodywave magnitude from 4.7 to 6.3 and one typical noise sample are shown in Tables IV-3 to IV-5 for the vertical, transverse, and radial components of motion, respectively. Included in each table are the correlation coefficient for each site-event, the signal-to-noise ratio of the reference site data for each event, the average correlation coefficient for each event, and the correlation coefficient for each site averaged over all events. A dash indicates that data for that site-event were either not available or were not suitable for processing. No signal-to-noise ratio is listed for events whose noise gates contained other signals or spikes. Since no plane-wave anomalies were observed, cross-correlation

## TABLE IV-3

## CORRELATION COEFFICIENTS FOR VERTICAL COMPONENT

| Event Number | Reference Site S/N (dB) | 2 | 3 | 4 | 5 | 6 | 7 | Event Average Correlation Coefficient |
|---|---|---|---|---|---|---|---|---|
| 0766 | 36.2 | 0.80 | ---- | 0.83 | 0.65 | 0.80 | 0.95 | 0.81 |
| 0790 | 32.8 | ---- | ---- | 0.76 | 0.83 | 0.84 | 0.85 | 0.82 |
| 0824 | 19.6 | 0.54 | ---- | 0.56 | 0.65 | 0.77 | 0.20 | 0.53 |
| 0885 | ---- | 0.99 | ---- | ---- | 0.95 | 0.95 | 0.95 | 0.96 |
| 0886 | 60.2 | 0.84 | ---- | 0.82 | 0.82 | 0.93 | 0.78 | 0.84 |
| 0890 | 36.7 | 0.89 | ---- | 0.84 | 0.87 | 0.94 | 0.81 | 0.87 |
| 0900 | 38.0 | 0.84 | ---- | 0.84 | 0.80 | 0.95 | 0.78 | 0.84 |
| 1265 | ---- | 0.51 | ---- | 0.75 | 0.71 | ---- | 0.33 | 0.57 |
| 1295 | 31.4 | 0.93 | ---- | 0.90 | 0.93 | 0.91 | 0.89 | 0.91 |
| 1296 | 74.4 | 0.81 | ---- | 0.58 | 0.74 | 0.86 | 0.92 | 0.78 |
| 1321 | 45.1 | 0.86 | ---- | ---- | ---- | 0.84 | 0.81 | 0.83 |
| 1331 | 55.1 | 0.80 | ---- | ---- | ---- | 0.88 | 0.70 | 0.79 |
| 1395 | 34.9 | 0.85 | ---- | ---- | 0.77 | 0.90 | 0.91 | 0.86 |
| 1406 | 39.5 | 0.85 | 0.92 | ---- | 0.94 | 0.95 | 0.82 | 0.90 |
| 1413 | 50.4 | 0.91 | 0.96 | ---- | 0.92 | ---- | 0.87 | 0.91 |
| 1524 | 56.2 | 0.86 | 0.90 | 0.78 | ---- | 0.91 | ---- | 0.86 |
| 1544 | 33.9 | 0.92 | 0.95 | ---- | ---- | ---- | 0.82 | 0.90 |
| 1555 | 35.4 | 0.84 | 0.85 | ---- | 0.78 | 0.89 | 0.64 | 0.80 |
| 1574 | 30.5 | 0.76 | 0.87 | ---- | ---- | 0.82 | 0.62 | 0.77 |
| 1621 | 54.4 | ---- | 0.88 | 0.83 | ---- | ---- | 0.72 | 0.81 |
| 1625 | 33.1 | ---- | ---- | 0.87 | 0.84 | 0.91 | 0.78 | 0.85 |
| 1628 | 31.8 | ---- | ---- | 0.82 | 0.94 | 0.75 | ---- | 0.83 |
| Day 170 (1976) Noise Sample | ---- | 0.26 | ---- | -0.17 | -0.15 | -0.14 | -0.19 | -0.08 |
| Site Average (Excluding Events 824 and 1265) | ---- | 0.86 | 0.90 | 0.81 | 0.84 | 0.88 | 0.81 | ---- |

## TABLE IV-4

## CORRELATION COEFFICIENTS FOR TRANSVERSE COMPONENT

| Event Number | Reference Site S/N (dB) | 2 | 3 | 4 | 5 | 6 | 7 | Event Average Correlation Coefficient |
|---|---|---|---|---|---|---|---|---|
| 0766 | 41.3 | 0.81 | ---- | 0.87 | 0.89 | 0.96 | 0.92 | 0.89 |
| 0790 | 38.7 | ---- | ---- | 0.75 | 0.86 | 0.94 | 0.95 | 0.88 |
| 0824 | 22.0 | 0.71 | ---- | 0.54 | 0.65 | 0.78 | 0.62 | 0.66 |
| 0885 | ---- | 0.82 | ---- | ---- | 0.86 | 0.95 | 0.79 | 0.86 |
| 0886 | 47.1 | 0.81 | ---- | 0.81 | 0.80 | 0.97 | 0.82 | 0.84 |
| 0890 | 36.7 | 0.89 | ---- | 0.84 | 0.87 | 0.96 | 0.88 | 0.89 |
| 0900 | 41.5 | 0.82 | ---- | 0.75 | 0.76 | 0.94 | 0.82 | 0.82 |
| 1265 | ---- | 0.57 | ---- | 0.62 | 0.55 | ---- | 0.60 | 0.58 |
| 1295 | 37.0 | 0.92 | ---- | 0.76 | 0.92 | 0.84 | 0.86 | 0.86 |
| 1296 | 68.3 | 0.85 | ---- | 0.81 | 0.84 | 0.89 | 0.85 | 0.85 |
| 1321 | 50.4 | 0.94 | ---- | ---- | ---- | 0.96 | 0.94 | 0.95 |
| 1331 | 45.6 | 0.85 | ---- | ---- | ---- | 0.93 | 0.83 | 0.87 |
| 1395 | 39.0 | 0.78 | ---- | ---- | 0.88 | 0.93 | 0.88 | 0.87 |
| 1406 | 36.3 | 0.72 | 0.89 | ---- | 0.68 | 0.89 | 0.66 | 0.77 |
| 1413 | 47.0 | 0.93 | 0.96 | ---- | 0.91 | ---- | 0.89 | 0.92 |
| 1524 | 57.5 | 0.85 | 0.89 | 0.86 | ---- | 0.91 | ---- | 0.88 |
| 1544 | 45.1 | 0.97 | 0.86 | ---- | ---- | ---- | 0.95 | 0.92 |
| 1555 | 30.4 | 0.87 | 0.87 | ---- | 0.82 | 0.92 | 0.96 | 0.97 |
| 1574 | 49.9 | 0.97 | 0.98 | ---- | ---- | 0.98 | 0.80 | 0.86 |
| 1621 | 60.3 | ---- | 0.97 | 0.87 | ---- | ---- | 0.92 | 0.92 |
| 1625 | 28.8 | ---- | ---- | 0.65 | 0.68 | 0.93 | 0.72 | 0.74 |
| 1628 | 34.2 | ---- | ---- | 0.75 | 0.95 | 0.58 | ---- | 0.76 |
| Day 170 (1976) Noise Sample | ---- | 0.10 | ---- | 0.06 | -0.14 | 0.21 | 0.21 | 0.09 |
| Site Average (Excluding Events 824 and 1265) | ---- | 0.86 | 0.92 | 0.79 | 0.84 | 0.91 | 0.86 | ---- |

## TABLE IV-5

## CORRELATION COEFFICIENTS FOR THE RADIAL COMPONENT

| Event Number | Reference Site S/N (dB) | 2 | 3 | 4 | 5 | 6 | 7 | Event Average Correlation Coefficient |
|---|---|---|---|---|---|---|---|---|
| 0766 | 33.9 | 0.78 | ---- | 0.76 | 0.74 | 0.75 | 0.89 | 0.78 |
| 0790 | 36.5 | ---- | ---- | 0.73 | 0.72 | 0.83 | 0.91 | 0.80 |
| 0824 | 23.6 | 0.70 | ---- | 0.55 | 0.66 | 0.75 | 0.57 | 0.65 |
| 0885 | ---- | 0.99 | ---- | ---- | 0.95 | 0.94 | 0.94 | 0.95 |
| 0886 | 50.3 | 0.79 | ---- | 0.82 | 0.79 | 0.87 | 0.74 | 0.80 |
| 0890 | 34.5 | 0.85 | ---- | 0.85 | 0.83 | 0.91 | 0.78 | 0.84 |
| 0900 | 37.4 | 0.76 | ---- | 0.81 | 0.74 | 0.93 | 0.69 | 0.79 |
| 1265 | ---- | 0.59 | ---- | 0.69 | 0.72 | ---- | 0.53 | 0.63 |
| 1295 | 34.3 | 0.82 | ---- | 0.75 | 0.91 | 0.82 | 0.86 | 0.83 |
| 1296 | 73.3 | 0.80 | ---- | 0.47 | 0.63 | 0.77 | 0.76 | 0.69 |
| 1321 | 49.2 | 0.84 | ---- | ---- | ---- | 0.78 | 0.66 | 0.76 |
| 1331 | 47.2 | 0.82 | ---- | ---- | ---- | 0.83 | 0.68 | 0.78 |
| 1395 | 36.2 | 0.56 | ---- | ---- | 0.58 | 0.68 | 0.89 | 0.68 |
| 1406 | 37.7 | 0.86 | 0.86 | ---- | 0.87 | 0.90 | 0.85 | 0.87 |
| 1413 | 50.7 | 0.92 | 0.94 | ---- | 0.85 | ---- | 0.90 | 0.90 |
| 1524 | 56.4 | 0.67 | 0.84 | 0.74 | ---- | 0.87 | ---- | 0.78 |
| 1544 | 38.2 | 0.78 | 0.93 | ---- | ---- | ---- | 0.69 | 0.80 |
| 1555 | 39.0 | 0.82 | 0.79 | ---- | 0.65 | 0.79 | 0.68 | 0.74 |
| 1574 | 38.2 | 0.41 | 0.60 | ---- | ---- | 0.77 | 0.42 | 0.55 |
| 1621 | 53.5 | ---- | 0.87 | 0.77 | ---- | ---- | 0.50 | 0.71 |
| 1625 | 32.8 | ---- | ---- | 0.80 | 0.73 | 0.93 | 0.69 | 0.79 |
| 1628 | 32.5 | ---- | ---- | 0.74 | 0.93 | 0.81 | ---- | 0.83 |
| Day 170 (1976) Noise Sample | ---- | -0.18 | ---- | 0.17 | -0.17 | 0.21 | 0.20 | 0.05 |
| Site Average (Excluding Events 824 and 1265) | ---- | 0.78 | 0.83 | 0.75 | 0.78 | 0.83 | 0.75 | ---- |

lag data are omitted. The data in these tables are interpreted from the standpoint that a correlation coefficient of 1 computed using data recorded at the reference site and data site i would indicate that the waveforms at these sites are identical, a correlation coefficient of zero would indicate that the waveforms at these sites are wholly unlike each other, and a correlation coefficient of -1 would indicate that the waveforms at these sites differ by a phase shift of 180°.

The following points should be noted from this data:

- Events with low correlation coefficients were reprocessed using site 2 as reference to determine if site 1 was producing anamolous values. The results were not significantly different.
- The low correlation coefficients for event 824 appear to be a result of low signal-to-noise ratio. Note that this event has the lowest signal-to-noise ratio of the suite of events.
- Event 1265 also displayed low correlation coefficients. Plots of the raw data of this event showed the data to be corrupted with high frequency noise. Examination of the field tape logs for this time period revealed that transmission errors occurred during the recording of this event.
- The transverse component yielded larger correlation coefficients than either the vertical or radial components, being greater than 0.8 for all large events.
- The radial component yielded on average the lowest correlation coefficients. This is perhaps reflected in the results of peak signal suppression due to beamforming the radial component as shown in Table IV-2.

- Overall, sites 3 and 6 yield better correlation coefficients with the reference site than do the other sites. Site 4 on the average, yields the lowest correlation coefficients.
- As expected, the noise sample yielded very low correlation coefficients.
- The peak signal suppressions noted in Table IV-2 appear to be reflected by the less than perfect site-to-site similarities.

# SECTION V
# ILPA DETECTION CAPABILITY

## A. DISCUSSION

In past evaluation tasks, detection statistics were derived from an event population for every member of which a clear detection/non-detection decision could be made; i.e., the analyst could state that he either saw the sought-for signal or he saw seismic noise. Unfortunately, the world does not always present the analyst with such a clear-cut case. Mixed events, system failures resulting in no data being recorded, and malfunctions all tend to obscure the detection capability picture.

The term 'mixed event' refers to the case where the sought-for signal is obscured or completely masked by a second signal. This can happen either when the two signals arrive at the station at essentially the same time or when a larger signal arrives before the signal under analysis, burying this signal in its coda. The term 'system failure' refers to the total shutting down of the station so that no data is recorded. The term 'malfunction' refers to any partial failure of the system, from sensor unit to reception of data at the Seismic Data Analysis Center, which causes degradation of the seismic data.

The problem of mixed events is often difficult for the analyst to resolve and is probably the major source of false alarms. (The term 'false alarm' in this context means declaring a detection when in fact the observed signal is from an event other than that under analysis.) When a signal is observed in the time gate of the event under analysis, the analyst first checks the waveforms on the three components of motion to see that their inter-relationships are correct. If still in doubt, the analyst checks available event lists to see whether any other reported event could have arrived in the signal gate. In general, the analyst declares a detection if a dispersed signal is observed having the correct inter-relationships between the Love and Rayleigh waves and if no other event has been reported which could be mistaken for the event under analysis.

Since mixed events and (secondarily) events for which no data were recorded or which contained malfunctions are a fairly common problem, the Iranian Long-Period Array detection capability estimates are calculated in two ways. The first of these is termed the absolute detection capability estimate. When computing this estimate, all mixed events, events for which no data were recorded, and events containing malfunctions are counted as non-detections when forming the detection statistics. This approach gives a real-world detection capability estimate.

The second of these estimates is termed the conditional detection capability estimate. When computing this estimate, all mixed events, events for which no data were recorded, and events containing malfunctions are rejected from the detection statistics. This approach gives an ideal detection capability estimate. The value of this ideal estimate is that it shows the detection capability improvement possible if the reliability of the instrumentation can be improved and if methods of separating mixed events can be found.

The number used to represent detection capability is the 50 percent detection threshold, denoted by '$m_{b50}$'. The 50 percent detection threshold is the bodywave magnitude for which the probability of detection is 0.5. It is computed by fitting the Gaussian probability function to the detection statistics by a maximum likelihood method (Ringdal, 1974). Hereafter, this will be referred to as the maximum likelihood curve.

It must be kept in mind that, since the data base was derived from the NORSAR and NEIS event bulletins, all detection capability estimates are in terms of a combined 'NORSAR - NEIS' $m_b$ unit. This fact is important, since NORSAR $m_b$ units are not the same as those from the National Earthquake Information Service (NEIS) event lists.

Depending on the quantity of data available, one of three levels of confidence is placed on each 50 percent detection threshold. If a 50 percent detection threshold is given to two decimal places (e.g., $m_{b50} = 4.56$), sufficient detection statistics were available to compute a reliable detection capability estimate. If a 50 percent detection threshold is enclosed in parentheses and given to only one decimal place, (e.g., $m_{b50} = (4.6)$) the detection statistics were sparse and the detection capability estimate can be considered to be only a first approximation. Finally, if a 50 percent detection threshold is expressed as greater than some value (e.g., $m_b > 5.0$), the detection statistics were too sparse to allow fitting of a maximum likelihood curve. In most cases, this is due to a lack of detected events. When this occurred, the value given is the $m_b$ of the largest non-detected event.

## B. ILPA LONG-PERIOD DETECTION CAPABILITY ESTIMATES

This subsection examines the estimates of detection capability made from the accumulated detection statistics for the reference site and beam data. The criteria used by the analyst which determine whether an event was detected are:

- The presence of dispersion in the signal gate.
- A peak in the dispersed wavetrain 3 dB or more above any peak outside the dispersed wavetrain and inside a time gate starting 600 seconds before the predicted Love wave arrival time and ending 600 seconds after the estimated Rayleigh wave end time.
- Occurrence of signal onset within ±180 seconds of the predicted signal onset time.

- Detection of the signal on at least two of the three components of motion.

These criteria were used as a guide to aid the analyst in determining the detection status of processed events. The first criterion was always followed for the events processed in this evaluation, since this is the primary visual difference between seismic signals and noise. The second criterion was occasionally disregarded, since bodywaves such as SS or isolated noise pulses would be at times visible within the specified time gate. If the event under analysis was visible, it was declared detected even if one of these was also visible. The third criterion was also occasionally not followed. When a waveform in the signal gate was observed to arrive later than this criterion allowed, the event lists were checked to ensure that this waveform was not due to some other event. If no other event could be found whose surface waves would arrive at the observed arrival time, the event under analysis was called a detection. The last criterion was rigidly followed, since it was imposed to reduce the probability of erroneously declaring an event to be detected.

The various detection capability estimates made for this evaluation are shown in Figures V-1 to V-4. Each 'sub-figure' of these figures consists of two parts. The upper part consists of a histogram showing the number of detected and non-detected events as a function of body-wave magnitude ($m_b$) for the particular data subset under consideration. The lower part shows the detection probability derived from these detection statistics as a function of bodywave magnitude. The percentage of events detected at each $m_b$ value is represented by an asterisk. The maximum likelihood curve fitted to these detection percentages is represented by a solid line. The 90 percent confidence limits of this curve are represented by dashed lines. The values for 'MB50' and 'MB90' shown on the figures represent the 50 and 90 percent detection thresholds respectively, as determined by the

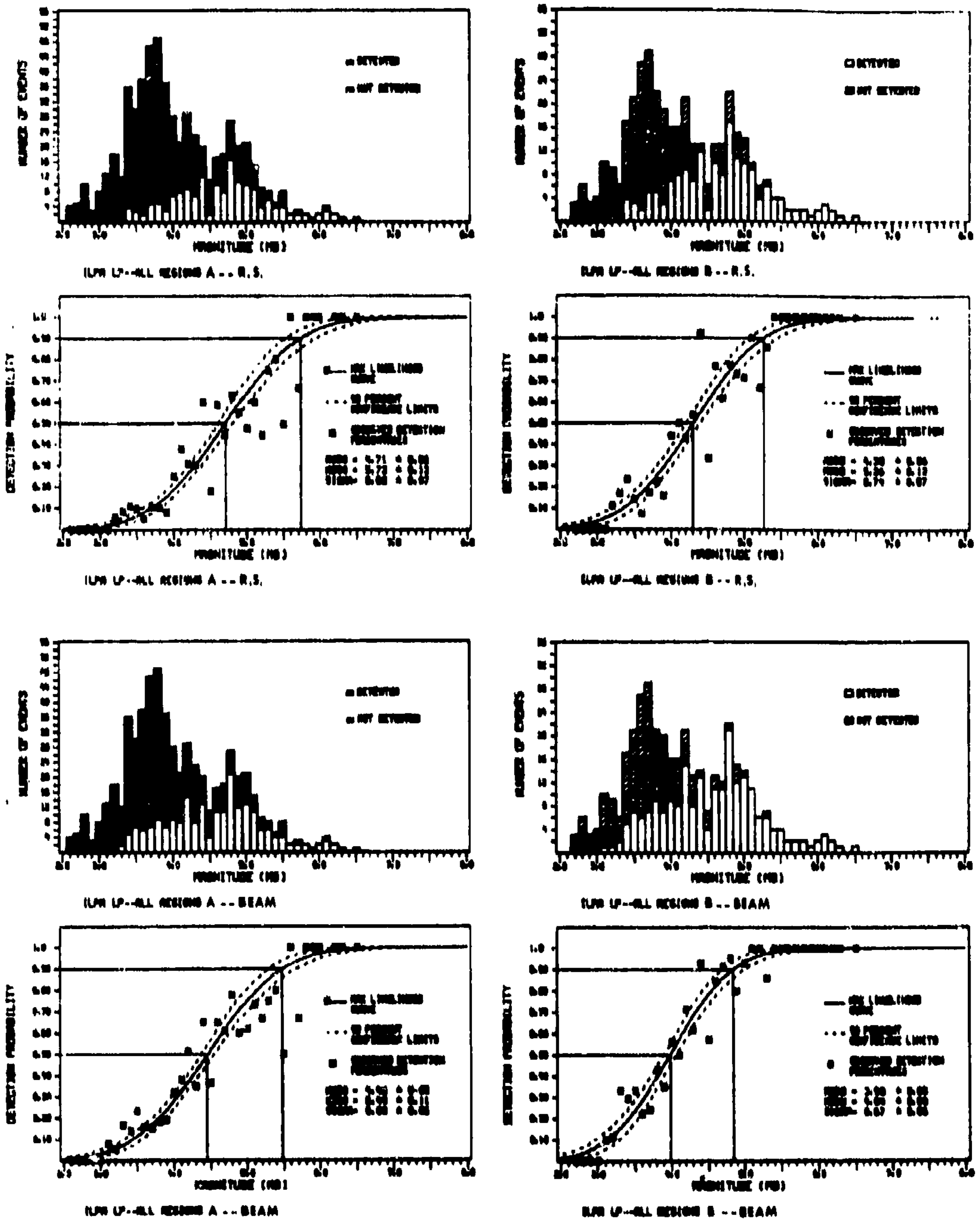

FIGURE V-1

ILPA LONG-PERIOD REFERENCE SITE AND
BEAM DETECTION STATISTICS
ALL REGIONS A AND B

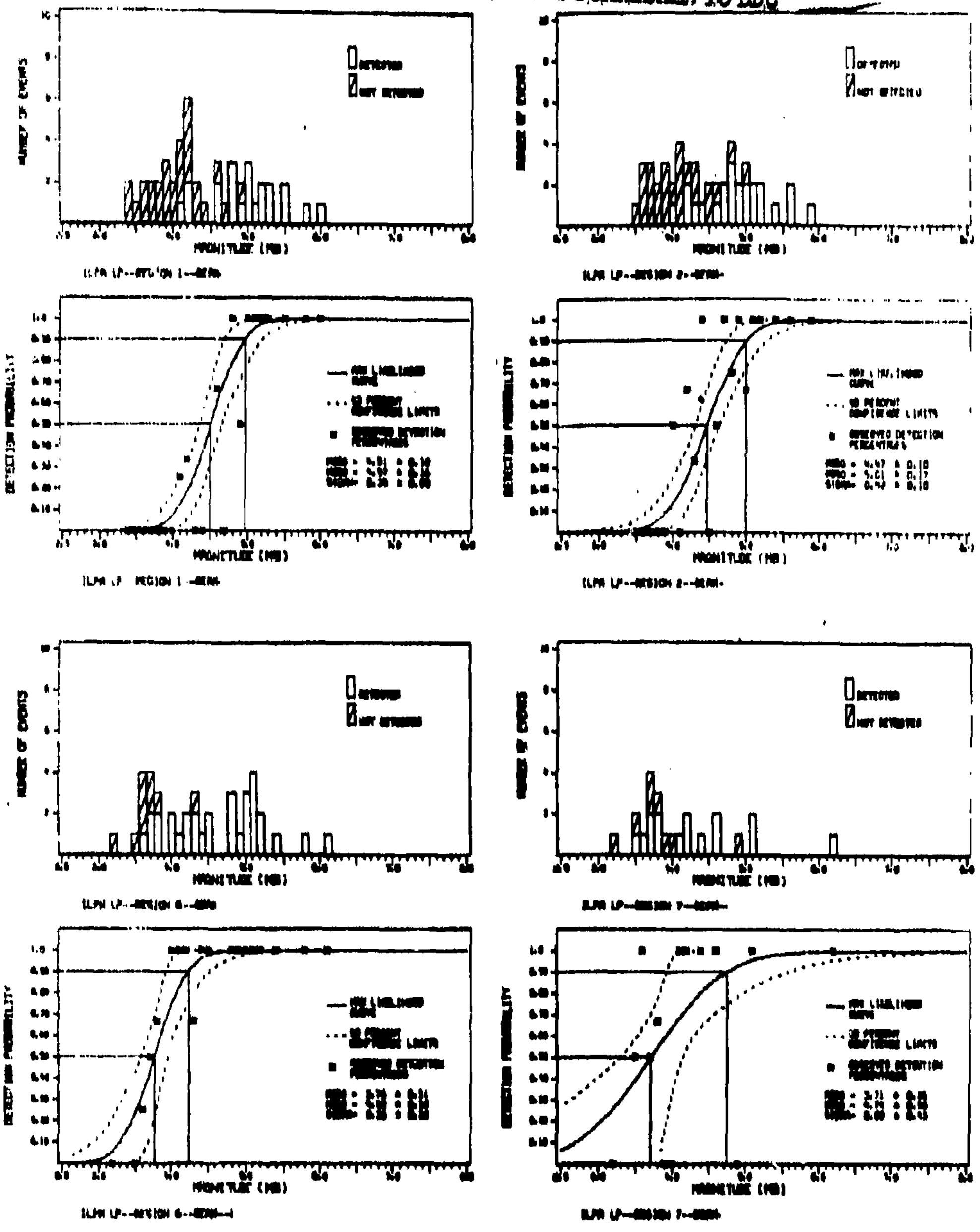

FIGURE V-2

ILPA LONG PERIOD BEAM DETECTION STATISTICS
REGIONS 1, 2, 6, AND 7

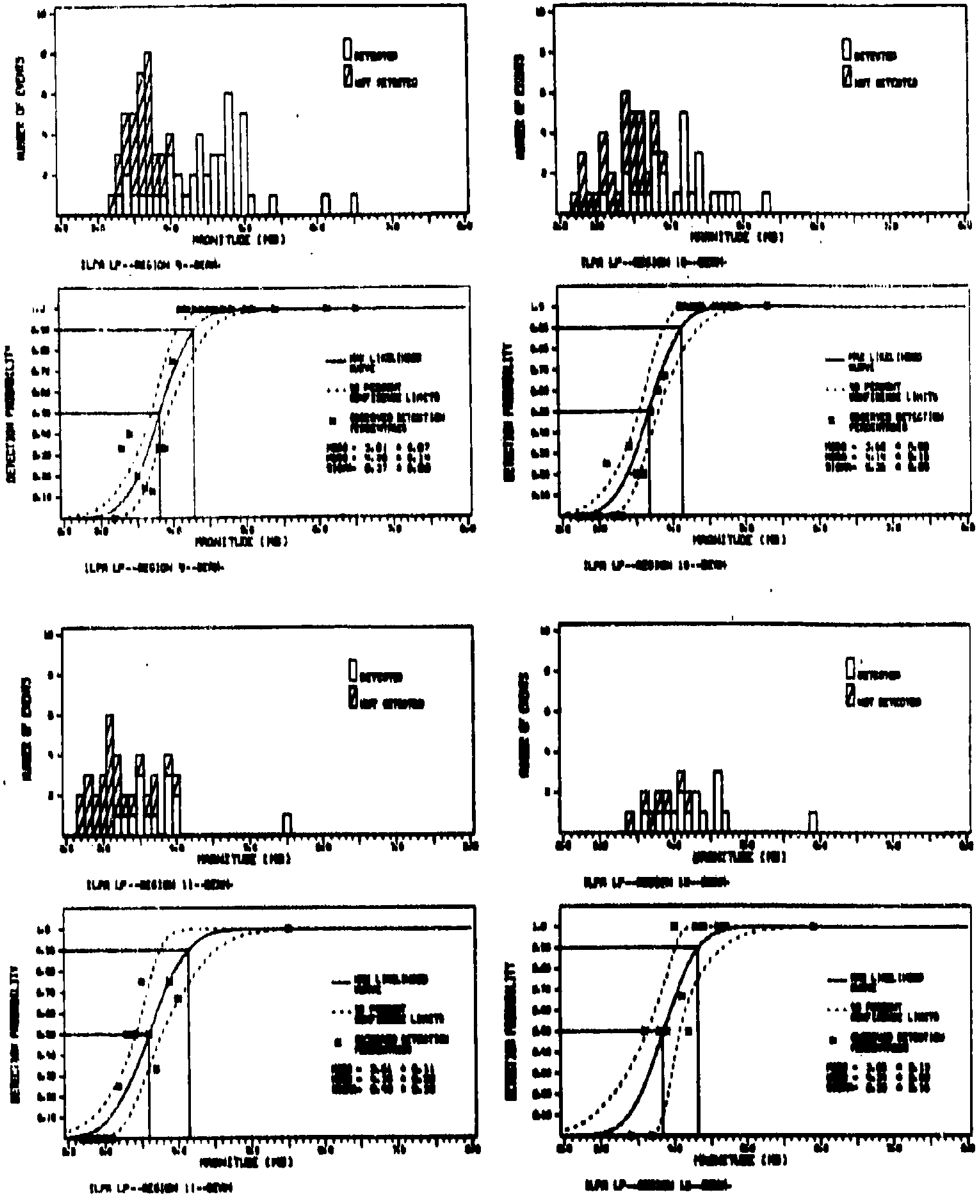

FIGURE V-3

ILPA LONG-PERIOD BEAM DETECTION STATISTICS
REGIONS 9, 10, 11, AND 12

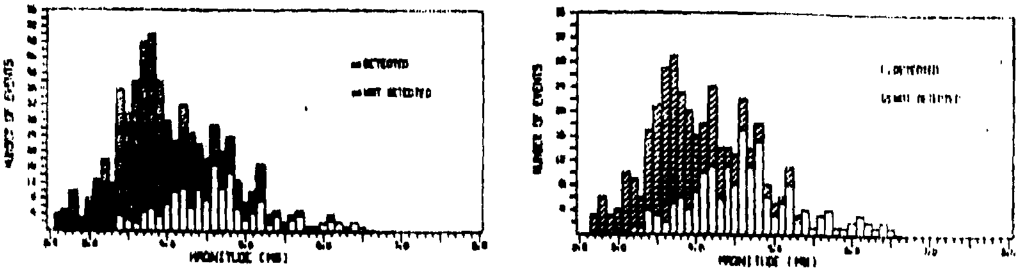

ILPA LP--ALL REGIONS A - R.S. NOR MB

ILPA LP--ALL REGIONS B - R.S. NOR MB

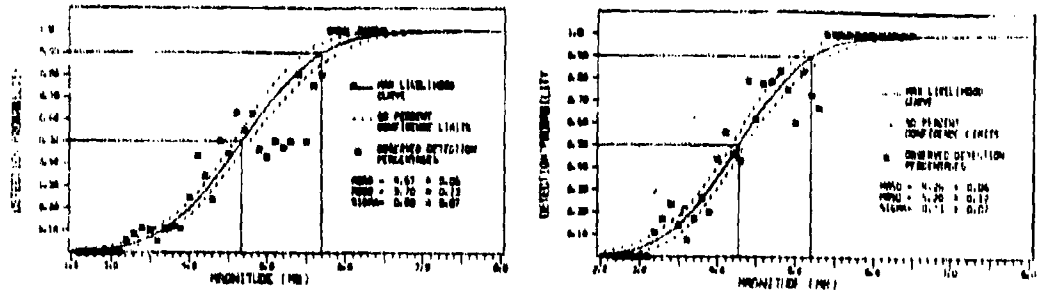

ILPA LP--ALL REGIONS A - R.S. NOR MB

ILPA LP--ALL REGIONS B - R.S. NOR MB

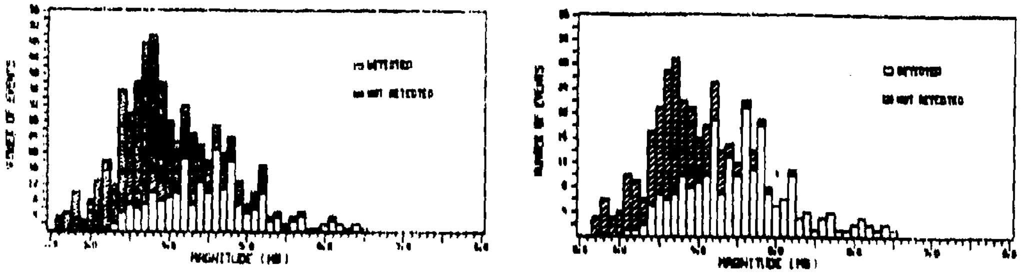

ILPA LP--ALL REGIONS A - BEAM NOR MB

ILPA LP--ALL REGIONS B - BEAM NOR MB

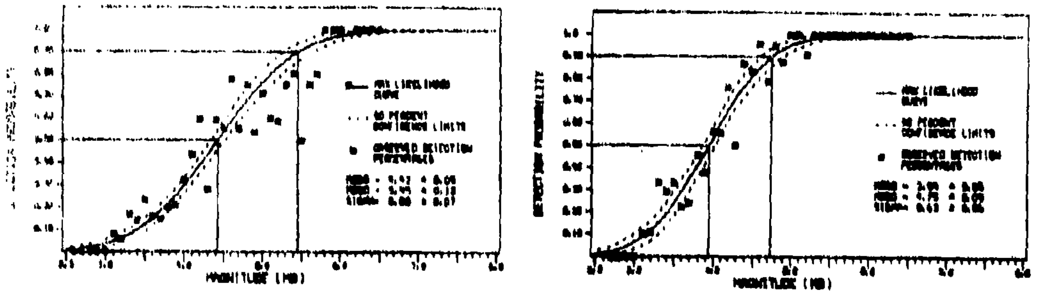

ILPA LP--ALL REGIONS A - BEAM NOR MB

ILPA LP--ALL REGIONS B - BEAM NOR MB

FIGURE V-4

ILPA LONG-PERIOD REFERENCE SITE AND
BEAM DETECTION STATISTICS
ALL REGIONS A AND B
(NORSAR $m_b$ VALUES)

maximum likelihood curve. Finally, the value given for 'SIGMA' is the standard deviation of the Gaussian probability function for the maximum likelihood curve.

Figure V-1 presents the reference site and beam detection capability estimates using the detection statistics of all the regions. These were made in two ways. In the first, denoted by 'ALL REGIONS A', mixed events, events for which no data were recorded, and events containing malfunctions were counted as non-detections. This forms the previously defined absolute detection capability estimate. In the second, denoted by 'ALL REGIONS B', mixed events, events for which no data were recorded, and events containing malfunctions were rejected from the detection statistics. This forms the previously defined conditional detection capability estimate.

Figures V-2 and V-3 show the detection capability estimates for the beam data on a regionalized basis. These estimates are conditional detection capability estimates. The paucity of detection statistics makes these regionalized estimates valid as first approximations only.

The detection statistics of Figures V-1 to V-3 were derived from earthquakes whose event parameters were taken from either the NORSAR or the NEIS event bulletins. Since the two event bulletins partially overlap in the time frame each covers, it was possible to compare the $m_b$ values that each reports. A total of 518 Eurasian events were found to be reported by both event bulletins. By fitting a straight line to the NORSAR $m_b$ - NEIS $m_b$ pairs so found, using an algorithm which treats neither variable as dependent, the following relationship between the two types of $m_b$ was derived:

$$\text{NORSAR}\, m_b = 1.11\ \text{NEIS}\, m_b - 0.71 \qquad (\text{variance} = 0.03).$$

Figure V-4 was formed by converting all NEIS-reported $m_b$ values in the data base to NORSAR $m_b$ values using the above relationship. Like Figure V-1, this figure shows the single-site and beam detection capability estimates using 'ALL REGIONS A' and 'ALL REGIONS B' detection statistics. The purpose of this is to estimate the effects of the $m_b$ conversion on the detection capability estimates.

The various detection capability estimates are summarized in Table V-1. Since the prime purpose of this section is to estimate the array detection capability, no regionalized reference site detection capability estimates were made. The following points should be noted from the data presented in Table V-1:

- Mixed events, events for which no data were recorded, and malfunctions raised the 50 percent detection threshold by 0.4 - 0.5 $m_b$ units.
- The beamforming process lowered the 50 percent detection threshold by 0.25 - 0.30 $m_b$ units.
- The conversion of NEIS $m_b$ values to NORSAR $m_b$ values had essentially no effect on the ILPA detection capability.
- The regionalized ILPA detection capability estimates can be considered as first approximations only, due to the limited detection statistics available.

It should be noted that, although the conversion of NEIS $m_b$ values to NORSAR $m_b$ values had essentially no effect on these detection capability estimates, the authors feel that in any future work this matter should be considered again. For the data base used in this report, the ratio of NORSAR events to NEIS events was approximately 4 to 1. Future increases in the data base will raise the number of NEIS events in the data base (since the NORSAR event bulletin ceased being issued 30 September 1976) and hence will increase the relative effect of NEIS $m_b$ values on the detection capability estimates.

## TABLE V-1

## ILPA LONG-PERIOD DETECTION CAPABILITY

| Region | NORSAR & NEIS $m_b$'s |  | NORSAR $m_b$'s |  | Mean Distance in Degrees |
|---|---|---|---|---|---|
|  | Reference | Beam | Reference | Beam |  |
| All Regions A | 4.71 | 4.46 | 4.67 | 4.42 | 36.5 |
| All Regions B | 4.30 | 3.98 | 4.26 | 3.94 |  |
| 1 | ---- | (4.5) | ---- | (4.5) | 71.8 |
| 2 | ---- | (4.5) | ---- | (4.4) | 69.6 |
| 5 | ---- | >4.0 | ---- | >4.3 | 40.7 |
| 6 | ---- | (3.8) | ---- | (3.7) | 36.9 |
| 7 | ---- | (3.7) | ---- | (3.7) | 31.6 |
| 9 | ---- | (3.8) | ---- | (3.8) | 8.6 |
| 10 | ---- | (3.7) | ---- | (3.7) | 17.2 |
| 11 | ---- | (3.6) | ---- | (3.6) | 24.7 |
| 12 | ---- | (3.8) | ---- | (3.8) | 53.9 |

Note:

1. Detection capability is estimated in terms of the 50 percent detection threshold.
2. All Regions A - Mixed, no data recorded, and malfunctions are counted as non-detections.
3. All Regions B - Mixed, no data recorded, and malfunctions are rejected from detection statistics.

# SECTION VI

# EARTHQUAKE-PRESUMED EXPLOSION DISCRIMINATION

## A. DISCUSSION

This section considers the question of discriminating between earthquakes and presumed nuclear explosions using long-period data. The discrimination method used is the surface-wave magnitude ($M_s$) versus bodywave magnitude ($m_b$) plot. This plot of $M_s$ versus $m_b$ is expected to function as an earthquake-presumed nuclear explosion discriminant since, for a given $m_b$, an explosion generates much lower Rayleigh and Love waves than does an earthquake. (Theoretically, an explosion should generate no Love waves, since the source is completely compressional. However, some Love wave energy is radiated from tectonic strain release (Sun, 1977) subsequent to the explosion.) Therefore, a plot of $M_s$ versus $m_b$ can be expected to show a separation of the data points into an earthquake population and an explosion population.

The data base for this discrimination study is comprised of all events which were visually detected on bandpass-filtered (0.023 - 0.059 Hz passband) plots.

## B. COMPUTATION OF SURFACE WAVE MAGNITUDES

In earlier evaluation tasks, the signal amplitude and period values used in computing surface wave magnitudes ($M_s$) were measured manually on the filtered signal plots at various periods. The computation of $M_s$ then used the equation:

$$M_s = \mathrm{LOG}_{10}\left[\frac{A*SF}{T*Q*G}\right] = \mathrm{LOG}_{10}\Delta + 1.12$$

where: $A$ = peak-to-peak amplitude measured in inches on the plot.

$SF$ = plot scale factor in computer counts per inch.

$T$ = period in seconds of the measured amplitude.

$Q$ = quantization factor ( 20.951 computer counts per millimicron).

$G$ = instrument response correction factor, and

$\Delta$ = epicentral distance in degrees.

This approach has several disadvantages. First, the analyst is apt to have difficulties finding the largest peak at each desired period - it is sometimes necessary to measure the periods of a number of waveforms before finding the desired period. Next, having found the waveform for which $M_s$ is to be measured, the analyst may make a measurement error. Finally, errors are apt to occur either in transcribing the measured values or in calculating the surface-wave magnitude from these values.

In order to avoid these problems and make the process of obtaining $M_s$ values less tiresome, a program was written to perform the measurements and calculations automatically. This program operates by first finding the times of all zero crossings in a given time gate and the maximum absolute amplitude in millimicrons between each pair of adjacent zero crossings. The waveform period is then simply:

$$T = 2*[\text{Time of Zero}_{i+1} - \text{Time of Zero}_i].$$

The program reads the epicentral distance from the event header. The quantization factor and instrument response corrections are built into the program. (The instrument response corrections are derived from the instrument response curve of Figure VI-1.)

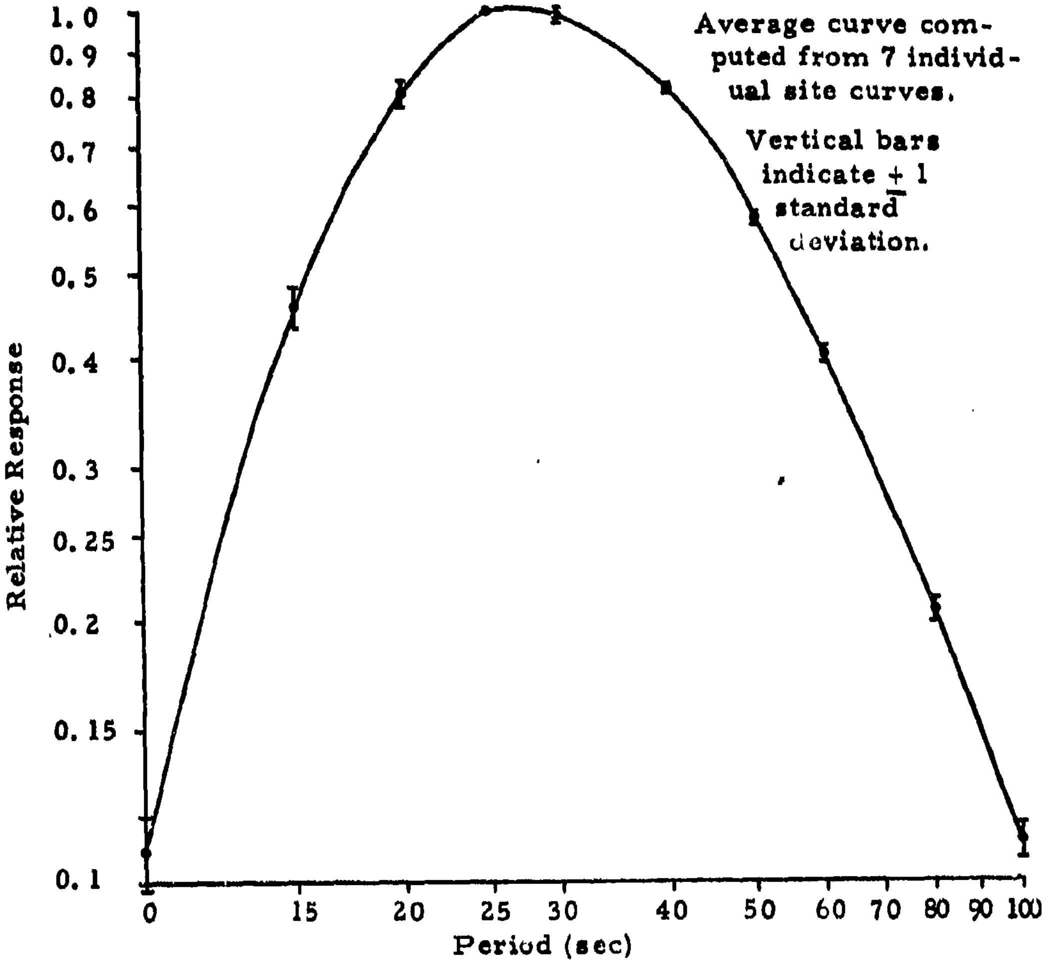

FIGURE VI-1

ILPA INSTRUMENT RESPONSE
NORMALIZED AT 25 SECONDS

The program uses the above information to compute a surface-wave magnitude for each amplitude-period pair. These $M_s$ values with their associated periods and times of measurement are printed out. Finally the program picks the largest $M_s$ value at each specified period of interest and prints it out. The analyst now checks these largest $M_s$ values against the plot of the data. If he does not like an $M_s$ value at a particular period (for example, if the $M_s$ value appears to be associated with a noise pulse in the signal gate) he can select another value from the $M_s$ list generated by the program.

By using this program, measurement errors have been eliminated and transcription errors greatly reduced (since the analyst only writes down the final $M_s$ value and none of the intermediate computational values). Also, the time required to arrive at the $M_s$ values for an event has been reduced.

A further benefit to the evaluation task was found once this program was put into use. Since measurements were no longer being made directly on the plot, it was possible to reduce the length of the plots by one-half. When measurements were made on the plot, a horizontal scale of 100 seconds per inch was considered necessary to minimize measurement errors. Plots are now made with a horizontal scale of 200 seconds per inch. This reduces the amount of plot paper and plot time by one-half and produces more manageable plots.

During the preliminary Iranian Long-Period Array evaluation, $M_s$ was measured at periods of 20, 30, and 40 seconds. However, measureable 40 second energy was not often found - only half as many 40 second $M_s$ values were measured as 20 second or 30 second $M_s$ values. It was also noted that events close to the array have the majority of their energy concentrated at or near 25 seconds period. For these reasons, it has been decided to drop the measurement of 40 second $M_s$ and add the measurement of 25 second $M_s$.

## C. DISCRIMINATION RESULTS

Table VI-1 lists those events of the data base which may be termed presumed nuclear explosions. They were selected on the basis of their epicentral locations and bodywave magnitudes. These events were selected because their epicenters are at or very close to the eastern Kazakh test site and their bodywave magnitudes are larger than most earthquakes from that area.

Figures VI-2 to VI-14 show the $M_s$-$m_b$ plots for the Iranian Long-Period Array data. The values are plotted for the array with three plots encompassing data from all regions showing surface wave magnitude measured at 20, 25, and 30 seconds, followed by individual plots for 25-second surface wave magnitudes from each region. The symbols used in these plots are:

O - earthquake with depth less than 60 km or depth unknown.
\+ - earthquake with depth greater than 60 km.
* - presumed nuclear explosion from Region 8.

Such depth information as was available came from the National Earthquake Information Service bulletins. The straight line in each plot represents the equation of the $M_s$-$m_b$ relationship for that data set. This was computed using the data points for earthquakes with depth less than 60 km or depth unknown. The relationship is computed with a linear fitting algorithm which treats neither variable as dependent. The earthquakes with depths known to be greater than 60 km were excluded from the fitting procedures to avoid biassing the fit. (Deeper events tend to generate relatively lower $M_s$ values.) The slopes and intercepts of the lines fitted to the 20, 25, and 30 second $M_s$ data are given in Table VI-2. The lines fitted to the data of the individual regions are based for the most part on rather sparse populations

## TABLE VI-1

## LIST OF PRESUMED NUCLEAR EXPLOSIONS

| Event Number | $m_b$ | Region | Processing Results |
|---|---|---|---|
| 839 | 4.6 | 8 | Detected |
| 958 | 5.3 | 8 | Detected |
| 1368 | 6.0 | 8 | Detected |
| 1549 | 5.3 | 8 | Not Recorded |
| 1558 | 5.9 | 8 | Detected |
| 1624 | 4.9 | 8 | Detected |

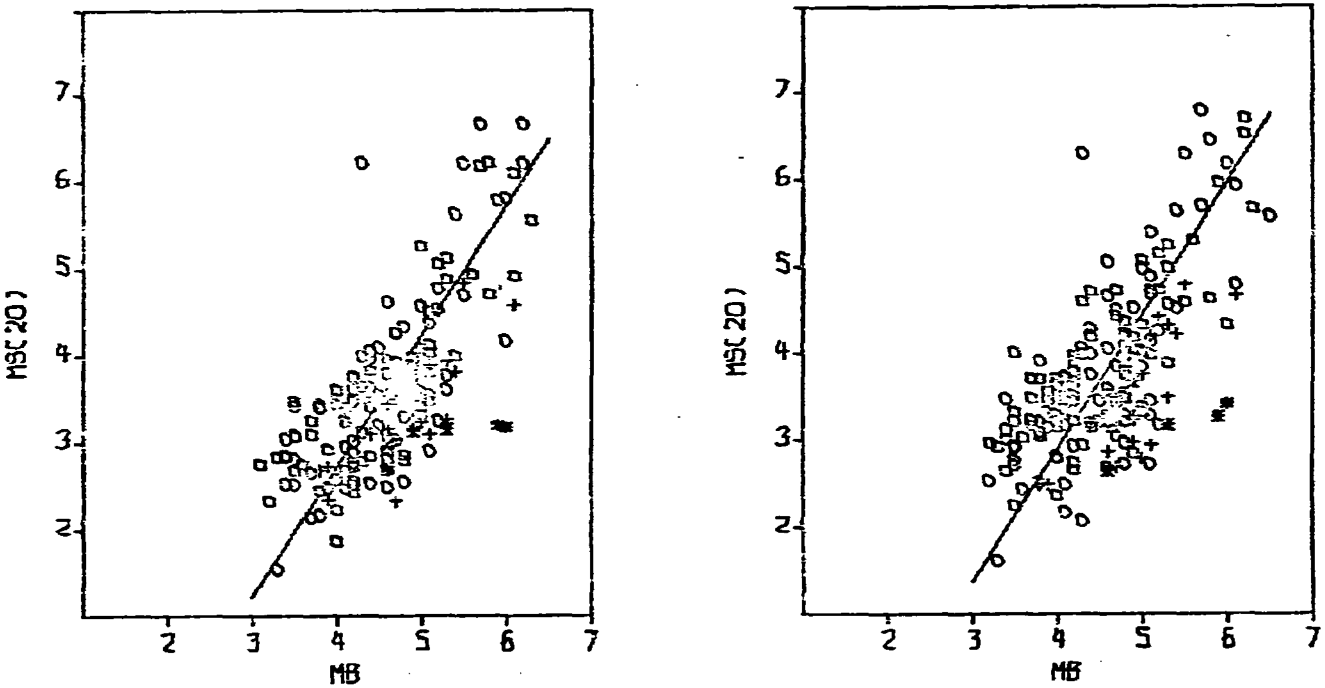

VERTICAL

TRANSVERSE

FIGURE VI-2

ILPA $M_s$-$m_b$ PLOT FOR $M_s$ MEASURED AT 20 SECONDS PERIOD
ALL REGIONS

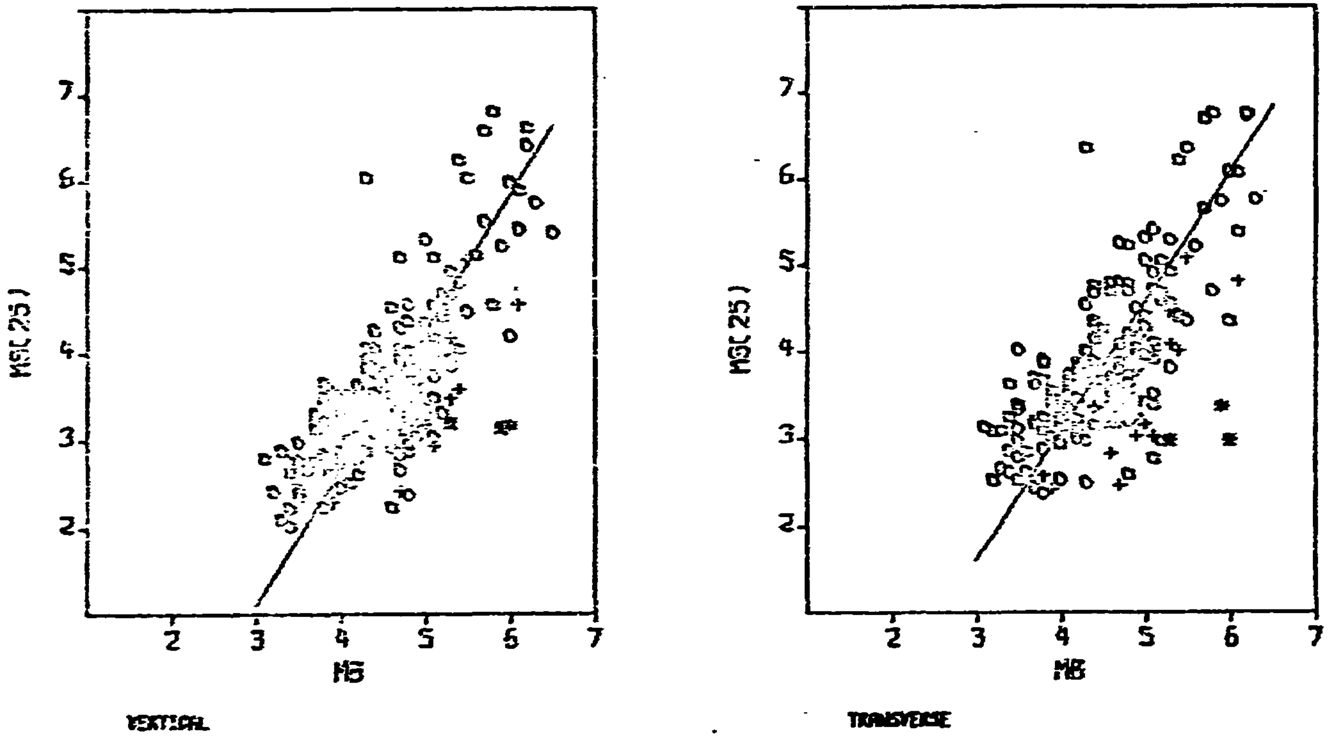

FIGURE VI-3

ILPA $M_s$-$m_b$ PLOT FOR $M_s$ MEASURED AT 25 SECONDS PERIOD
ALL REGIONS

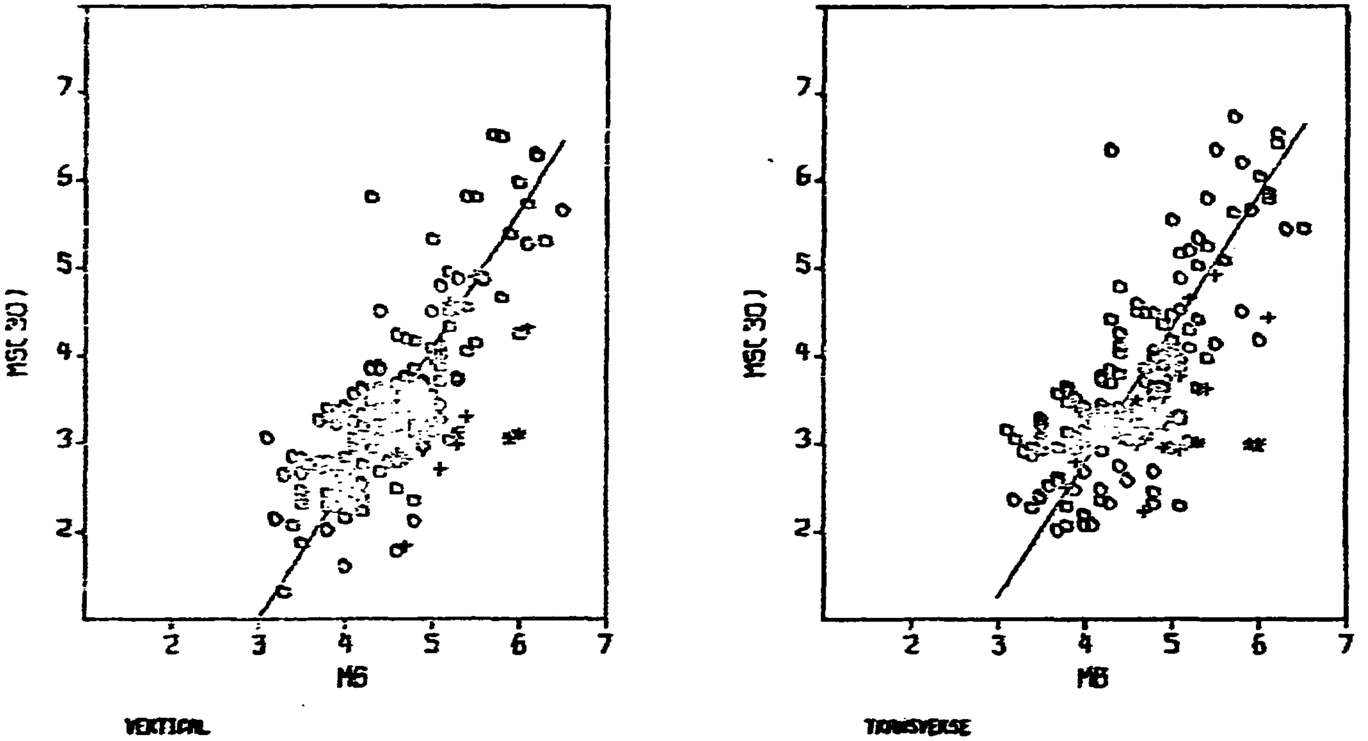

FIGURE VI-4

ILPA $M_s$-$m_b$ PLOT FOR $M_s$ MEASURED AT 30 SECONDS PERIOD
ALL REGIONS

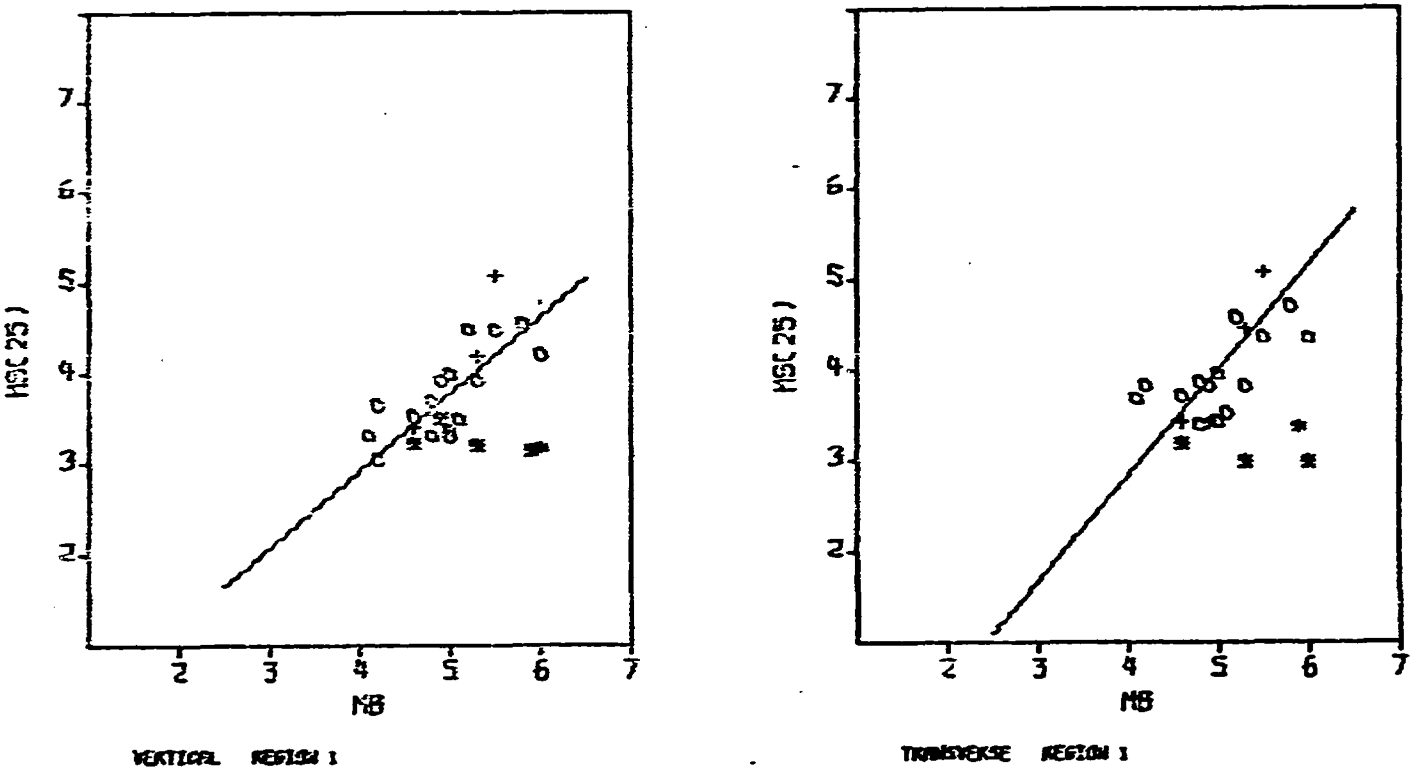

FIGURE VI-5

ILPA $M_s$-$m_b$ PLOT FOR $M_s$ MEASURED AT 25 SECONDS PERIOD
REGION 1 EARTHQUAKES

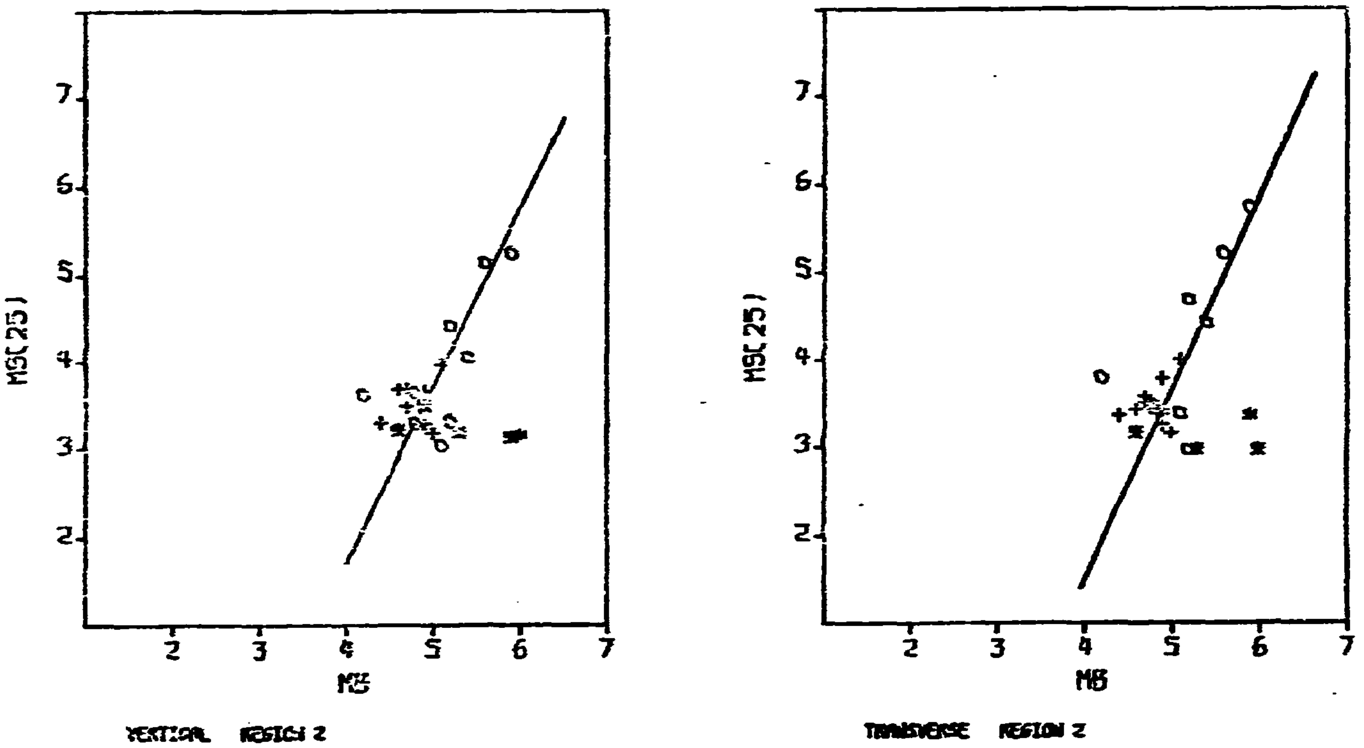

FIGURE VI-6

ILPA $M_s$-$m_b$ PLOT FOR $M_s$ MEASURED AT 25 SECONDS PERIOD
REGION 2 EARTHQUAKES

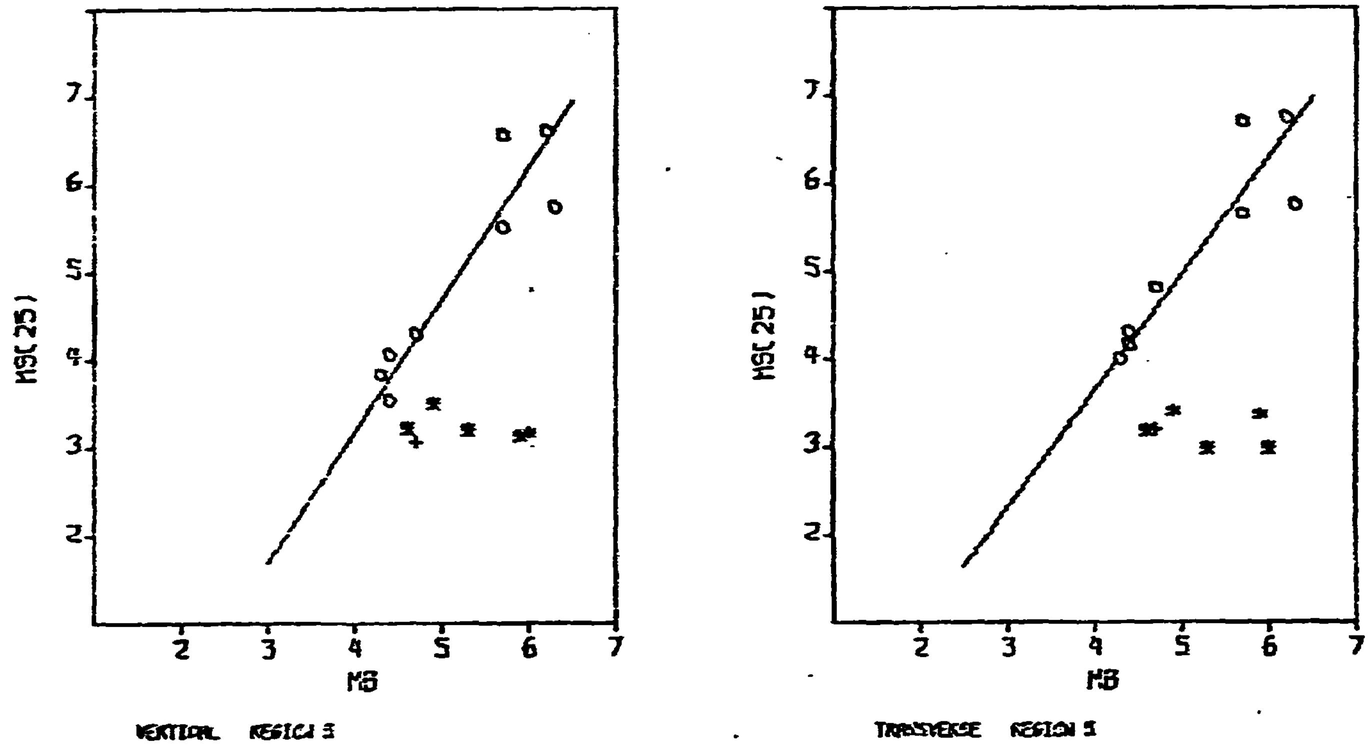

FIGURE VI-7

ILPA $M_s$-$m_b$ PLOT FOR $M_s$ MEASURED AT 25 SECONDS PERIOD
REGION 5 EARTHQUAKES

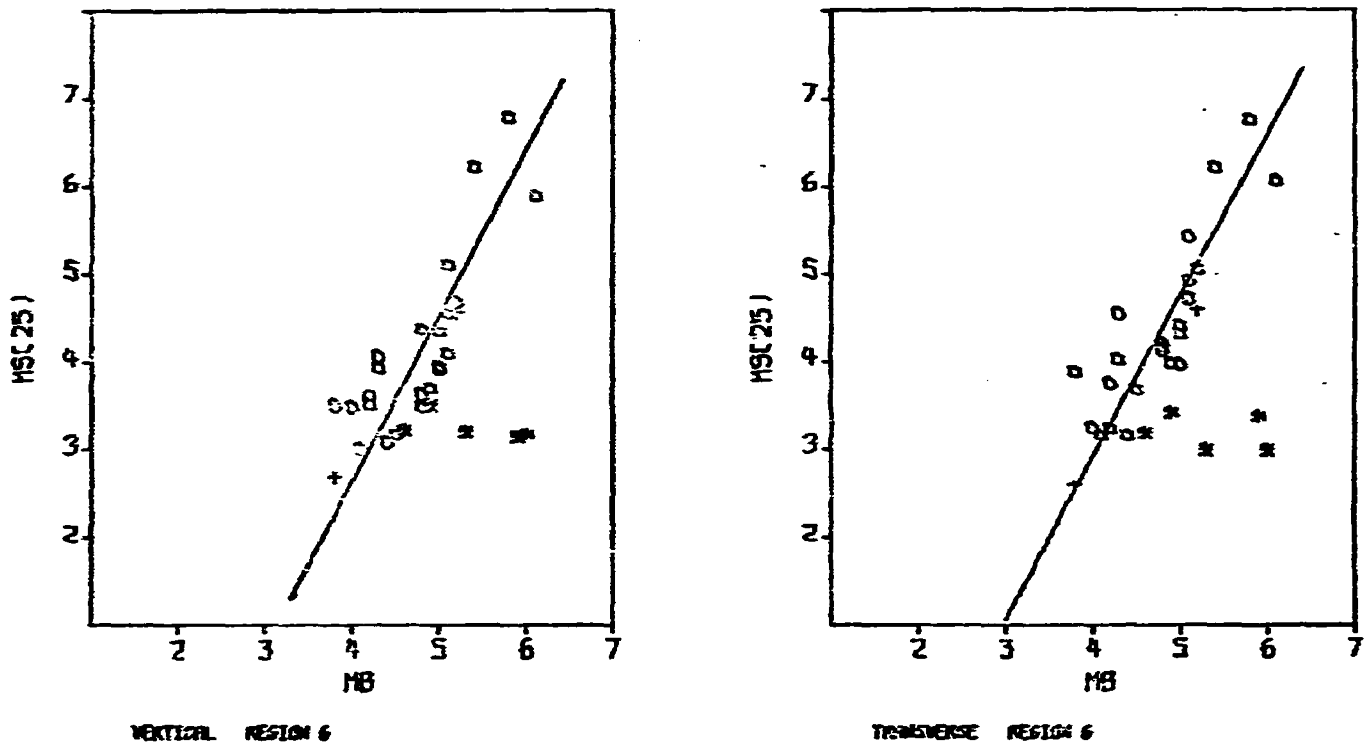

FIGURE VI-8

ILPA $M_s$-$m_b$ PLOT FOR $M_s$ MEASURED AT 25 SECONDS PERIOD
REGION 6 EARTHQUAKES

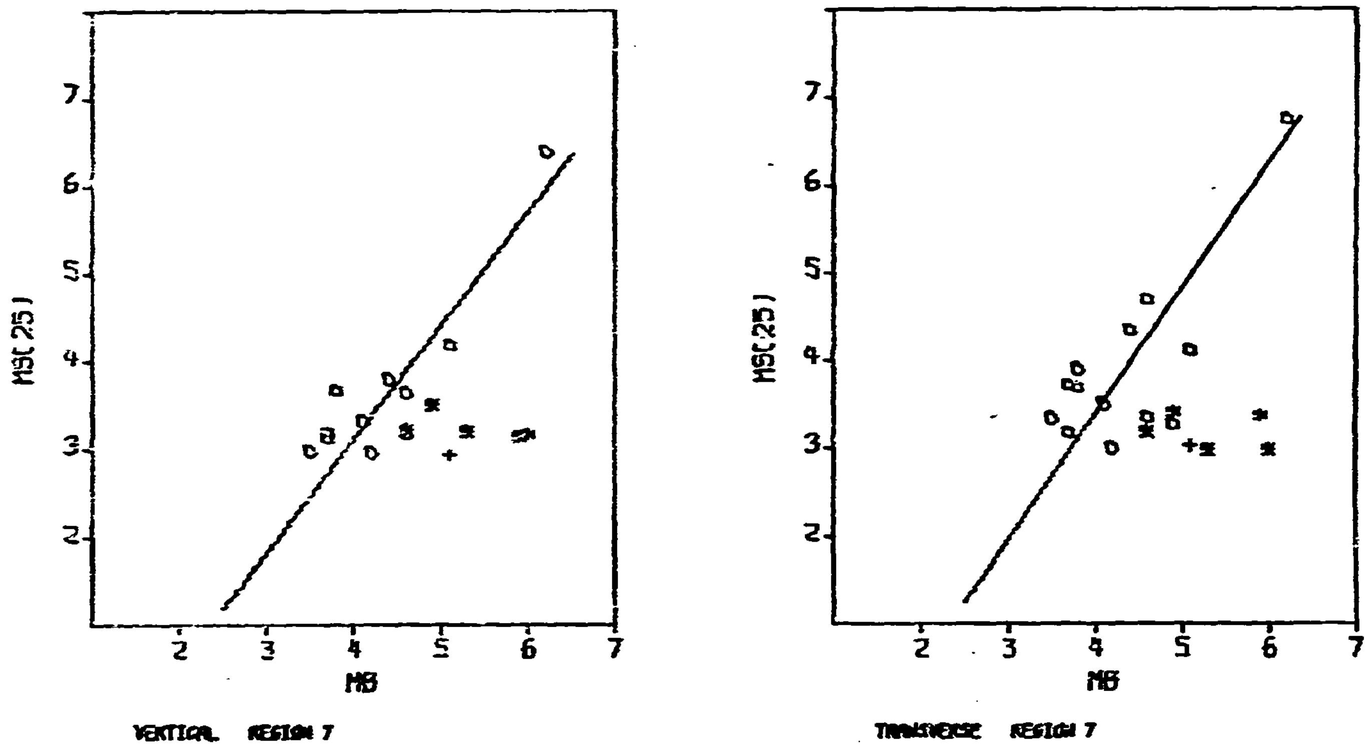

FIGURE VI-9

ILPA $M_s$-$m_b$ PLOT FOR $M_s$ MEASURED AT 25 SECONDS PERIOD
REGION 7 EARTHQUAKES

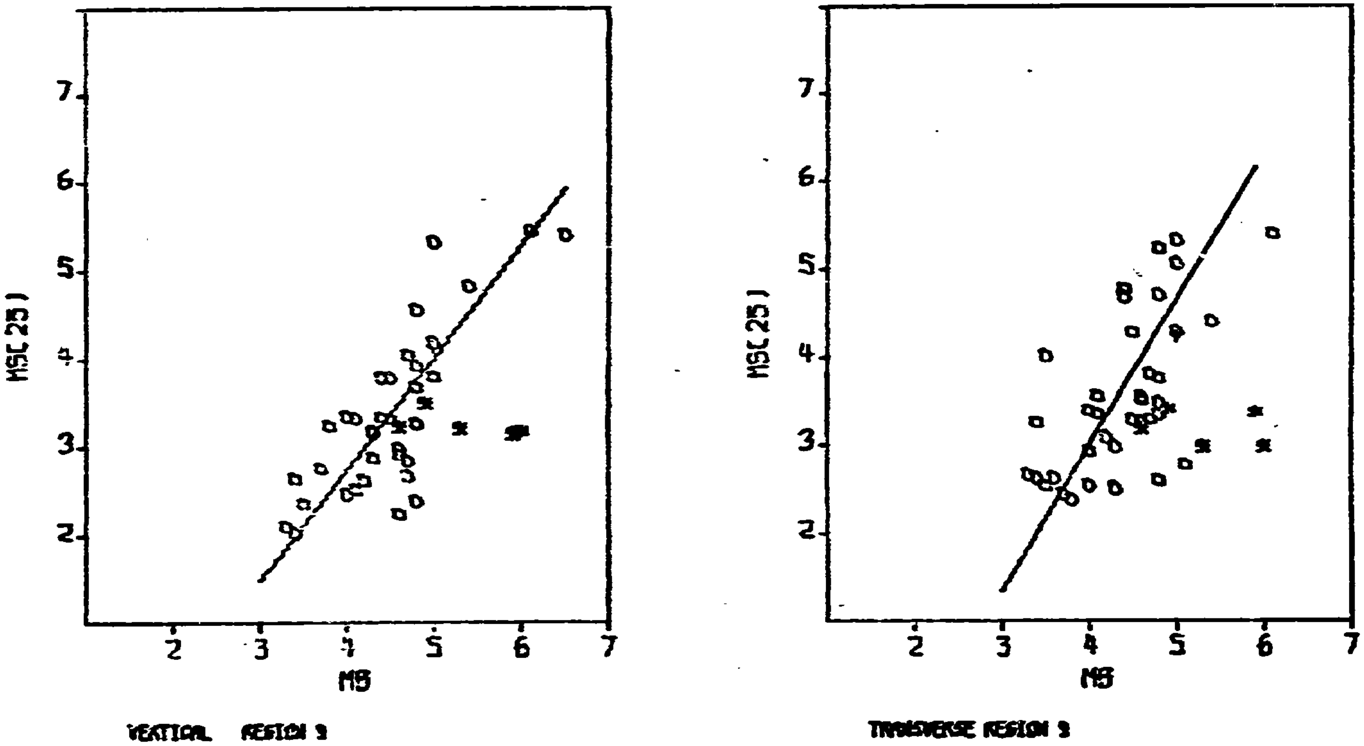

FIGURE VI-10

ILPA $M_s$-$m_b$ PLOT FOR $M_s$ MEASURED AT 25 SECONDS PERIOD
REGION 9 EARTHQUAKES

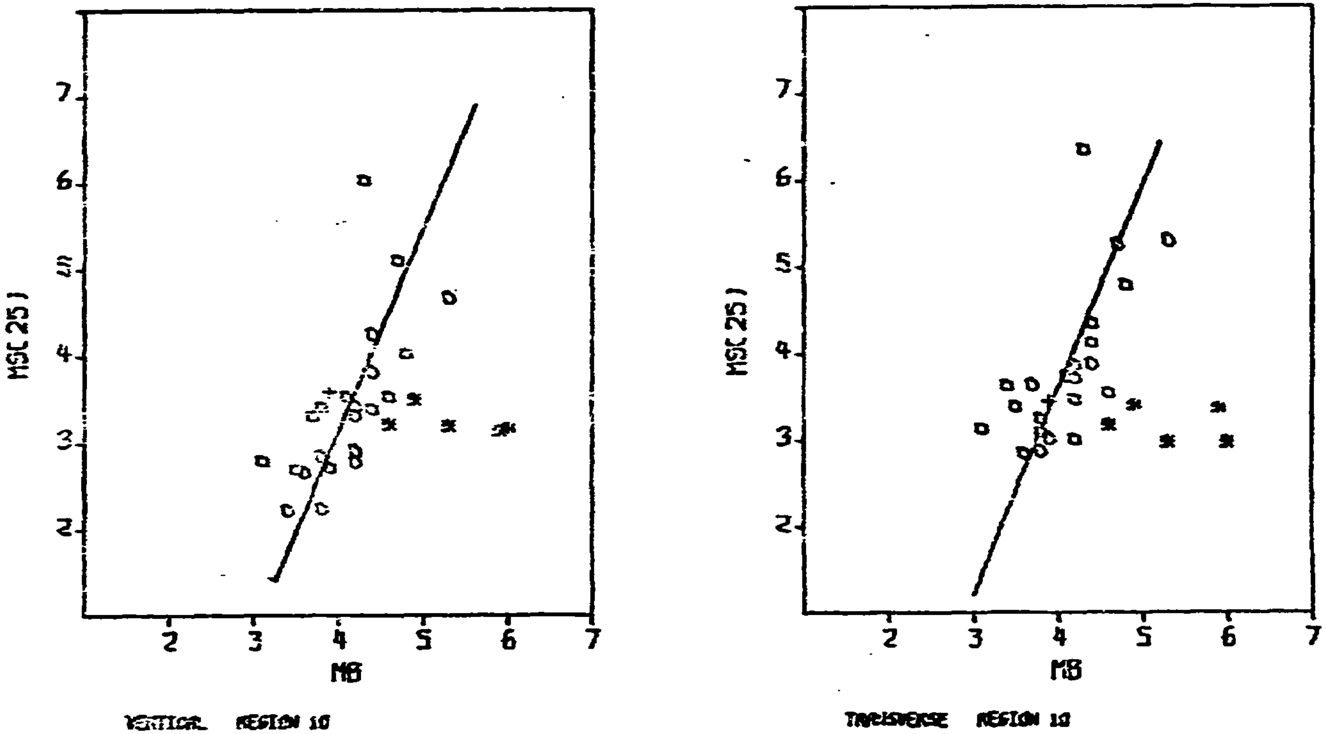

FIGURE VI-11

ILPA $M_s$-$m_b$ PLOT FOR $M_s$ MEASURED AT 25 SECONDS PERIOD
REGION 10 EARTHQUAKES

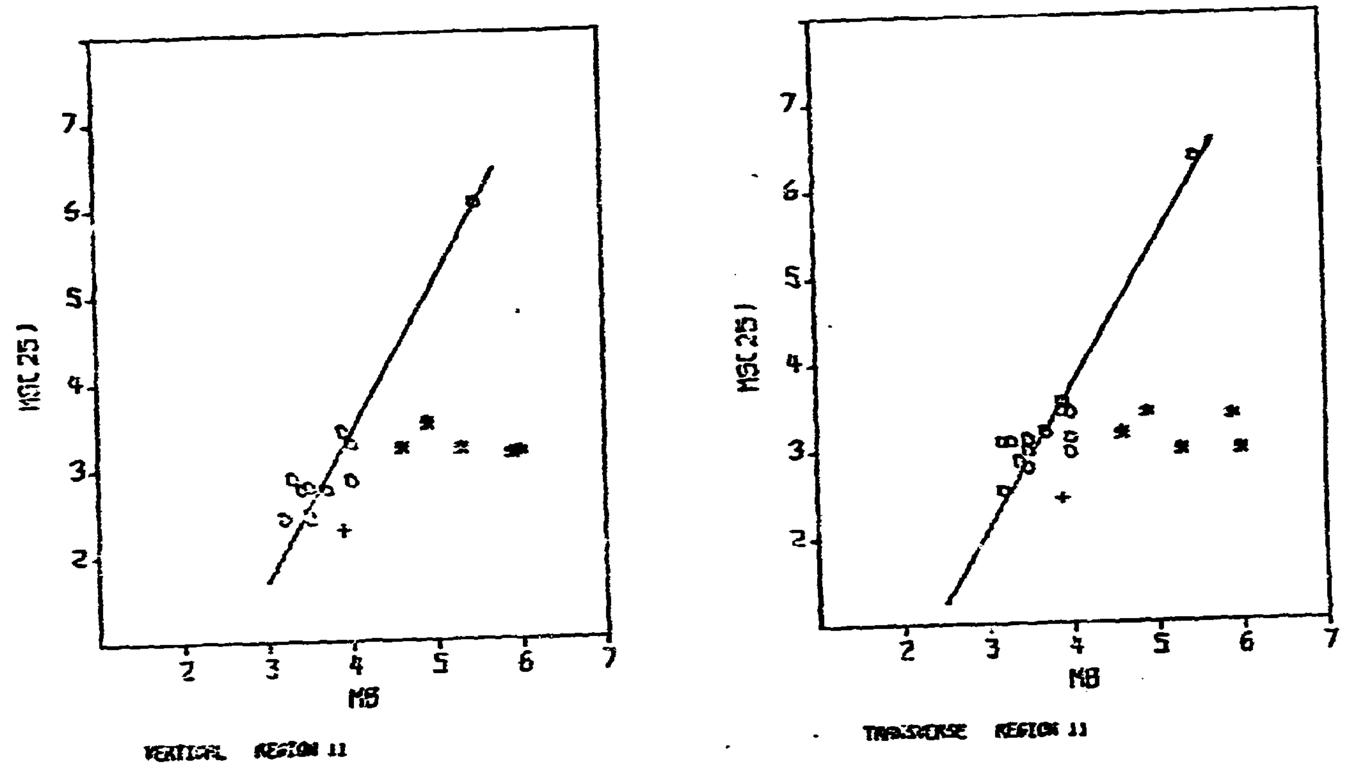

FIGURE VI-12

ILPA $M_s$-$m_b$ PLOT FOR $M_s$ MEASURED AT 25 SECONDS PERIOD
REGION 11 EARTHQUAKES

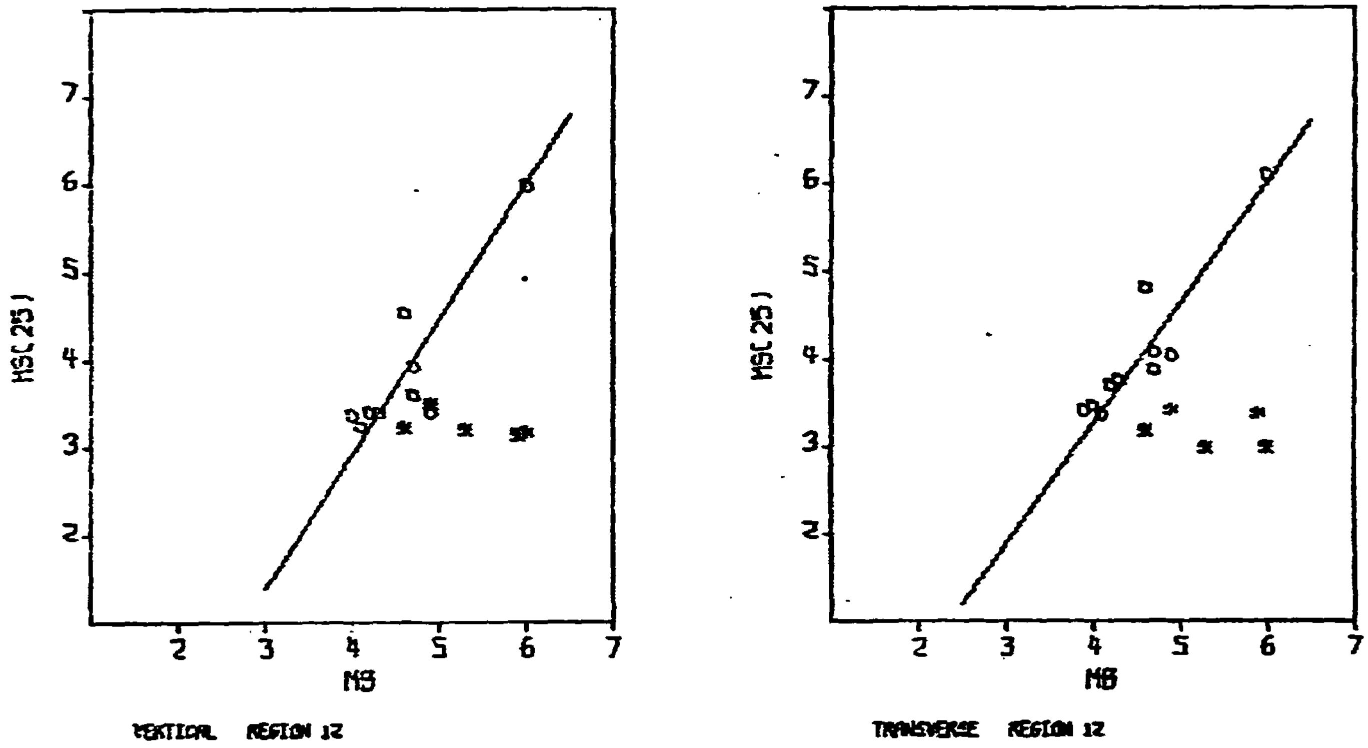

FIGURE VI-13

ILPA $M_s$-$m_b$ PLOT FOR $M_s$ MEASURED AT 25-SECOND PERIOD
REGION 12 EARTHQUAKES

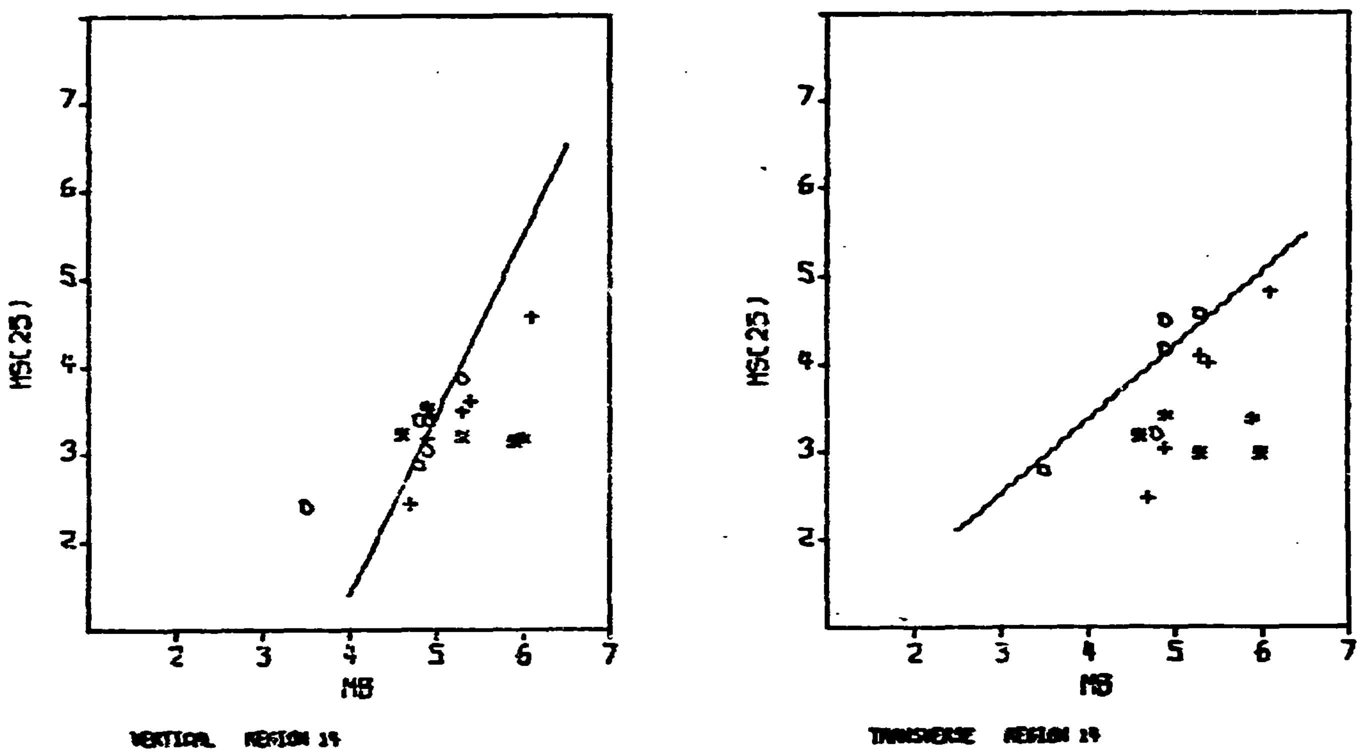

FIGURE VI-14

ILPA $M_s$-$m_b$ PLOT FOR $M_s$ MEASURED AT 25 SECONDS PERIOD
REGION 14 EARTHQUAKES

## TABLE VI-2

## $M_s$-$m_b$ FIT
## SLOPE AND INTERCEPT VALUES

| Period | Component | a | b | $\sigma^2$ | Center of Mass | | |
|---|---|---|---|---|---|---|---|
| | | | | | $m_b$ | $M_s$ | n |
| 20 | Vertical | 1.51 | -3.34 | 0.20 | 4.73 | 3.83 | 138 |
| | Transverse | 1.51 | -3.09 | 0.21 | 4.64 | 3.89 | 152 |
| 25 | Vertical | 1.61 | -3.81 | 0.18 | 4.71 | 3.76 | 147 |
| | Transverse | 1.49 | -2.92 | 0.21 | 4.62 | 3.97 | 157 |
| 30 | Vertical | 1.58 | -3.80 | 0.20 | 4.80 | 3.78 | 119 |
| | Transverse | 1.56 | -3.48 | 0.23 | 4.72 | 3.89 | 131 |

where $M_s = am_b + b$

and are intended to be used only as a visual aid in separating earthquakes from presumed nuclear explosions. Little emphasis should be placed on their particular slopes and intercepts.

Considering the individual events of Table VI-1 for which surface wave magnitudes could be measured, the following points should be noted from Figures VI-2 to VI-14:

| | | |
|---|---|---|
| ● | Event 839 | The surface wave magnitudes for this event fall well within the earthquake population. Therefore, based on this discriminant, this event is classified as an earthquake. |
| ● | Event 958 | The surface wave magnitudes for this event fall at the lower edge of the earthquake population. Therefore, based on this discriminant, this event cannot be classified as an earthquake or explosion. |
| ● | Event 1368 | The surface wave magnitudes for this event show excellent separation from the earthquake population. Therefore, based on this discriminant, this event is classified as an explosion. |
| ● | Event 1558 | The surface wave magnitudes of this event show excellent separation from the earthquake population. Therefore, based on this discriminant, this event is classified as an explosion. |
| ● | Event 1624 | The surface wave magnitudes for this event fall well within the earthquake population. Therefore, based on this discriminant, this event is classified as an earthquake. |

## SECTION VII

## COMPARISON OF SINGLE-SITE STATION AND ARRAY EVALUATION RESULTS

The goal of this section is to determine the differences in performance between the seven-element Iranian Long-Period Array and a single-site station. The single-site station chosen for this comparison is Mashhad (MAIO) of the Seismic Research Observatory Network, located approximately 700 km from ILPA. This station was selected because it is closest to ILPA of the available single-site stations and has the same sensor system as the individual remote sites of ILPA. All data for MAIO are taken from the current report on the evaluation of the Seismic Research Observatory stations (Strauss, 1977).

If the problems which have shut down ILPA in the past as described in Section II do not recur, the reliability of the array as a whole is assessed as 0.8 (where a reliability factor of 1.0 would be perfect.) At MAIO, this reliability factor is assessed at 0.9. The difference in these reliability estimates can be ascribed to the greater complexity of instrumentation at ILPA, resulting in a higher probability of hardware failure and consequent down-time at the array.

The comparison of mixed event probabilities is presented in Table VII-1. Note that while at MAIO the probability of an event being mixed remains fairly constant for all ranges of bodywave magnitude considered, it tends to drop for increasing bodywave magnitude at ILPA. This difference is due to the process of beamforming array data. If the event causing the mixing is well off the azimuth of the event under analysis and

# TABLE VII-1

# COMPARISON OF MIXED EVENT PROBABILITIES

| $m_b$ Range | P(MIX) | |
|---|---|---|
| | MAIO | ILPA Beam |
| 3.1 - 3.5 | 0.29 | 0.30 |
| 3.6 - 4.0 | 0.36 | 0.31 |
| 4.1 - 4.5 | 0.34 | 0.19 |
| 4.6 - 5.0 | 0.25 | 0.15 |

if the amplitudes of the two events as recorded at the array are roughly the same, beamforming will suppress the off-azimuth signal and reveal the signal under analysis. This change from mixed event on single-site to detected event on beam occurred for events processed at the higher values of body-wave magnitude.

Table VII-2 presents the comparison of RMS noise levels measured in the 0.023 - 0.059 Hz passband at MAIO and ILPA. Note first that the RMS noise at MAIO is slightly less than the RMS noise measured at the ILPA reference site. Beamforming the noise recorded at ILPA lowers the ILPA noise levels by 4.7 dB for the vertical component, 3.4 dB for the north component, and 2.0 dB for the east component relative to the MAIO RMS noise levels. For the two highest components, this is an average noise suppression of 4.0 dB relative to MAIO. (This averaging is justified by the consideration that an event is considered to be detected if it is detected on two of the three components and that it is most likely to be detected on the components with highest noise suppression.) From this one can predict that the detection capability of ILPA relative to MAIO (as measured by the 50 percent detection threshold) should be about 0.20 $m_b$ units lower.

Table VII-3 presents the comparison of MAIO and ILPA detection capability. The values of mean epicentral distance ('MEAN DELTA') are presented as an indication that the MAIO and ILPA data bases from which the detection capability estimates were determined had overall essentially the same epicentral distances. Therefore, the comparison is not obscured by differences in detection capability due to differences in epicenter-station separations. The terms 'ALL REGIONS A' and 'ALL REGIONS B' are as previously defined in Section V, where 'ALL REGIONS A' represents the absolute detection capability estimate and 'ALL REGIONS B' represents the conditional detection capability estimate.

## TABLE VII-2

## COMPARISON OF RMS NOISE LEVELS
## (ALL VALUES IN mμ)

| Station | Vertical | | North | | East | |
|---|---|---|---|---|---|---|
| | Mean | S. D. * | Mean | S. D. * | Mean | S. D. * |
| MAIO | 8.20 | 4.37 | 7.89 | 3.45 | 8.19 | 4.00 |
| ILPA Reference Site | 9.58 | 2.19 | 9.34 | 2.56 | 9.86 | 2.98 |
| ILPA BEAM | 4.77 | 1.44 | 5.36 | 1.82 | 6.51 | 2.31 |

* S.D. = Standard Deviation

Note: RMS noise computed in 0.023 - 0.059 Hz passband (no correction for instrument response)

## TABLE VII-3

## COMPARISON OF ILPA AND MAIO DETECTION CAPABILITY

| Type of Detection Statistics | MAIO | | ILPA | |
|---|---|---|---|---|
| | $m_{b50}$ | Mean Delta (degrees) | $m_{b50}$ | Mean Delta (degrees) |
| All Regions A | 4.55 | 38.5 | 4.42 | 36.5 |
| All Regions B | 4.13 | | 3.94 | |

The data of Table VII-3 show that the ILPA detection capability is affected slightly more than the MAIO detection capability by the aggregate of mixed events, malfunctions, and system failures causing no data to be recorded. (Note that ILPA is evaluated only for those times when it was nominally operational.) For ILPA, the absolute and conditional detection capability estimates differ by 0.48 $m_b$ units, while for MAIO the difference is 0.42 $m_b$ units. Considering the mixed event probabilities of Table VII-1, this difference must be a direct result of the lower reliability of ILPA.

A value of 0.20 $m_b$ units was predicted from the relative ILPA and MAIO RMS noise levels as the improvement in the ILPA detection capability relative to the MAIO detection capability. Since this does not take into account the effects of mixed events, malfunctions, and system failures resulting in no data being recorded, it represents an improvement in the conditional detection capability estimates. From Table VII-3, the ILPA conditional detection capability estimate ('ALL REGIONS B') is 0.19 $m_b$ units lower than that of MAIO, which agrees quite well with the predicted improvement.

# SECTION VIII
# CONCLUSIONS

This section summarizes the results of the continued evaluation of the Iranian Long-Period Array (ILPA) and presents plans for necessary future work. The major conclusions are:

## A. DATA QUALITY

- In general, the data quality is fairly good. Of 680 events examined, 6.6% were lost due to unreadable data, 6.2% were lost due to gaps in the recorded data, and 4.1% were lost due to uncorrectable system malfunctions.
- Estimates of array reliability were based on estimates of array up time, frequency of occurrence of recorded and readable data, and frequency of occurrance of system malfunctions. The worst case estimate of ILPA reliability is 0.54 and the best case estimate is 0.79.
- The probability of an event being mixed was estimated at approximately 0.25 for a range of $m_b$ values from 3.1 t0 5.0.

## B. NOISE ANALYSIS

- RMS noise amplitudes do not vary greatly from site to site.
- Noise suppression due to beamforming is greater on the vertical component than on either of the horizontal components.
- For all sites except site 1, the RMS noise amplitudes for periods above 25 seconds are higher on the horizontal components than on the vertical component.

- At periods above 25 seconds, beamforming lowers the vertical component RMS amplitude spectrum much more than the horizontal spectra.
- The above points indicate that use of a 0.033 - 0.050 Hz passband filter in place of the 0.023 - 0.059 Hz passband filter previously used may significantly enhance the signal-to-noise ratio of the ILPA data.
- Multichannel noise coherencies for the 7-element ILPA array are quite similar in level as a function of frequency to those determined from the inner-ring sites of the Norwegian Seismic Array.
- The level of multichannel coherence in the 0.023-0.059 Hz filter passband is high enough that multichannel filtering may be effective.
- There is very little 0.01172 Hz propagating noise arriving at ILPA.
- The majority of 0.04297 Hz and 0.05859 Hz propagating noise with signal phase velocities have arrival azimuths directed toward the south, away from the general seismic area of interest.

## C. SIGNAL ANALYSIS

- The highest gain in signal-to-noise ratio due to beamforming was 6.9 dB on the vertical component. Gains on the transverse and radial components were 4.4 and 4.0 dB, respectively.
- The LQ-transverse component yielded larger correlation coefficients than either the LR-vertical or LR-radial components.

The LR-radial component produced the lowest correlation coefficients on average. Sites 3 and 6 gave the highest correlation coefficients, while site 4 yielded the lowest correlation coefficients.

## D. DETECTION CAPABILITY

- The absolute 50 percent detection capability estimate for ILPA beam data using NORSAR $m_b$ values is at $m_b = 4.42$ for Eurasian events. The absolute detection capability estimate was computed by including all mixed events, events for which no data were available and events containing malfunctions as non-detections.
- The conditional 50 percent detection capability estimate for ILPA beam data using NORSAR $m_b$ values is at $m_b = 3.94$ for Eurasian events. The conditional detection capability estimate was computed by excluding all mixed events, events for which no data were available and events containing malfunctions from the detection statistics.
- Mixed events, events for which no data were available and malfunctions raised the 50 percent detection threshold for the reference site and beam by 0.41 and 0.48 $m_b$ units, respectively.

## E. DISCRIMINATION

- Events 839 and 1624 show surface wave magnitudes indicating that they are earthquakes.
- Event 958 could not be classified as either earthquake or explosion.
- Events 1368 and 1558 show surface wave magnitudes indicating that they are nuclear explosions.

## F. COMPARISON WITH A SINGLE-SITE STATION

- ILPA reliability is estimated at 0.8, in comparison with 0.9 at MAIO. This reflects the greater system complexity of ILPA.
- Due to the beamforming process, the probability of an event being mixed decreases with increasing bodywave magnitude at ILPA while remaining fairly constant at MAIO.
- While the RMS noise levels at ILPA are slightly greater than those at MAIO, beamforming produces an average noise suppression of 4.0 dB at ILPA relative to MAIO.
- The conditional detection capability estimate at ILPA is approximately 0.2 $m_b$ units lower than that of MAIO.

## G. FUTURE WORK

The following items should be investigated to complete the evaluation of the Iranian Long-Period Array:

- Investigate the long-period noise field in more detail. Points covered should include RMS noise levels in different passbands, reasons for increased horizontal component noise at periods beyond 30 seconds, and frequency-wavenumber spectra for more noise samples to better define source azimuths of propagating noise.
- Refine regionalized detection capability estimates. This will require processing and analyzing approximately 500 more events.
- Process more presumed nuclear explosions to better estimate the ILPA discrimination capability.

- Process a suite of detected and non-detected events with the 0.033 - 0.050 Hz passband to determine the effect of removing the elevated noise levels beyond 30 seconds on detection capability.
- Completely evaluate the single recorded component of short-period data in terms of noise characteristics, detection capability, and discrimination capability.

# SECTION IX

# REFERENCES

Flinn, E. A., and Engdahl, E. R., 1965, A Proposed Basis for Geographical and Seismic Regionalization; Reviews of Geophysics, Volume 3, Number 1, February 1965, pp. 123-149.

Laun, P. R., Shen, W., and Swindell, W. H., 1973, Evaluation of the Norwegian Long-Period Seismic Array - Final Report; Special Report Number 12, ALEX(01)-STR-73-12, AFTAC Contract Number F33657-72-C-0725, Texas Instruments Incorporated, Dallas, Texas.

Ringdal, F., 1974, VLPE Network Evaluation and Automatic Processing Research; Technical Report Number 2, ALEX(01)-TR-74-02, AFTAC Contract Number F08606-74-C-0033, Texas Instruments Incorporated, Dallas, Texas.

Robinson, E. A., 1967, Statistical Communication and Detection with Special Reference to Digital Data Processing of Radar and Seismic Signals; Charles Griffin and Company Limited, London, England.

Strauss, A. C., 1976, Preliminary Evaluation of the Iranian Long-Period Array; Technical Report Number 1, ALEX(01)-TR-76-01, AFTAC Contract Number F08606-76-C-0011, Texas Instruments Incorporated, Dallas, Texas.

Strauss, A. C., 1977, Continuation of the Seismic Research Observatories Evaluation; Technical Report Number 2, ALEX(01)-TR-77-02, AFTAC Contract Number F08606-77-C-0004, Texas Instruments Incorporated, Dallas, Texas.

Texas Instruments, 1977, Iranian Long-Period Array Final Report; Contract Number 14-08-0001-14031, Texas Instruments Incorporated, Dallas, Texas.

# APPENDIX A

# THE DATA BASE

This appendix presents the parameters describing each event in the data base. The column headed 'EVNO' gives the number assigned to each event. (These event numbers are the same as those used in the Seismic Research Observatory evaluation.) The column headed 'DATE' gives the month, day, and year of occurrence of the event. The column headed 'TIME' gives the origin time of the event. The columns headed 'LAT.' and 'LONG.' give the latitude and longitude of the event epicenter, where a positive value indicates north latitude or east longitude (as appropriate) and a negative value indicates south latitude or west longitude. The column headed 'MB' gives the body-wave magnitude of the event. The column headed 'Q' gives the NORSAR quality rating of the event parameters, where

1 = good to excellent
2 = fair to good
3 = poor to fair.

A zero in this column indicates the event parameters came from the NEIS event bulletin. The column headed 'LOCATION' gives the general area in which the event occurred. Finally, the column headed 'SUBREG' gives the sub-region number of the event as defined by Flinn and Engdahl (Flinn and Engdahl, 1965).

## TABLE A-1

### DATA BASE
(PAGE 1 OF 16)

| EVNO | DATE | TIME | LAT. | LONG. | MB | Q | LOCATION | SUBREG |
|---|---|---|---|---|---|---|---|---|
| 715 | 5/ 1/76 | 8.28.59 | 34.0 | 80.0 | 3.7 | 3 | TIBET | 306 |
| 716 | 5/ 1/76 | 11.35.33 | 38.0 | 89.0 | 4.1 | 2 | S. SINKIANG PROV. | 321 |
| 717 | 5/ 1/76 | 16.30.10 | 32.0 | 62.0 | 3.8 | 3 | SW AFGHANISTAN | 350 |
| 718 | 5/ 1/76 | 19.34.12 | 41.0 | 142.0 | 4.9 | 1 | NEC HONSHU, JAPAN | 228 |
| 719 | 5/ 2/76 | 0.25.29 | 35.0 | 27.0 | 3.5 | 3 | CRETE | 370 |
| 720 | 5/ 2/76 | 15.20.25 | 50.0 | 155.0 | 4.1 | 2 | KURILE ISLANDS | 221 |
| 721 | 5/ 2/76 | 15.41.30 | 39.0 | 64.0 | 3.6 | 3 | UZBEK SSR | 339 |
| 722 | 5/ 2/76 | 16.37.30 | 53.0 | 158.0 | 3.7 | 3 | NEC KAMCHATKA | 218 |
| 723 | 5/ 2/76 | 16.57.26 | 30.0 | 51.0 | 4.1 | 2 | IRAN | 348 |
| 724 | 5/ 3/76 | 11. 3.29 | 40.0 | 76.0 | 3.7 | 2 | KIRGIZ-SINKIANG BOR. | 320 |
| 725 | 5/ 4/76 | 3.29.39 | 47.0 | 154.0 | 4.2 | 1 | KURILE ISLANDS | 221 |
| 726 | 5/ 4/76 | 5.23. 9 | 32.0 | 50.0 | 3.5 | 2 | WESTERN IRAN | 347 |
| 727 | 5/ 4/76 | 6. 1.51 | 29.0 | 99.0 | 4.3 | 2 | TIBET | 306 |
| 728 | 5/ 4/76 | 7. 5.11 | 27.0 | 81.0 | 3.5 | 2 | NORTHERN INDIA | 308 |
| 729 | 5/ 5/76 | 10. 2.36 | 42.0 | 141.0 | 3.8 | 3 | HOKKAIDO, JAPAN REG. | 224 |
| 730 | 5/ 5/76 | 13.26.18 | 45.0 | 149.0 | 4.6 | 1 | KURILE ISLANDS | 221 |
| 731 | 5/ 5/76 | 16.13.22 | 44.0 | 146.0 | 3.5 | 3 | HOKKAIDO, JAPAN REG. | 224 |
| 732 | 5/ 6/75 | 8.21.35 | 31.0 | 77.0 | 4.2 | 2 | NORTHERN INDIA | 308 |
| 733 | 5/ 6/76 | 11.13. 2 | 44.0 | 149.0 | 4.0 | 2 | KURILE ISLANDS | 221 |
| 734 | 5/ 6/76 | 16.53.20 | 43.0 | 80.0 | 4.2 | 2 | KIRGIZ-SINKIANG BOR. | 320 |
| 735 | 5/ 6/76 | 17.42.43 | 44.0 | 147.0 | 4.7 | 1 | KURILE ISLANDS | 221 |
| 736 | 5/ 6/76 | 17.59. 4 | 35.0 | 24.0 | 4.7 | 2 | CRETE | 370 |
| 737 | 5/ 6/76 | 20.36. 7 | 39.0 | 54.0 | 3.8 | 2 | UZBEK SSR | 339 |
| 738 | 5/ 7/76 | 0.10.42 | 39.0 | 64.0 | 4.5 | 1 | UZBEK SSR | 339 |
| 739 | 5/ 7/76 | 2. 9.54 | 43.0 | 140.0 | 4.0 | 2 | HOKKAIDO, JAPAN REG. | 224 |
| 740 | 5/ 7/76 | 4.34.20 | 48.0 | 154.0 | 3.9 | 2 | KURILE ISLANDS | 221 |
| 741 | 5/ 7/76 | 18. 2.53 | 32.0 | 78.0 | 3.8 | 3 | KASHMIR-TIBET BOR. | 304 |
| 742 | 5/ 7/76 | 23. 5.23 | 40.0 | 29.0 | 3.6 | 3 | TURKEY | 366 |
| 743 | 5/ 9/76 | 2.55.38 | 40.0 | 30.0 | 3.8 | 3 | TURKEY | 366 |
| 744 | 5/ 9/76 | 5.53.45 | 36.0 | 22.0 | 3.6 | 3 | MEDITERRANEAN SEA | 400 |
| 745 | 5/ 9/76 | 7.51.25 | 41.0 | 63.0 | 5.0 | 2 | UZBEK SSR | 339 |
| 746 | 5/ 9/76 | 8.13. 4 | 45.0 | 149.0 | 3.5 | 3 | KURILE ISLANDS | 221 |
| 747 | 5/ 9/76 | 11.19.47 | 40.0 | 30.0 | 4.0 | 3 | TURKEY | 366 |
| 748 | 5/ 9/76 | 13.14.27 | 35.0 | 140.0 | 4.2 | 2 | NEC HONSHU, JAPAN | 228 |
| 749 | 5/ 9/76 | 15. 1.25 | 40.0 | 30.0 | 4.1 | 2 | TURKEY | 366 |
| 750 | 5/ 9/76 | 16.30.25 | 46.0 | 150.0 | 3.6 | 2 | KURILE ISLANDS | 221 |
| 751 | 5/ 9/76 | 20.11. 8 | 40.0 | 30.0 | 3.3 | 3 | TURKEY | 366 |
| 752 | 5/ 9/76 | 22. 5.17 | 46.0 | 35.0 | 2.6 | 3 | CRIMEA REGION | 361 |
| 753 | 5/10/76 | 4.34.31 | 39.0 | 19.0 | 3.5 | 3 | GREECE-ALBANIA BOR. | 392 |
| 754 | 5/10/75 | 8.14.56 | 39.0 | 15.0 | 3.3 | 2 | SICILY | 398 |

## TABLE A-1

## DATA BASE

(PAGE 2 OF 16)

| EVNO | DATE | TIME | LAT. | LONG. | MB | Q | LOCATION | SUBREG |
|---|---|---|---|---|---|---|---|---|
| 755 | 5/10/76 | 12. 1.38 | 40.0 | 29.0 | 4.2 | 3 | TURKEY | 366 |
| 756 | 5/10/76 | 15.20.49 | 39.0 | 30.0 | 4.2 | 2 | TURKEY | 366 |
| 757 | 5/10/76 | 18.37.24 | 29.0 | 82.0 | 4.0 | 3 | NEPAL | 310 |
| 758 | 5/10/76 | 18.43.40 | 29.0 | 83.0 | 5.0 | 2 | NEPAL-INDIA BOR. | 309 |
| 759 | 5/10/76 | 23.34.15 | 46.0 | 36.0 | 2.8 | 3 | SOUTHWESTERN RUSSIA | 357 |
| 760 | 5/10/76 | 23.54.14 | 40.0 | 30.0 | 4.3 | 2 | TURKEY | 366 |
| 761 | 5/11/76 | 3. 2. 3 | 30.0 | 81.0 | 3.4 | 3 | NEPAL | 310 |
| 762 | 5/11/76 | 3.32. 8 | 40.0 | 30.0 | 4.2 | 3 | TURKEY | 366 |
| 763 | 5/11/76 | 4. 4.16 | 36.0 | 141.0 | 4.1 | 2 | NEC HONSHU, JAPAN | 228 |
| 764 | 5/11/76 | 7.14.13 | 33.0 | 53.0 | 3.8 | 3 | IRAN | 348 |
| 765 | 5/11/76 | 13.26.51 | 45.0 | 149.0 | 4.2 | 2 | KURILE ISLANDS | 221 |
| 766 | 5/11/76 | 17. 0.23 | 41.0 | 21.0 | 5.5 | 2 | GREECE-ALBANIA BOR. | 392 |
| 767 | 5/11/76 | 17. 9.55 | 36.0 | 22.0 | 5.2 | 2 | MEDITERRANEAN SEA | 400 |
| 768 | 5/11/76 | 19.25. 0 | 32.0 | 49.0 | 3.4 | 3 | WESTERN IRAN | 347 |
| 769 | 5/11/76 | 21.11.51 | 36.0 | 22.0 | 4.0 | 3 | MEDITERRANEAN SEA | 400 |
| 770 | 5/12/76 | 5.11.49 | 40.0 | 30.0 | 4.1 | 2 | TURKEY | 366 |
| 771 | 5/12/76 | 5.26.16 | 38.0 | 21.0 | 3.2 | 3 | IONIAN SEA | 399 |
| 772 | 5/12/76 | 16.45.40 | 52.0 | 160.0 | 4.1 | 2 | OEC KAMCHATKA | 219 |
| 773 | 5/12/76 | 18. 5.20 | 38.0 | 21.0 | 2.9 | 3 | IONIAN SEA | 399 |
| 774 | 5/12/76 | 18.40.15 | 42.0 | 145.0 | 4.4 | 2 | OC HOKKAIDO, JAPAN | 225 |
| 775 | 5/13/76 | 3.44.48 | 43.0 | 20.0 | 4.0 | 2 | YUGOSLAVIA | 383 |
| 776 | 5/13/76 | 9.50.10 | 44.0 | 149.0 | 3.9 | 2 | KURILE ISLANDS | 221 |
| 777 | 5/13/76 | 11. 0. 8 | 36.0 | 140.0 | 3.8 | 3 | HONSHU, JAPAN | 227 |
| 778 | 5/13/76 | 13.18.29 | 40.0 | 30.0 | 3.6 | 3 | TURKEY | 366 |
| 779 | 5/13/76 | 14.47.34 | 36.0 | 22.0 | 3.5 | 3 | MEDITERRANEAN SEA | 400 |
| 780 | 5/13/76 | 19.23. 1 | 38.0 | 21.0 | 2.8 | 3 | IONIAN SEA | 399 |
| 781 | 5/13/76 | 20.28.46 | 35.0 | 140.0 | 4.5 | 2 | NEC HONSHU, JAPAN | 228 |
| 782 | 5/13/76 | 20.44.32 | 35.0 | 24.0 | 4.2 | 2 | CRETE | 370 |
| 783 | 5/13/76 | 21.13. 5 | 38.0 | 21.0 | 3.1 | 3 | IONIAN SEA | 399 |
| 784 | 5/13/76 | 22.17.18 | 36.0 | 22.0 | 4.0 | 2 | MEDITERRANEAN SEA | 400 |
| 785 | 5/13/76 | 23.17.21 | 40.0 | 143.0 | 3.8 | 2 | NEC HONSHU, JAPAN | 228 |
| 786 | 5/14/76 | 1.23.17 | 38.0 | 32.0 | 3.5 | 3 | TURKEY | 366 |
| 787 | 5/14/76 | 11. 6.17 | 39.0 | 30.0 | 3.9 | 3 | TURKEY | 366 |
| 788 | 5/14/76 | 15. 1.30 | 43.0 | 149.0 | 4.2 | 2 | KURILE ISLANDS REG. | 222 |
| 789 | 5/14/76 | 20.24.53 | 39.0 | 142.0 | 3.9 | 3 | NEC HONSHU, JAPAN | 228 |
| 790 | 5/14/76 | 20.40.13 | 41.0 | 144.0 | 5.2 | 1 | HOKKAIDO, JAPAN | 224 |
| 791 | 5/14/76 | 22.27.54 | 40.0 | 143.0 | 3.9 | 2 | NEC HONSHU, JAPAN | 228 |
| 792 | 5/15/76 | 3. 3.25 | 35.0 | 24.0 | 4.2 | 2 | CRETE | 370 |
| 793 | 5/15/76 | 4.24. 3 | 35.0 | 27.0 | 3.5 | 3 | CRETE | 370 |
| 794 | 5/15/76 | 6.55.54 | 24.0 | 94.0 | 3.5 | 3 | BURMA-INDIA BOR. | 294 |

## TABLE A-1

## DATA BASE

(PAGE 3 OF 16)

| EVNO | DATE | TIME | LAT. | LONG. | MB | Q | LOCATION | SUBREG |
|---|---|---|---|---|---|---|---|---|
| 795 | 5/15/76 | 8.11.59 | 19.0 | 95.0 | 4.8 | 1 | BURMA | 296 |
| 796 | 5/15/76 | 11. 6. 6 | 40.0 | 30.0 | 3.4 | 2 | TURKEY | 366 |
| 797 | 5/15/76 | 19.12.28 | 38.0 | 21.0 | 2.8 | 3 | IONIAN SEA | 399 |
| 798 | 5/15/76 | 22.23.29 | 42.0 | 141.0 | 3.7 | 3 | HOKKAIDO, JAPAN REG. | 224 |
| 799 | 5/15/76 | 23. 5.23 | 38.0 | 144.0 | 3.8 | 3 | OEC HONSHU, JAPAN | 229 |
| 800 | 5/16/76 | 8. 1.16 | 36.0 | 51.0 | 3.7 | 2 | IRAN | 348 |
| 801 | 5/16/76 | 15.40.36 | 36.0 | 74.0 | 3.5 | 3 | NORTHWESTERN KASHMIR | 720 |
| 802 | 5/16/76 | 20.25.16 | 48.0 | 154.0 | 4.2 | 2 | KURILE ISLANDS | 221 |
| 803 | 5/17/76 | 2.58.35 | 39.0 | 54.0 | 6.5 | 1 | UZBEK SSR | 339 |
| 804 | 5/17/76 | 3.21.30 | 39.0 | 64.0 | 4.3 | 2 | UZBEK SSR | 339 |
| 805 | 5/17/76 | 3.29.14 | 39.0 | 64.0 | 4.1 | 2 | UZBEK SSR | 339 |
| 806 | 5/17/76 | 3.57.25 | 41.0 | 62.0 | 4.1 | 2 | TURKMEN SSR | 340 |
| 807 | 5/17/76 | 4.14.26 | 42.0 | 52.0 | 4.4 | 2 | UZBEK SSR | 339 |
| 808 | 5/17/76 | 4.34.33 | 39.0 | 65.0 | 3.5 | 2 | TURKMEN SSR | 340 |
| 809 | 5/17/76 | 4.54.15 | 42.0 | 61.0 | 4.7 | 2 | TURKMEN SSR | 340 |
| 810 | 5/17/76 | 5.53.10 | 39.0 | 64.0 | 4.0 | 2 | UZBEK SSR | 339 |
| 811 | 5/17/76 | 6. 6.32 | 39.0 | 54.0 | 3.2 | 3 | TURKMEN SSR | 340 |
| 812 | 5/17/76 | 6.37. 8 | 41.0 | 61.0 | 3.8 | 2 | UZBEK SSR | 339 |
| 813 | 5/17/76 | 6.58.11 | 39.0 | 64.0 | 3.9 | 2 | UZBEK SSR | 339 |
| 814 | 5/17/76 | 7.20. 3 | 41.0 | 63.0 | 3.6 | 3 | UZBEK SSR | 339 |
| 815 | 5/17/76 | 8.10.26 | 39.0 | 64.0 | 3.8 | 2 | TURKMEN SSR | 340 |
| 816 | 5/17/76 | 10.44.12 | 41.0 | 63.0 | 3.4 | 2 | UZBEK SSR | 339 |
| 817 | 5/17/76 | 11. 1.36 | 41.0 | 62.0 | 4.0 | 2 | UZBEK SSR | 339 |
| 818 | 5/17/76 | 15.39.16 | 40.0 | 30.0 | 3.7 | 3 | TURKEY | 366 |
| 819 | 5/17/76 | 16.11.36 | 38.0 | 21.0 | 3.7 | 3 | IONIAN SEA | 399 |
| 820 | 5/17/76 | 16.38.10 | 41.0 | 63.0 | 3.2 | 3 | UZBEK SSR | 339 |
| 821 | 5/17/76 | 17.46.18 | 40.0 | 64.0 | 4.7 | 2 | UZBEK SSR | 339 |
| 822 | 5/17/76 | 20.18.24 | 42.0 | 62.0 | 3.5 | 3 | UZBEK SSR | 339 |
| 823 | 5/17/76 | 21.52.28 | 41.0 | 52.0 | 3.7 | 2 | UZBEK SSR | 339 |
| 824 | 5/17/76 | 22.18.25 | 56.0 | 162.0 | 4.8 | 1 | NEC KAMCHATKA | 218 |
| 825 | 5/18/76 | 5.35.37 | 43.0 | 61.0 | 3.4 | 3 | UZBEK SSR | 339 |
| 826 | 5/18/76 | 7.59.41 | 35.0 | 27.0 | 3.3 | 3 | CRETE | 370 |
| 827 | 5/18/76 | 8.30.14 | 35.0 | 27.0 | 4.2 | 3 | CRETE | 370 |
| 828 | 5/18/76 | 8.57.37 | 41.0 | 63.0 | 4.6 | 1 | UZBEK SSR | 339 |
| 829 | 5/18/76 | 13.54.33 | 41.0 | 62.0 | 4.8 | 1 | TURKMEN SSR | 340 |
| 830 | 5/18/76 | 16.15.50 | 38.0 | 21.0 | 3.5 | 3 | IONIAN SEA | 399 |
| 831 | 5/18/76 | 17. 7.51 | 38.0 | 21.0 | 2.8 | 3 | IONIAN SEA | 399 |
| 832 | 5/18/76 | 20.11.39 | 39.0 | 64.0 | 3.7 | 2 | TURKMEN SSR | 340 |
| 833 | 5/18/76 | 20.22. 2 | 33.0 | 64.0 | 3.6 | 2 | UZBEK SSR | 339 |
| 834 | 5/18/76 | 20.24.29 | 39.0 | 145.0 | 3.6 | 3 | OEC HONSHU, JAPAN | 229 |

## TABLE A-1

## DATA BASE
(PAGE 4 OF 16)

| EVNO | DATE | TIME | LAT. | LONG. | MB | Q | LOCATION | SUBREG |
|---|---|---|---|---|---|---|---|---|
| 835 | 5/18/76 | 22.48.47 | 39.0 | 64.0 | 3.4 | 2 | TURKMEN SSR | 340 |
| 836 | 5/18/76 | 23. 9.47 | 36.0 | 22.0 | 3.5 | 3 | MEDITERRANEAN SEA | 400 |
| 837 | 5/19/76 | 1.11.12 | 39.0 | 64.0 | 4.2 | 1 | UZBEK SSR | 339 |
| 838 | 5/19/76 | 2.26. 9 | 41.0 | 63.0 | 3.5 | 3 | UZBEK SSR | 339 |
| 839 | 5/19/76 | 2.56.46 | 49.0 | 80.0 | 4.6 | 1 | EASTERN KAZAKH SSR | 329 |
| 840 | 5/19/76 | 7.30.16 | 39.0 | 55.0 | 3.6 | 3 | TURKMEN SSR | 340 |
| 841 | 5/19/76 | 15.54.54 | 41.0 | 62.0 | 4.8 | 1 | TURKMEN SSR | 340 |
| 842 | 5/19/76 | 16.44. 9 | 38.0 | 21.0 | 3.0 | 3 | IONIAN SEA | 399 |
| 843 | 5/20/76 | 6.43.33 | 33.0 | 55.0 | 3.9 | 2 | IRAN | 348 |
| 844 | 5/20/76 | 11.37.15 | 39.0 | 54.0 | 3.9 | 2 | UZBEK SSR | 339 |
| 845 | 5/20/76 | 19.42.40 | 46.0 | 152.0 | 4.3 | 2 | KURILE ISLANDS | 221 |
| 846 | 5/20/76 | 22. 4.24 | 45.0 | 149.0 | 3.8 | 2 | KURILE ISLANDS | 221 |
| 847 | 5/21/76 | 0.50.41 | 51.0 | 155.0 | 3.7 | 3 | KURILE ISLANDS | 221 |
| 848 | 5/21/76 | 8.33.38 | 41.0 | 63.0 | 3.8 | 2 | UZBEK SSR | 339 |
| 849 | 5/21/76 | 13. 9.19 | 37.0 | 140.0 | 3.6 | 3 | HONSHU, JAPAN | 227 |
| 850 | 5/21/76 | 16. 5.21 | 39.0 | 64.0 | 4.2 | 1 | UZBEK SSR | 339 |
| 851 | 5/21/76 | 18.28.50 | 39.0 | 54.0 | 3.9 | 2 | UZBEK SSR | 339 |
| 852 | 5/22/76 | 18. 2. 8 | 40.0 | 29.0 | 3.9 | 3 | TURKEY | 366 |
| 853 | 5/22/76 | 18.37.36 | 31.0 | 76.0 | 3.8 | 2 | NORTHERN INDIA | 308 |
| 854 | 5/22/76 | 18.51.11 | 46.0 | 148.0 | 3.8 | 2 | KURILE ISLANDS | 221 |
| 855 | 5/23/76 | 3.53.50 | 39.0 | 30.0 | 3.6 | 3 | TURKEY | 366 |
| 856 | 5/23/76 | 9.20.52 | 38.0 | 21.0 | 2.8 | 3 | IONIAN SEA | 399 |
| 857 | 5/23/76 | 9.49.10 | 39.0 | 64.0 | 4.0 | 2 | UZBEK SSR | 339 |
| 858 | 5/23/76 | 10.58.33 | 40.0 | 143.0 | 4.1 | 2 | NEC HONSHU, JAPAN | 228 |
| 859 | 5/23/76 | 13.26.48 | 39.0 | 54.0 | 3.4 | 2 | UZBEK SSR | 339 |
| 860 | 5/24/76 | 6.10.46 | 39.0 | 64.0 | 3.8 | 2 | UZBEK SSR | 339 |
| 861 | 5/24/76 | 6.49.44 | 47.0 | 152.0 | 3.8 | 3 | KURILE ISLANDS | 221 |
| 862 | 5/24/76 | 14.56.25 | 41.0 | 62.0 | 4.3 | 2 | UZBEK SSR | 339 |
| 863 | 5/24/76 | 17.52. 7 | 44.0 | 12.0 | 3.7 | 3 | CENTRAL ITALY | 381 |
| 864 | 5/25/76 | 4.48.49 | 27.0 | 94.0 | 4.6 | 1 | EASTERN INDIA | 317 |
| 865 | 5/25/76 | 7.29.41 | 44.0 | 149.0 | 3.6 | 3 | KURILE ISLANDS | 221 |
| 866 | 5/25/76 | 9. 9.17 | 53.0 | 158.0 | 5.5 | 1 | NEC KAMCHATKA | 218 |
| 867 | 5/25/76 | 8.16.53 | 53.0 | 158.0 | 5.7 | 1 | NEC KAMCHATKA | 218 |
| 868 | 5/25/76 | 10.53.16 | 53.0 | 158.0 | 4.0 | 2 | NEC KAMCHATKA | 218 |
| 869 | 5/25/76 | 11. 9.42 | 50.0 | 158.0 | 4.6 | 2 | KURILE ISLANDS | 221 |
| 870 | 5/25/76 | 11.17. 3 | 52.0 | 160.0 | 3.9 | 2 | OEC KAMCHATKA | 219 |
| 871 | 5/25/76 | 12.12.42 | 32.0 | 50.0 | 3.4 | 3 | WESTERN IRAN | 347 |
| 872 | 5/25/76 | 15.34.20 | 51.0 | 158.0 | 4.1 | 2 | KURILE ISLANDS | 221 |
| 873 | 5/25/76 | 18.43.25 | 39.0 | 30.0 | 4.6 | 2 | TURKEY | 366 |
| 874 | 5/27/76 | 2.19.49 | 31.0 | 83.0 | 3.6 | 3 | TIBET | 306 |

## TABLE A-1

## DATA BASE

(PAGE 5 OF 16)

| EVNO | DATE | TIME | LAT. | LONG. | MB | Q | LOCATION | SUBREG |
|---|---|---|---|---|---|---|---|---|
| 875 | 5/27/76 | 6.44.15 | 40.0 | 58.0 | 3.7 | 2 | UZBEK SSR | 339 |
| 876 | 5/28/76 | 3.36.43 | 36.0 | 139.0 | 3.9 | 2 | HONSHU, JAPAN | 227 |
| 877 | 5/28/76 | 14. 5.30 | 39.0 | 64.0 | 4.8 | 1 | UZBEK SSR | 339 |
| 878 | 5/28/76 | 23. 2.19 | 39.0 | 30.0 | 4.4 | 2 | TURKEY | 366 |
| 879 | 5/28/76 | 23. 9.54 | 43.0 | 36.0 | 3.2 | 3 | BLACK SEA | 360 |
| 880 | 5/29/76 | 1.59. 9 | 35.0 | 140.0 | 3.7 | 3 | NEC HONSHU, JAPAN | 228 |
| 881 | 5/29/76 | 3.45.33 | 39.0 | 30.0 | 3.9 | 2 | TURKEY | 366 |
| 882 | 5/29/76 | 8.38.22 | 39.0 | 114.0 | 3.7 | 3 | NORTHEASTERN CHINA | 658 |
| 883 | 5/29/76 | 10.21.13 | 38.0 | 21.0 | 2.8 | 3 | IONIAN SEA | 399 |
| 884 | 5/29/76 | 11.42.47 | 56.0 | 152.0 | 3.7 | 3 | NEC KAMCHATKA | 218 |
| 885 | 5/29/76 | 11.58.39 | 27.0 | 97.0 | 4.7 | 1 | BURMA | 296 |
| 886 | 5/29/76 | 12.23.13 | 24.0 | 100.0 | 5.7 | 1 | BURMA-CHINA BORDER | 297 |
| 887 | 5/29/76 | 12.35.36 | 28.0 | 96.0 | 4.2 | 2 | INDIA-CHINA BORDER | 313 |
| 888 | 5/29/76 | 12.59. 5 | 25.0 | 97.0 | 3.9 | 3 | BURMA-CHINA BORDER | 297 |
| 889 | 5/29/76 | 13.55.51 | 28.0 | 95.0 | 4.0 | 3 | INDIA-CHINA BORDER | 313 |
| 890 | 5/29/76 | 14. 0.16 | 24.0 | 99.0 | 6.2 | 1 | BURMA-CHINA BORDER | 297 |
| 891 | 5/29/76 | 14.11.14 | 28.0 | 95.0 | 3.8 | 3 | INDIA-CHINA BORDER | 313 |
| 892 | 5/29/76 | 14.28.32 | 28.0 | 96.0 | 3.7 | 3 | INDIA-CHINA BORDER | 313 |
| 893 | 5/29/76 | 14.32. 7 | 27.0 | 97.0 | 4.7 | 2 | BURMA | 296 |
| 894 | 5/29/76 | 14.53.10 | 26.0 | 98.0 | 4.4 | 2 | BURMA-CHINA BORDER | 297 |
| 895 | 5/29/76 | 15. 3. 9 | 28.0 | 95.0 | 3.7 | 3 | INDIA-CHINA BORDER | 313 |
| 896 | 5/29/76 | 15.26.15 | 40.0 | 30.0 | 3.4 | 3 | TURKEY | 366 |
| 897 | 5/29/76 | 16. 5.44 | 24.0 | 98.0 | 3.8 | 3 | BURMA-CHINA BORDER | 297 |
| 898 | 5/29/76 | 17. 9.15 | 27.0 | 97.0 | 3.8 | 3 | BURMA | 296 |
| 899 | 5/29/76 | 18.25.53 | 31.0 | 77.0 | 3.2 | 3 | NORTHERN INDIA | 308 |
| 900 | 5/29/76 | 19.37.25 | 28.0 | 96.0 | 5.1 | 2 | INDIA-CHINA BORDER | 313 |
| 901 | 5/29/76 | 21.57.13 | 41.0 | 20.0 | 3.2 | 3 | GREECE-ALBANIA BOR. | 392 |
| 902 | 5/29/76 | 22. 5.19 | 35.0 | 24.0 | 3.5 | 2 | CRETE | 370 |
| 903 | 5/29/76 | 23.12.11 | 37.0 | 140.0 | 4.3 | 2 | HONSHU, JAPAN | 227 |
| 904 | 5/29/76 | 23.31.29 | 25.0 | 99.0 | 3.8 | 3 | YUNNAN PROV. CHINA | 318 |
| 905 | 5/30/76 | 0.40.12 | 28.0 | 99.0 | 3.9 | 3 | BURMA-CHINA BORDER | 297 |
| 906 | 5/30/76 | 3.15.19 | 39.0 | 64.0 | 3.4 | 3 | UZBEK SSR | 339 |
| 907 | 5/30/76 | 4.19. 4 | 27.0 | 97.0 | 4.9 | 2 | BURMA | 296 |
| 908 | 5/30/76 | 4.53.52 | 43.0 | 17.0 | 3.1 | 3 | ADRIATIC SEA | 382 |
| 909 | 5/30/76 | 5.32.34 | 34.0 | 47.0 | 3.7 | 2 | WESTERN IRAN | 347 |
| 910 | 5/30/76 | 8. 1.48 | 52.0 | 150.0 | 4.0 | 1 | OEC KAMCHATKA | 219 |
| 911 | 5/30/76 | 13.11.47 | 53.0 | 157.0 | 4.3 | 1 | KAMCHATKA | 217 |
| 912 | 5/30/76 | 13.46.11 | 41.0 | 21.0 | 3.3 | 2 | GREECE-ALBANIA BOR. | 392 |
| 913 | 5/30/76 | 16.27.21 | 41.0 | 21.0 | 3.2 | 2 | GREECE-ALBANIA BOR. | 392 |
| 914 | 5/30/76 | 17.31.18 | 34.0 | 48.0 | 3.3 | 3 | WESTERN IRAN | 347 |

## TABLE A-1

## DATA BASE

## (PAGE 6 OF 16)

| EVNO | DATE | TIME | LAT. | LONG. | MB | Q | LOCATION | SUBREG |
|---|---|---|---|---|---|---|---|---|
| 915 | 5/30/76 | 19.43.39 | 25.0 | 97.0 | 3.7 | 3 | BURMA-CHINA BORDER | 297 |
| 916 | 5/30/76 | 21.12.43 | 43.0 | 13.0 | 3.2 | 3 | CENTRAL ITALY | 381 |
| 917 | 5/30/76 | 22.16.20 | 41.0 | 77.0 | 3.8 | 3 | KIRGIZ-SINKIANG BOR. | 320 |
| 918 | 5/30/76 | 22.31.31 | 24.0 | 98.0 | 4.4 | 1 | BURMA-CHINA BORDER | 297 |
| 919 | 5/31/76 | 4.57.10 | 36.0 | 51.0 | 3.9 | 3 | IRAN | 348 |
| 920 | 5/31/76 | 5. 8.35 | 25.0 | 99.0 | 5.3 | 1 | YUNNAN PROV. CHINA | 318 |
| 921 | 5/31/76 | 8. 6. 7 | 32.0 | 61.0 | 4.6 | 2 | IRAN | 348 |
| 922 | 5/31/76 | 13.17.19 | 47.0 | 154.0 | 4.6 | 1 | KURILE ISLANDS | 221 |
| 923 | 5/31/76 | 18.35.35 | 28.0 | 96.0 | 5.1 | 2 | INDIA-CHINA BORDER | 313 |
| 924 | 5/31/76 | 20.31.48 | 38.0 | 21.0 | 3.1 | 3 | IONIAN SEA | 399 |
| 925 | 5/31/76 | 20.51.38 | 43.0 | 150.0 | 3.6 | 3 | KURILE ISLANDS REG. | 222 |
| 926 | 6/ 1/76 | 1.37.41 | 40.0 | 29.0 | 2.8 | 3 | TURKEY | 366 |
| 927 | 6/ 1/76 | 1.59. 2 | 27.0 | 97.0 | 3.9 | 3 | BURMA | 296 |
| 928 | 6/ 1/76 | 10.59.16 | 28.0 | 94.0 | 4.9 | 1 | INDIA-CHINA BORDER | 313 |
| 929 | 6/ 1/76 | 20.39.35 | 27.0 | 97.0 | 4.0 | 3 | BURMA | 296 |
| 930 | 6/ 2/76 | 5.49.27 | 41.0 | 142.0 | 5.1 | 1 | NEC HONSHU JAPAN | 228 |
| 931 | 6/ 2/76 | 16.28.29 | 38.0 | 21.0 | 2.9 | 3 | IONIAN SEA | 399 |
| 932 | 6/ 2/76 | 18. 5. 3 | 30.0 | 51.0 | 4.1 | 1 | IRAN | 348 |
| 933 | 6/ 2/76 | 21.58.49 | 49.0 | 24.0 | 3.1 | 3 | RUMANIA | 358 |
| 934 | 6/ 3/76 | 18. 5.14 | 24.0 | 98.0 | 4.5 | 3 | BURMA-CHINA BORDER | 297 |
| 935 | 6/ 3/76 | 21.36.54 | 40.0 | 30.0 | 3.9 | 3 | TURKEY | 366 |
| 936 | 6/ 4/76 | 5. 7.48 | 35.0 | 48.0 | 3.5 | 3 | WESTERN IRAN | 347 |
| 937 | 6/ 4/76 | 5.26.59 | 39.0 | 142.0 | 3.9 | 2 | NEC HONSHU JAPAN | 228 |
| 938 | 6/ 4/76 | 5.44.52 | 38.0 | 21.0 | 3.0 | 3 | IONIAN SEA | 399 |
| 939 | 6/ 4/76 | 6.28.50 | 41.0 | 21.0 | 3.6 | 2 | GREECE-ALBANIA BORDE | 392 |
| 940 | 6/ 4/76 | 9.23.45 | 47.0 | 43.0 | 3.0 | 3 | SW RUSSIA | 357 |
| 941 | 6/ 4/76 | 11.13.26 | 41.0 | 143.0 | 4.3 | 2 | NEC HONSHU JAPAN | 228 |
| 942 | 6/ 5/76 | 10.46.24 | 28.0 | 95.0 | 3.9 | 2 | INDIA-CHINA BORDER | 313 |
| 943 | 6/ 5/76 | 14.21.29 | 41.0 | 21.0 | 3.6 | 2 | GREECE-ALBANIA BOR | 392 |
| 944 | 6/ 5/76 | 20.30.38 | 41.0 | 21.0 | 3.7 | 2 | GREECE-ALBANIA BOR | 392 |
| 945 | 6/ 5/76 | 22.22.27 | 41.0 | 21.0 | 3.9 | 2 | GREECE-ALBANIA BOR | 392 |
| 946 | 6/ 6/76 | 13.51.44 | 47.0 | 154.0 | 4.1 | 2 | KURILE IS | 221 |
| 947 | 6/ 6/76 | 14. 1.13 | 35.0 | 140.0 | 5.0 | 1 | NSC HONSHU JAPAN | 230 |
| 948 | 6/ 6/76 | 14. 6.59 | 38.0 | 21.0 | 3.1 | 3 | IONIAN SEA | 399 |
| 949 | 6/ 6/76 | 14.43.53 | 38.0 | 21.0 | 3.9 | 2 | IONIAN SEA | 399 |
| 950 | 6/ 7/76 | 4.31.41 | 39.0 | 74.0 | 3.7 | 3 | S SINKIANG PROV | 321 |
| 951 | 6/ 7/76 | 10.45.49 | 38.0 | 21.0 | 2.7 | 3 | IONIAN SEA | 399 |
| 952 | 6/ 7/76 | 11.59.30 | 39.0 | 64.0 | 3.7 | 2 | TURKMEN SSR | 340 |
| 953 | 6/ 8/76 | 7.37.22 | 27.0 | 94.0 | 3.7 | 3 | EASTERN INDIA | 317 |
| 954 | 6/ 8/76 | 18.33.43 | 38.0 | 21.0 | 3.6 | 2 | IONIAN SEA | 399 |

THIS PAGE IS BEST QUALITY PRACTICABLE
FROM COPY FURNISHED TO DDC

## TABLE A-1

## DATA BASE
(PAGE 7 OF 16)

| EVNO | DATE | TIME | LAT. | LONG. | MB | Q | LOCATION | SUBREG |
|---|---|---|---|---|---|---|---|---|
| 955 | 6/ 8/76 | 22.31.31 | 33.0 | 89.0 | 4.0 | 3 | TIBET | 306 |
| 956 | 6/ 8/76 | 23.15. 6 | 28.0 | 96.0 | 4.3 | 2 | INDIA-CHINA BORDER | 313 |
| 957 | 6/ 9/76 | 0.20.56 | 27.0 | 97.0 | 5.7 | 1 | BURMA | 296 |
| 958 | 6/ 9/76 | 3. 2.48 | 50.0 | 81.0 | 5.3 | 1 | EASTERN KAZAKH SSR | 329 |
| 959 | 6/ 9/76 | 10. 2.42 | 40.0 | 29.0 | 4.4 | 2 | TURKEY | 366 |
| 960 | 6/ 9/76 | 17.41.14 | 31.0 | 96.0 | 4.2 | 3 | TIBET | 306 |
| 961 | 6/ 9/76 | 18.47.49 | 43.0 | 13.0 | 3.7 | 3 | CENTRAL ITALY | 381 |
| 962 | 6/ 9/76 | 20.58.54 | 40.0 | 64.0 | 3.6 | 2 | UZBEK SSR | 339 |
| 963 | 6/ 9/76 | 23.41.27 | 38.0 | 21.0 | 2.8 | 3 | IONIAN SEA | 399 |
| 964 | 6/10/76 | 0.38.30 | 27.0 | 94.0 | 3.6 | 3 | EASTERN INDIA | 317 |
| 965 | 6/10/76 | 5.55.12 | 35.0 | 24.0 | 3.9 | 2 | CRETE | 370 |
| 966 | 6/11/76 | 0.52.44 | 40.0 | 30.0 | 3.7 | 2 | TURKEY | 366 |
| 967 | 6/11/76 | 5. 8.50 | 40.0 | 76.0 | 4.6 | 1 | KIRGIZ-SINKIANG BOR | 320 |
| 968 | 6/11/76 | 9. 7.54 | 47.0 | 42.0 | 3.1 | 3 | SW RUSSIA | 357 |
| 969 | 6/11/76 | 9.55.19 | 39.0 | 30.0 | 3.8 | 3 | TURKEY | 366 |
| 970 | 6/11/76 | 10. 5.31 | 39.0 | 30.0 | 3.4 | 3 | TURKEY | 366 |
| 971 | 6/11/76 | 10.25.56 | 38.0 | 21.0 | 2.7 | 3 | IONIAN SEA | 399 |
| 972 | 6/11/76 | 18.27. 0 | 43.0 | 17.0 | 3.9 | 2 | ADRIATIC SEA | 392 |
| 973 | 6/12/76 | 0.11.49 | 37.0 | 21.0 | 2.8 | 3 | MEDITERRANEAN SEA | 400 |
| 974 | 6/12/76 | 0.59.28 | 38.0 | 22.0 | 5.3 | 2 | GREECE | 364 |
| 975 | 6/12/76 | 2.41.16 | 35.0 | 24.0 | 3.8 | 2 | CRETE | 370 |
| 976 | 6/12/76 | 3.41.37 | 37.0 | 22.0 | 3.9 | 3 | SOUTHERN GREECE | 368 |
| 977 | 6/12/76 | 4.55.26 | 41.0 | 21.0 | 4.0 | 2 | GREECE-ALBANIA BOR | 392 |
| 978 | 6/12/76 | 10.25.33 | 41.0 | 20.0 | 3.5 | 2 | ALBANIA | 391 |
| 979 | 6/13/76 | 0.20.24 | 40.0 | 19.0 | 3.9 | 2 | GREECE-ALBANIA BOR | 392 |
| 980 | 6/13/76 | 1.42.41 | 41.0 | 63.0 | 3.6 | 3 | UZBEK SSR | 339 |
| 981 | 6/13/76 | 8.25. 7 | 29.0 | 86.0 | 3.8 | 3 | TIBET | 306 |
| 982 | 6/13/76 | 11.47. 2 | 32.0 | 85.0 | 3.8 | 3 | TIBET | 306 |
| 983 | 6/13/76 | 16.34. 0 | 35.0 | 139.0 | 3.8 | 2 | HONSHU JAPAN | 227 |
| 984 | 6/13/76 | 16.54.17 | 27.0 | 57.0 | 3.6 | 3 | SOUTHERN IRAN | 353 |
| 985 | 6/13/76 | 17.20.39 | 38.0 | 21.0 | 3.1 | 3 | IONIAN SEA | 399 |
| 986 | 6/14/76 | 0.16.39 | 33.0 | 94.0 | 3.8 | 3 | TSINGHAI PROV CHINA | 325 |
| 987 | 6/14/76 | 6.52.43 | 40.0 | 29.0 | 4.4 | 2 | TURKEY | 366 |
| 988 | 6/14/76 | 11.10.19 | 33.0 | 86.0 | 4.1 | 2 | TIBET | 306 |
| 989 | 6/14/76 | 20.14.34 | 53.0 | 157.0 | 4.8 | 1 | KAMCHATKA | 217 |
| 990 | 6/15/76 | 0. 9.11 | 41.0 | 21.0 | 3.4 | 3 | ALBANIA | 391 |
| 991 | 6/15/76 | 0. 9.55 | 40.0 | 27.0 | 3.6 | 2 | TURKEY | 366 |
| 992 | 6/15/76 | 6.38. 4 | 31.0 | 96.0 | 3.7 | 3 | TIBET | 306 |
| 993 | 6/15/76 | 12.21.57 | 27.0 | 95.0 | 3.9 | 3 | BURMA-INDIA BOR | 294 |
| 994 | 6/15/76 | 12.46.25 | 35.0 | 24.0 | 4.4 | 2 | CRETE | 370 |

## TABLE A-1

## DATA BASE

(PAGE 8 OF 16)

| EVNO | DATE | TIME | LAT. | LONG. | MB | Q | LOCATION | SUBREG |
|---|---|---|---|---|---|---|---|---|
| 995 | 6/15/76 | 16.22.33 | 46.0 | 151.0 | 3.9 | 2 | KURILE IS | 221 |
| 996 | 6/15/76 | 18. 1.19 | 40.0 | 29.0 | 3.4 | 3 | TURKEY | 366 |
| 997 | 6/15/76 | 20.33.59 | 35.0 | 140.0 | 4.9 | 1 | NEC HONSHU JAPAN | 230 |
| 998 | 6/16/76 | 0. 5.23 | 37.0 | 139.0 | 4.3 | 2 | HONSHU JAPAN | 227 |
| 999 | 6/16/76 | 4.20.13 | 36.0 | 77.0 | 3.7 | 2 | EASTERN KASHMIR | 302 |
| 1000 | 6/16/76 | 13.33.59 | 48.0 | 47.0 | 3.2 | 3 | SW RUSSIA | 357 |
| 1001 | 6/16/76 | 13.50.47 | 27.0 | 89.0 | 3.8 | 2 | SIKKIM | 311 |
| 1002 | 6/17/76 | 18.39.56 | 33.0 | 143.0 | 4.0 | 2 | OFF E C HONSHU | 229 |
| 1003 | 6/18/76 | 22.19.15 | 36.0 | 139.0 | 4.3 | 2 | HONSHU JAPAN | 227 |
| 1004 | 6/19/76 | 8.52.28 | 36.0 | 22.0 | 3.5 | 3 | MEDITERRANEAN SEA | 400 |
| 1005 | 6/19/76 | 14.25.33 | 40.0 | 29.0 | 3.5 | 3 | TURKEY | 366 |
| 1006 | 6/19/76 | 16.12.16 | 41.0 | 39.0 | 3.6 | 3 | TURKEY | 366 |
| 1007 | 6/19/76 | 16.17.23 | 39.0 | 64.0 | 3.5 | 3 | TURKMEN SSR | 340 |
| 1008 | 6/20/76 | 2.33.28 | 27.0 | 97.0 | 4.4 | 3 | BURMA | 296 |
| 1009 | 6/20/76 | 2.48. 7 | 39.0 | 21.0 | 3.4 | 3 | GREECE | 364 |
| 1010 | 6/20/76 | 4.51.41 | 41.0 | 21.0 | 4.3 | 2 | GREECE-ALBANIA BOR | 392 |
| 1011 | 6/20/76 | 15.28.32 | 28.0 | 95.0 | 4.0 | 3 | INDIA-CHINA BOR | 313 |
| 1012 | 6/20/76 | 15.30. 2 | 27.0 | 97.0 | 4.3 | 2 | BURMA | 296 |
| 1013 | 6/20/76 | 23.33.56 | 41.0 | 63.0 | 5.4 | 1 | UZBEK SSR | 339 |
| 1014 | 6/21/76 | 1.28.17 | 41.0 | 77.0 | 3.8 | 2 | KIRGIZ-SINKIANG BOR | 320 |
| 1015 | 6/21/76 | 9.11.27 | 39.0 | 48.0 | 3.7 | 2 | NW IRAN-USSR BORDER | 344 |
| 1016 | 6/21/76 | 10.59.40 | 37.0 | 23.0 | 3.8 | 2 | SOUTHERN GREECE | 368 |
| 1017 | 6/21/76 | 20. 4.53 | 34.0 | 141.0 | 4.3 | 2 | HONSHU JAPAN | 227 |
| 1018 | 6/22/76 | 18.48.53 | 32.0 | 56.0 | 3.4 | 3 | IRAN | 348 |
| 1075 | 7/ 8/76 | 10.41.39 | 45.0 | 36.0 | 2.7 | 3 | CRIMEA REGION | 361 |
| 1076 | 7/ 8/76 | 11. 2.34 | 35.0 | 24.0 | 3.4 | 3 | CRETE | 370 |
| 1077 | 7/ 8/76 | 15.20. 9 | 35.0 | 24.0 | 4.5 | 2 | CRETE | 370 |
| 1079 | 7/ 8/76 | 18.15.53 | 31.0 | 51.0 | 3.4 | 3 | IRAN | 348 |
| 1240 | 8/ 4/76 | 9.28.17 | 27.0 | 98.0 | 4.0 | 3 | BURMA | 296 |
| 1241 | 8/ 5/76 | 4.26.40 | 49.0 | 152.0 | 3.9 | 3 | KURILE IS | 221 |
| 1242 | 8/ 5/76 | 10.24.12 | 28.0 | 92.0 | 4.4 | 2 | INDIA-CHINA BOR REG | 313 |
| 1243 | 8/ 5/76 | 18.26.23 | 45.0 | 148.0 | 4.0 | 2 | KURILE IS | 221 |
| 1244 | 8/ 6/76 | 20. 0. 1 | 39.0 | 143.0 | 3.6 | 3 | NEAR E COAST HONSHU | 228 |
| 1245 | 8/ 7/76 | 18.43. 1 | 46.0 | 153.0 | 3.7 | 3 | KURILE IS | 221 |
| 1246 | 8/ 8/76 | 1.56.59 | 48.0 | 154.0 | 4.2 | 3 | KURILE IS | 221 |
| 1247 | 8/ 8/76 | 22.41.33 | 40.0 | 119.0 | 4.6 | 2 | NE CHINA | 658 |
| 1248 | 8/ 8/76 | 23.12. 7 | 41.0 | 21.0 | 3.2 | 3 | GREECE-ALBANIA BOR R | 392 |
| 1249 | 8/ 8/76 | 23.36. 8 | 40.0 | 121.0 | 3.6 | 3 | NE CHINA | 658 |
| 1250 | 8/ 9/76 | 1.12.27 | 38.0 | 21.0 | 2.7 | 3 | IONIAN SEA | 399 |
| 1251 | 8/ 9/76 | 3.20.32 | 47.0 | 152.0 | 3.4 | 3 | KURILE IS | 221 |

# TABLE A-1

## DATA BASE

## (PAGE 9 OF 16)

| EVNO | DATE | TIME | LAT. | LONG. | MB | Q | LOCATION | SUBREG |
|---|---|---|---|---|---|---|---|---|
| 1252 | 8/ 9/76 | 4.35.41 | 39.0 | 64.0 | 3.9 | 2 | UZBEK SSR | 339 |
| 1253 | 8/ 9/76 | 5.46. 6 | 33.0 | 145.0 | 3.4 | 3 | OFF E COAST HONSHU | 229 |
| 1254 | 8/ 9/76 | 8.50.46 | 33.0 | 97.0 | 3.8 | 3 | TSINGHAI PROV | 325 |
| 1255 | 8/ 9/76 | 10.29. 0 | 33.0 | 97.0 | 4.4 | 2 | TSINGHAI PROV | 325 |
| 1256 | 8/10/76 | 6.32.20 | 29.0 | 78.0 | 3.7 | 2 | NORTHERN INDIA | 308 |
| 1257 | 8/10/76 | 19.18.26 | 52.0 | 152.0 | 3.4 | 3 | OEC KAMCHATKA | 219 |
| 1258 | 8/10/76 | 22.38.26 | 42.0 | 119.0 | 3.4 | 3 | NE CHINA | 658 |
| 1259 | 8/10/76 | 23.32.32 | 30.0 | 79.0 | 3.2 | 3 | NORTHERN INDIA | 308 |
| 1260 | 8/11/76 | 0.15. 9 | 38.0 | 21.0 | 2.6 | 3 | IONIAN SEA | 399 |
| 1261 | 8/11/76 | 6.57.31 | 34.0 | 91.0 | 3.8 | 3 | TSINGHAI PROV | 325 |
| 1262 | 8/11/76 | 9.40.45 | 46.0 | 153.0 | 3.6 | 2 | KURILE IS REG | 222 |
| 1263 | 8/12/76 | 6.17.58 | 38.0 | 13.0 | 3.1 | 2 | SICILY | 398 |
| 1264 | 8/12/76 | 14. 1.22 | 52.0 | 44.0 | 3.1 | 3 | SW RUSSIA | 357 |
| 1265 | 8/12/76 | 23.26.53 | 27.0 | 97.0 | 6.3 | 1 | BURMA-INDIA BOR REG | 294 |
| 1266 | 8/12/76 | 23.28.18 | 43.0 | 144.0 | 5.0 | 2 | HOKKAIDO JAPAN REG | 224 |
| 1267 | 8/13/76 | 0. 6.35 | 28.0 | 96.0 | 4.0 | 2 | INDIA-CHINA BOR REG | 313 |
| 1268 | 8/13/76 | 2.58.23 | 29.0 | 95.0 | 3.7 | 2 | INDIA-CHINA BOR REG | 313 |
| 1269 | 8/13/76 | 23.22.13 | 35.0 | 138.0 | 4.5 | 1 | NEAR S COAST HONSHU | 230 |
| 1270 | 8/13/76 | 23.55.33 | 28.0 | 96.0 | 3.7 | 2 | INDIA-CHINA BOR REG | 313 |
| 1271 | 8/13/76 | 23.56.10 | 40.0 | 121.0 | 3.9 | 3 | NE CHINA | 658 |
| 1272 | 8/14/76 | 1.23.40 | 28.0 | 96.0 | 4.4 | 1 | INDIA-CHINA BOR REG | 313 |
| 1273 | 8/14/76 | 4.33.34 | 35.0 | 27.0 | 3.2 | 3 | CRETE | 370 |
| 1274 | 8/14/76 | 7.10.49 | 40.0 | 121.0 | 3.5 | 3 | NE CHINA | 658 |
| 1275 | 8/14/76 | 8.22.50 | 32.0 | 62.0 | 3.7 | 2 | SW AFGHANISTAN | 350 |
| 1276 | 8/14/76 | 8.48.35 | 45.0 | 40.0 | 2.8 | 3 | SW RUSSIA | 357 |
| 1277 | 8/14/76 | 9.26.46 | 31.0 | 53.0 | 3.3 | 3 | IRAN | 348 |
| 1278 | 8/14/76 | 10.16.47 | 43.0 | 29.0 | 3.1 | 3 | BLACK SEA | 360 |
| 1279 | 8/14/76 | 16. 2.38 | 40.0 | 121.0 | 4.2 | 2 | NE CHINA | 658 |
| 1280 | 8/14/76 | 22.56.22 | 28.0 | 51.0 | 3.5 | 3 | SOUTHERN IRAN | 353 |
| 1281 | 8/15/76 | 3.40.48 | 42.0 | 141.0 | 4.0 | 2 | HOKKAIDO JAPAN REG | 224 |
| 1282 | 8/15/76 | 5.18.51 | 21.0 | 94.0 | 3.7 | 2 | BURMA | 296 |
| 1283 | 8/15/76 | 9.37. 6 | 36.0 | 74.0 | 3.6 | 2 | NW KASHMIR | 720 |
| 1284 | 8/15/76 | 10.21.17 | 40.0 | 119.0 | 4.0 | 3 | NE CHINA | 658 |
| 1285 | 8/15/76 | 10.28.32 | 38.0 | 117.0 | 3.9 | 3 | NE CHINA | 658 |
| 1286 | 8/15/76 | 10.53. 9 | 38.0 | 119.0 | 3.8 | 3 | NE CHINA | 658 |
| 1287 | 8/15/76 | 12.42.48 | 36.0 | 139.0 | 3.5 | 3 | HONSHU JAPAN | 227 |
| 1288 | 8/15/76 | 14.32.58 | 39.0 | 119.0 | 3.6 | 2 | NE CHINA | 658 |
| 1289 | 8/15/76 | 22.39.44 | 39.0 | 118.0 | 3.9 | 2 | NE CHINA | 658 |
| 1290 | 8/16/76 | 2. 6.21 | 48.0 | 152.0 | 3.2 | 3 | KURILE IS | 221 |
| 1291 | 8/16/76 | 4.11.52 | 39.0 | 43.0 | 3.5 | 3 | NW IRAN | 345 |

## TABLE A-1

## DATA BASE
(PAGE 10 OF 16)

| EVNO | DATE | TIME | LAT. | LONG. | MB | Q | LOCATION | SUBREG |
|---|---|---|---|---|---|---|---|---|
| 1292 | 8/16/76 | 7.25.32 | 36.0 | 79.0 | 3.7 | 2 | KASHMIR-SINKIANG BOR | 324 |
| 1293 | 8/16/76 | 8.42. 8 | 35.0 | 24.0 | 3.5 | 3 | CRETE | 370 |
| 1294 | 8/16/76 | 9.34.51 | 46.0 | 45.0 | 2.9 | 3 | SW RUSSIA | 357 |
| 1295 | 8/16/76 | 12.29.28 | 52.0 | 159.0 | 5.2 | 1 | NEC KAMCHATKA | 218 |
| 1296 | 8/16/76 | 14. 6.54 | 34.0 | 104.0 | 6.2 | 1 | KANSU PROV CHINA | 322 |
| 1297 | 8/16/76 | 14.56.25 | 31.0 | 105.0 | 3.8 | 2 | SZECHWAN CHINA | 307 |
| 1298 | 8/16/76 | 14.57.40 | 35.0 | 103.0 | 3.8 | 0 | TSINGHAI PROV CHINA | 325 |
| 1299 | 8/16/76 | 15. 0.54 | 33.0 | 105.0 | 4.5 | 1 | SZECHWAN PROV CHINA | 307 |
| 1300 | 8/16/76 | 15.26.14 | 33.0 | 105.0 | 4.4 | 1 | SZECHWAN PROV CHINA | 307 |
| 1301 | 8/16/76 | 18.15.54 | 35.0 | 103.0 | 4.0 | 2 | TSINGHAI PROV CHINA | 325 |
| 1302 | 8/16/76 | 18.54.35 | 33.0 | 105.0 | 3.4 | 3 | SZECHWAN PROV CHINA | 307 |
| 1303 | 8/16/76 | 20.26.50 | 33.0 | 104.0 | 3.7 | 2 | SZECHAN PROV CHINA | 307 |
| 1304 | 8/16/76 | 21.20.17 | 40.0 | 117.0 | 3.4 | 3 | NE CHINA | 658 |
| 1305 | 8/16/76 | 21.23.34 | 26.0 | 81.0 | 3.2 | 3 | NORTHERN INDIA | 308 |
| 1306 | 8/16/76 | 21.30.32 | 31.0 | 105.0 | 3.9 | 2 | SZECHWAN PROV CHINA | 307 |
| 1307 | 8/16/76 | 22. 6.38 | 33.0 | 105.0 | 3.8 | 2 | SZECHWAN PROV CHINA | 307 |
| 1308 | 8/16/76 | 22.41.26 | 41.0 | 39.0 | 3.1 | 3 | TURKEY | 366 |
| 1309 | 8/17/76 | 2. 3. 5 | 43.0 | 149.0 | 4.4 | 1 | KURILE ISLANDS | 222 |
| 1310 | 8/17/76 | 2. 3.33 | 39.0 | 64.0 | 3.8 | 2 | UZBEK SSR | 339 |
| 1311 | 8/17/76 | 2.27.43 | 35.0 | 103.0 | 3.4 | 3 | TSINGHAI PROV CHINA | 325 |
| 1312 | 8/17/76 | 3.48.27 | 38.0 | 100.0 | 3.6 | 3 | TSINGHAI PROV CHINA | 325 |
| 1313 | 8/17/76 | 5.19.54 | 35.0 | 103.0 | 3.4 | 2 | TSINGHAI PROV CHINA | 325 |
| 1314 | 8/17/76 | 17.19. 9 | 35.0 | 138.0 | 4.8 | 1 | HONSHU JAPAN | 227 |
| 1315 | 8/17/76 | 22.17.31 | 34.0 | 104.0 | 3.9 | 2 | KANSU PROV CHINA | 322 |
| 1316 | 8/18/76 | 0.58.24 | 39.0 | 24.0 | 3.6 | 3 | AEGEAN SEA | 365 |
| 1317 | 8/18/76 | 2.25.37 | 38.0 | 21.0 | 2.7 | 3 | IONIAN SEA | 399 |
| 1318 | 8/18/76 | 2.30.53 | 39.0 | 94.0 | 3.7 | 2 | INDIA-CHINA BOR REG | 313 |
| 1319 | 8/18/76 | 17. 6.11 | 35.0 | 27.0 | 3.8 | 3 | CRETE | 370 |
| 1320 | 8/19/76 | 7.52.29 | 53.0 | 158.0 | 3.9 | 2 | NEC KAMCHATKA | 218 |
| 1321 | 8/19/76 | 12.49.45 | 33.0 | 105.0 | 5.2 | 1 | SZECHWAN PROV CHINA | 307 |
| 1322 | 8/19/76 | 19. 2.16 | 41.0 | 21.0 | 3.4 | 3 | GREECE | 364 |
| 1323 | 8/20/76 | 1. 9.43 | 43.0 | 141.0 | 3.6 | 2 | HOKKAIDO, JAPAN REG. | 228 |
| 1324 | 8/20/76 | 15.41.44 | 40.0 | 29.0 | 3.0 | 3 | TURKEY | 366 |
| 1325 | 8/20/76 | 19. 5.25 | 36.0 | 74.0 | 3.4 | 2 | NW KASHMIR | 720 |
| 1326 | 8/20/76 | 21. 1.23 | 37.0 | 77.5 | 3.4 | 3 | KASHMIR-SINKIANG BOR | 324 |
| 1327 | 8/20/76 | 22.18. 2 | 39.0 | 82.0 | 3.2 | 3 | S SINKIANG PROV | 321 |
| 1328 | 8/20/76 | 23.43.36 | 43.0 | 148.0 | 4.2 | 2 | OFF COAST HOKKAIDO | 225 |
| 1329 | 8/21/76 | 8. 9.20 | 26.0 | 95.0 | 4.1 | 2 | BURMA-INDIA BOR REG | 294 |
| 1330 | 8/21/76 | 20. 2. 2 | 40.0 | 121.0 | 3.4 | 3 | NE CHINA | 658 |
| 1331 | 8/21/76 | 21.49.54 | 32.0 | 104.0 | 6.1 | 1 | SZECHWAN PROV CHINA | 307 |

THIS PAGE IS BEST QUALITY PRACTICABLE
FROM COPY FURNISHED TO DDC

## TABLE A-1

## DATA BASE

(PAGE 11 OF 16)

| EVNO | DATE | TIME | LAT. | LONG. | MB | Q | LOCATION | SUBREG |
|---|---|---|---|---|---|---|---|---|
| 1332 | 8/21/76 | 22.40.50 | 33.0 | 105.0 | 3.7 | 3 | SZECHWAN PROV CHINA | 307 |
| 1333 | 8/22/76 | 3. 5.15 | 41.0 | 39.0 | 3.6 | 2 | TURKEY | 366 |
| 1334 | 8/22/76 | 8.48.20 | 43.0 | 17.0 | 3.4 | 2 | ADRIATIC SEA | 382 |
| 1335 | 8/22/76 | 9.42. 8 | 40.0 | 23.0 | 2.6 | 3 | GREECE | 364 |
| 1336 | 8/22/76 | 13.19.55 | 33.0 | 105.0 | 4.2 | 2 | SZECHWAN PROV CHINA | 307 |
| 1337 | 8/22/76 | 13.28.56 | 40.0 | 29.0 | 4.8 | 2 | TURKEY | 366 |
| 1338 | 8/22/76 | 14.46.19 | 38.0 | 14.0 | 3.2 | 3 | SICILY | 398 |
| 1339 | 8/22/76 | 16. 6.17 | 41.0 | 21.0 | 3.0 | 2 | GREECE-ALBANIA BOR | 392 |
| 1340 | 8/22/76 | 21.55.15 | 45.0 | 34.0 | 2.6 | 3 | CRIMEA REG | 361 |
| 1341 | 8/23/76 | 1.52. 9 | 27.0 | 96.0 | 3.9 | 2 | BURMA-INDIA BOR REG | 294 |
| 1342 | 8/23/76 | 3.15.40 | 41.0 | 20.0 | 4.3 | 2 | ALBANIA | 391 |
| 1343 | 8/23/76 | 3.30.22 | 34.0 | 103.0 | 6.1 | 1 | KANSU PROV CHINA | 322 |
| 1344 | 8/23/76 | 4.31.11 | 33.0 | 105.0 | 3.9 | 2 | SZECHWAN PROV CHINA | 307 |
| 1345 | 8/23/76 | 4.38.11 | 35.0 | 27.0 | 3.0 | 3 | CRETE | 370 |
| 1346 | 8/23/76 | 6.43.30 | 33.0 | 105.0 | 3.8 | 2 | SZECHWAN PROV CHINA | 307 |
| 1347 | 8/23/76 | 8.58.37 | 35.0 | 103.0 | 4.0 | 2 | KANSU PROV. CHINA | 322 |
| 1348 | 8/23/76 | 10.17. 6 | 35.0 | 140.0 | 3.9 | 2 | NEAR E COAST HONSHU | 228 |
| 1349 | 8/23/76 | 12.12.17 | 46.0 | 152.0 | 3.4 | 3 | KURILE IS | 221 |
| 1350 | 8/23/76 | 17.15.37 | 38.0 | 119.0 | 4.1 | 2 | NE CHINA | 658 |
| 1351 | 8/23/76 | 20.35.11 | 36.0 | 75.0 | 3.4 | 3 | NW KASHMIR | 720 |
| 1352 | 8/23/76 | 21. 2.29 | 35.0 | 103.0 | 4.2 | 2 | TSINGHAI PROV CHINA | 325 |
| 1353 | 8/24/76 | 0.52.16 | 32.0 | 49.0 | 3.3 | 3 | WESTERN IRAN | 347 |
| 1354 | 8/24/76 | 4.31.47 | 29.0 | 102.0 | 3.8 | 2 | SZECHWAN PROV CHINA | 307 |
| 1355 | 8/24/76 | 5.52.45 | 37.0 | 142.0 | 4.3 | 2 | NEAR COAST HONSHU | 228 |
| 1356 | 8/24/76 | 7.26.46 | 36.0 | 22.0 | 3.3 | 3 | MEDITERRANEAN SEA | 400 |
| 1357 | 8/24/76 | 8. 0. 6 | 38.0 | 21.0 | 3.0 | 3 | IONIAN SEA | 399 |
| 1358 | 8/24/76 | 16.10.36 | 41.0 | 21.0 | 3.1 | 2 | GREECE-ALBANIA BOR | 392 |
| 1359 | 8/24/76 | 23.26. 6 | 42.0 | 124.0 | 3.8 | 3 | NE CHINA | 658 |
| 1360 | 8/25/76 | 1.56.19 | 35.0 | 27.0 | 3.3 | 3 | CRETE | 370 |
| 1361 | 8/25/76 | 17.31.38 | 37.0 | 119.0 | 4.2 | 2 | NE CHINA | 658 |
| 1362 | 8/26/76 | 12. 5.31 | 42.0 | 142.0 | 4.2 | 2 | HOKKAIDO JAPAN REG | 224 |
| 1363 | 8/27/76 | 2.32.14 | 45.0 | 149.0 | 4.7 | 1 | KURILE IS | 221 |
| 1364 | 8/27/76 | 2.53.27 | 30.0 | 54.0 | 3.5 | 3 | IRAN | 348 |
| 1365 | 8/27/76 | 16. 1.31 | 38.0 | 78.0 | 3.6 | 3 | SOUTHERN SINKIANG | 321 |
| 1366 | 8/27/76 | 22.45.43 | 35.0 | 27.0 | 3.4 | 3 | CRETE | 370 |
| 1367 | 8/27/76 | 23.57.37 | 39.0 | 64.0 | 3.7 | 3 | UZBEK SSR | 339 |
| 1368 | 8/28/76 | 2.56.43 | 49.0 | 81.0 | 6.0 | 1 | EASTERN KAZAKH SSR | 329 |
| 1369 | 8/28/76 | 6.33.53 | 39.0 | 121.0 | 4.3 | 2 | NE CHINA | 658 |
| 1370 | 8/28/76 | 10.32.53 | 36.0 | 101.0 | 3.9 | 3 | TSINGHAI PROV CHINA | 325 |
| 1371 | 8/28/76 | 16.23.48 | 45.0 | 117.0 | 4.1 | 3 | NE CHINA | 658 |

## TABLE A-1

## DATA BASE
(PAGE 12 OF 16)

| EVNO | DATE | TIME | LAT. | LONG. | MB | Q | LOCATION | SUBREG |
|---|---|---|---|---|---|---|---|---|
| 1372 | 8/28/76 | 18.59.55 | 35.0 | 103.0 | 3.8 | 3 | TSINGHAI PROV CHINA | 325 |
| 1373 | 8/28/76 | 23. 1.12 | 38.0 | 78.0 | 4.2 | 1 | S SINKIANG PROV | 321 |
| 1374 | 8/29/76 | 0.14.56 | 26.0 | 91.0 | 3.3 | 3 | EASTERN INDIA | 317 |
| 1375 | 8/29/76 | 1.51.25 | 41.0 | 143.0 | 3.7 | 3 | HOKKAIDO, JAPAN REG. | 224 |
| 1376 | 8/29/76 | 16.49.52 | 36.0 | 140.0 | 3.7 | 3 | NEAR S COAST HONSHU | 230 |
| 1377 | 8/29/76 | 19.31. 7 | 43.0 | 20.0 | 3.0 | 2 | YUGOSLAVIA | 383 |
| 1378 | 8/29/76 | 20. 1.21 | 31.0 | 47.0 | 4.4 | 2 | IRAN-IRAQ BOR REG | 346 |
| 1379 | 8/29/76 | 23.39. 7 | 44.0 | 142.0 | 4.2 | 2 | HOKKAIDO JAP REG | 224 |
| 1380 | 8/30/76 | 0. 8.18 | 20.0 | 96.0 | 3.9 | 2 | BURMA | 296 |
| 1381 | 8/30/76 | 15.49.47 | 44.0 | 147.0 | 4.3 | 2 | KURILE IS | 221 |
| 1382 | 8/30/76 | 17.41.16 | 42.0 | 143.0 | 4.3 | 2 | HOKKAIDO JAP | 224 |
| 1383 | 8/31/76 | 3.25. 5 | 37.0 | 122.0 | 4.9 | 2 | NE CHINA | 658 |
| 1384 | 8/31/76 | 11.20.23 | 43.0 | 23.0 | 3.3 | 2 | BULGARIA | 359 |
| 1385 | 9/ 1/76 | 1. 7.14 | 35.0 | 103.0 | 4.6 | 2 | TSINGHAI PROV. CHINA | 325 |
| 1386 | 9/ 2/76 | 11.15.10 | 39.0 | 64.0 | 3.7 | 3 | TURKMEN SSR | 340 |
| 1387 | 9/ 2/76 | 19.54. 6 | 32.0 | 49.0 | 4.0 | 2 | WESTERN IRAN | 347 |
| 1388 | 9/ 2/76 | 21.37. 3 | 38.0 | 21.0 | 3.4 | 3 | IONIAN SEA | 399 |
| 1389 | 9/ 3/76 | 9.57.39 | 29.0 | 99.0 | 4.9 | 1 | SZECHWAN PROV. CHINA | 307 |
| 1390 | 9/ 5/76 | 0.14. 6 | 41.0 | 122.0 | 4.3 | 2 | NORTHEASTERN CHINA | 658 |
| 1391 | 9/ 5/76 | 9.54.32 | 36.0 | 80.0 | 3.6 | 3 | KASHMIR-TIBET BORDER | 304 |
| 1392 | 9/ 5/76 | 10.42.16 | 44.0 | 142.0 | 5.0 | 1 | HOKKAIDO JAPAN REG | 224 |
| 1393 | 9/ 5/76 | 16.43. 8 | 31.0 | 51.0 | 5.6 | 1 | IRAN | 348 |
| 1394 | 9/ 5/76 | 20.33.13 | 51.0 | 158.0 | 3.7 | 3 | KURILE ISLANDS | 221 |
| 1395 | 9/ 5/76 | 22. 7.58 | 41.0 | 40.0 | 4.7 | 2 | TURKEY | 366 |
| 1396 | 9/ 6/76 | 7. 7.39 | 36.0 | 64.0 | 3.3 | 3 | TURKMEN-AFGHANISTAN | 342 |
| 1397 | 9/ 6/76 | 11. 2.44 | 46.0 | 48.0 | 3.9 | 3 | SOUTHWESTERN RUSSIA | 357 |
| 1398 | 9/ 6/76 | 16. 4.41 | 31.0 | 51.0 | 4.5 | 1 | IRAN | 348 |
| 1399 | 9/ 6/76 | 17. 1.38 | 37.0 | 122.0 | 4.4 | 2 | NORTHEASTERN CHINA | 658 |
| 1400 | 9/ 7/76 | 3.27.57 | 45.0 | 130.0 | 4.1 | 2 | NORTHEASTERN CHINA | 658 |
| 1401 | 9/ 7/76 | 6. 3.21 | 39.0 | 143.0 | 4.8 | 2 | OEC HONSHU JAPAN | 229 |
| 1402 | 9/ 7/76 | 9.20.27 | 39.0 | 115.0 | 4.1 | 3 | NORTHEASTERN CHINA | 658 |
| 1403 | 9/ 7/76 | 17.37.51 | 43.0 | 23.0 | 3.7 | 2 | BULGARIA | 359 |
| 1404 | 9/ 7/76 | 19.27.18 | 49.0 | 156.0 | 3.5 | 3 | KURILE ISLANDS REG | 222 |
| 1405 | 9/ 8/76 | 17.59.47 | 38.0 | 78.0 | 3.5 | 3 | SOUTHERN SINKIANG PR | 321 |
| 1406 | 9/ 8/76 | 20.13. 4 | 32.0 | 79.0 | 5.0 | 1 | TIBET-INDIA BORDER | 305 |
| 1407 | 9/12/76 | 6.43. 1 | 41.0 | 21.0 | 3.2 | 3 | GREECE-ALBANIA BORD | 392 |
| 1408 | 9/12/76 | 7.29.33 | 41.0 | 103.0 | 3.5 | 3 | NORTHERN CHINA | 323 |
| 1409 | 9/13/76 | 4.16.47 | 35.0 | 27.0 | 3.1 | 2 | CRETE | 370 |
| 1410 | 9/13/76 | 5.45.38 | 40.0 | 120.0 | 3.9 | 3 | NORTHEASTERN CHINA | 658 |
| 1411 | 9/13/76 | 19.41.53 | 44.0 | 12.0 | 3.5 | 3 | CENTRAL ITALY | 381 |

## TABLE A-1

## DATA BASE

(PAGE 13 OF 16)

| EVNO | DATE | TIME | LAT. | LONG. | MB | Q | LOCATION | SUBREG |
|---|---|---|---|---|---|---|---|---|
| 1412 | 9/13/76 | 19.57. 8 | 33.0 | 105.0 | 3.7 | 2 | SZECHWAN PROV. CHINA | 307 |
| 1413 | 9/14/76 | 6.43.52 | 30.0 | 89.0 | 5.2 | 1 | TIBET | 306 |
| 1414 | 9/14/76 | 10.52.19 | 41.0 | 81.0 | 3.7 | 3 | SOUTHERN SINKIANG | 321 |
| 1415 | 9/14/76 | 15.38.31 | 37.0 | 96.0 | 4.3 | 2 | TSINGHAI PROV. CHINA | 325 |
| 1416 | 9/14/76 | 18.23.43 | 27.0 | 86.0 | 3.6 | 3 | NEPAL | 310 |
| 1417 | 9/14/76 | 23.41.35 | 29.0 | 53.0 | 4.4 | 1 | SOUTHERN IRAN | 353 |
| 1418 | 9/15/76 | 8.20.16 | 39.0 | 143.0 | 4.8 | 1 | NEC HONSHU JAPAN | 228 |
| 1419 | 9/15/76 | 9.57.34 | 43.0 | 17.0 | 3.2 | 3 | ADRIATIC SEA | 382 |
| 1420 | 9/15/76 | 18.52.58 | 31.0 | 105.0 | 3.7 | 2 | SZECHWAN PROV. CHINA | 307 |
| 1421 | 9/15/76 | 20.59.10 | 37.0 | 139.0 | 4.1 | 2 | HONSHU JAPAN | 227 |
| 1422 | 9/16/76 | 1.45. 7 | 32.0 | 49.0 | 3.6 | 3 | WESTERN IRAN | 347 |
| 1423 | 9/17/76 | 11.11.19 | 44.0 | 151.0 | 4.2 | 2 | HOKKAIDO JAPAN REG | 224 |
| 1424 | 9/17/76 | 23. 7.24 | 33.0 | 59.0 | 4.0 | 2 | IRAN | 348 |
| 1425 | 9/18/76 | 11.48. 7 | 42.0 | 51.0 | 3.5 | 3 | CASPIAN SEA | 338 |
| 1426 | 9/18/76 | 19.14.59 | 40.0 | 120.0 | 4.7 | 2 | NORTHEASTERN CHINA | 658 |
| 1427 | 9/19/76 | 0.48.11 | 20.0 | 93.0 | 3.9 | 2 | BURMA | 296 |
| 1428 | 9/19/76 | 2. 1. 7 | 43.0 | 146.0 | 4.1 | 2 | HOKKAIDO, JAPAN REG. | 224 |
| 1513 | 11/ 1/76 | 4. 4.57 | 42.2 | 143.0 | 4.9 | 0 | HOKKAIDO, JAPAN REG | 224 |
| 1514 | 11/ 2/76 | 14.56. 2 | 56.2 | 111.6 | 5.1 | 0 | LAKE BAIKAL REG. | 327 |
| 1515 | 11/ 2/76 | 19.29.30 | 26.7 | 125.2 | 5.5 | 0 | NORTHEAST OF TAIWAN | 245 |
| 1516 | 11/ 3/76 | 3.59.52 | 39.6 | 143.7 | 5.0 | 0 | OEC HONSHU, JAPAN | 229 |
| 1517 | 11/ 3/76 | 5.41. 4 | 25.0 | 99.2 | 4.8 | 0 | YUNNAN PROV., CHINA | 310 |
| 1518 | 11/ 4/76 | 11.20. 7 | 42.1 | 144.3 | 5.1 | 0 | HOKKAIDO, JAPAN REG | 224 |
| 1519 | 11/ 5/76 | 3.59.57 | 61.5 | 112.7 | 5.3 | 0 | CENTRAL SIBERIA | 726 |
| 1520 | 11/ 5/76 | 6.30. 0 | 44.3 | 148.5 | 5.0 | 0 | KURILE ISLANDS | 221 |
| 1521 | 11/ 6/76 | 4.43.54 | 26.5 | 96.4 | 4.5 | 0 | BURMA | 296 |
| 1522 | 11/ 6/76 | 7.57.25 | 35.3 | 138.4 | 5.0 | 0 | HONSHU, JAPAN | 227 |
| 1523 | 11/ 6/76 | 15. 0.52 | 50.0 | 156.9 | 5.1 | 0 | KURILE ISLANDS | 221 |
| 1524 | 11/ 6/76 | 18. 4. 9 | 27.6 | 101.1 | 5.8 | 0 | SZECHWAN, CHINA | 307 |
| 1525 | 11/ 6/76 | 18.50.12 | 27.4 | 101.1 | 5.1 | 0 | SZECHWAN, CHINA | 307 |
| 1527 | 11/ 7/76 | 4. 0.50 | 33.7 | 59.2 | 5.0 | 0 | IRAN | 348 |
| 1528 | 11/ 7/76 | 8.14. 1 | 27.5 | 101.1 | 4.9 | 0 | SZECHWAN, CHINA | 307 |
| 1529 | 11/ 8/76 | 0. 0. 9 | 44.4 | 148.1 | 4.9 | 0 | KURILE ISLANDS | 221 |
| 1530 | 11/ 8/76 | 6.48.53 | 39.7 | 77.4 | 5.0 | 0 | SOUTHERN SINKIANG | 321 |
| 1531 | 11/ 8/76 | 8.19.27 | 38.1 | 142.2 | 5.9 | 0 | NEC HONSHU, JAPAN | 228 |
| 1532 | 11/ 8/76 | 9. 7.57 | 47.4 | 145.9 | 5.0 | 0 | SEA OF OKHOTSK | 663 |
| 1533 | 11/ 8/76 | 9. 7.59 | 47.8 | 146.3 | 4.2 | 0 | NW OF KURILE IS. | 220 |
| 1534 | 11/ 8/76 | 23.27.42 | 27.5 | 101.1 | 5.0 | 0 | SZECHWAN PROV. CHINA | 307 |
| 1535 | 11/ 9/76 | 22.49. 8 | 38.1 | 73.6 | 5.3 | 0 | TADZHIK-SINKIANG BOR | 719 |
| 1536 | 11/10/76 | 12.54. 8 | 36.4 | 70.3 | 4.7 | 0 | HINDU KUSH REGION | 718 |

## TABLE A-1

## DATA BASE
(PAGE 14 OF 16)

| EVNO | DATE | TIME | LAT. | LONG. | MB | Q | LOCATION | SUBREG |
|---|---|---|---|---|---|---|---|---|
| 1537 | 11/12/76 | 13.13.41 | 39.9 | 116.8 | 4.7 | 0 | NORTHEASTERN CHINA | 658 |
| 1538 | 11/13/76 | 10.12.33 | 28.2 | 57.4 | 5.0 | 0 | SOUTHERN IRAN | 353 |
| 1539 | 11/15/76 | 3.14.46 | 49.3 | 155.1 | 4.9 | 0 | KURILE ISLANDS | 221 |
| 1540 | 11/15/76 | 3.14.50 | 49.3 | 155.6 | 5.3 | 0 | KURILE ISLANDS | 221 |
| 1541 | 11/15/76 | 7. 6.34 | 38.6 | 130.8 | 4.8 | 0 | KYUSHU, JAPAN | 235 |
| 1542 | 11/15/76 | 8. 3.23 | 33.2 | 47.9 | 5.4 | 0 | WESTERN IRAN | 347 |
| 1543 | 11/15/76 | 13.53. 1 | 39.4 | 117.7 | 6.0 | 0 | NORTHEASTERN CHINA | 658 |
| 1544 | 11/17/76 | 5.33.37 | 51.3 | 156.3 | 5.5 | 0 | KAMCHATKA | 217 |
| 1545 | 11/17/76 | 17.23.24 | 36.5 | 71.2 | 5.4 | 0 | AFGHANISTAN-USSR BOR | 717 |
| 1546 | 11/19/76 | 18.11.32 | 24.4 | 122.7 | 4.6 | 0 | TAIWAN REGION | 243 |
| 1547 | 11/21/76 | 9.23. 7 | 29.9 | 139.4 | 4.6 | 0 | S. OF HONSHU, JAPAN | 211 |
| 1548 | 11/22/76 | 13. 6. 9 | 42.2 | 147.8 | 5.0 | 0 | OFF COAST HOKKAIDO | 225 |
| 1549 | 11/23/76 | 5. 3. 2 | 51.0 | 78.3 | 5.3 | 0 | EASTERN KAZAKH SSR | 329 |
| 1550 | 11/23/76 | 10.46.36 | 51.2 | 159.3 | 5.5 | 0 | OEC KAMCHATKA | 219 |
| 1551 | 11/24/76 | 16. 9.15 | 52.0 | 160.7 | 5.8 | 0 | OEC KAMCHATKA | 219 |
| 1552 | 12/ 1/76 | 9. 1.47 | 39.4 | 73.1 | 4.9 | 0 | TADZHIK-SINKIANG BOR | 719 |
| 1553 | 12/ 1/76 | 11.59.35 | 27.0 | 54.9 | 4.7 | 0 | SOUTHERN IRAN | 353 |
| 1554 | 12/ 2/76 | 0.42.58 | 39.7 | 117.5 | 4.9 | 0 | NORTHEASTERN CHINA | 658 |
| 1555 | 12/ 2/76 | 1.19.29 | 31.0 | 139.5 | 5.6 | 0 | S. OF HONSHU, JAPAN | 211 |
| 1556 | 12/ 3/76 | 13.57.26 | 31.1 | 139.3 | 4.6 | 0 | S. OF HONSHU, JAPAN | 211 |
| 1557 | 12/ 3/76 | 22.35.49 | 33.0 | 47.9 | 4.3 | 0 | IRAN-IRAQ BORDER | 346 |
| 1558 | 12/ 7/76 | 4.56.57 | 49.9 | 78.9 | 5.9 | 0 | EASTERN KAZAKH SSR | 329 |
| 1559 | 12/ 7/76 | 9.36.39 | 33.9 | 137.0 | 5.0 | 0 | NEAR S. COAST HONSHU | 230 |
| 1560 | 12/ 7/76 | 9.36.47 | 35.1 | 135.6 | 4.9 | 0 | SOUTHERN HONSHU | 232 |
| 1561 | 12/11/76 | 4. 9.26 | 33.7 | 46.5 | 5.0 | 0 | IRAN-IRAQ BORDER | 346 |
| 1562 | 12/11/76 | 5.36.57 | 41.9 | 142.5 | 4.9 | 0 | HOKKAIDO, JAPAN | 224 |
| 1563 | 12/11/76 | 8.39. 9 | 53.8 | 160.5 | 5.0 | 0 | NEC KAMCHATKA | 218 |
| 1564 | 12/12/76 | 7.54.20 | 39.0 | 44.2 | 4.8 | 0 | TURKEY-IRAN BORDER | 343 |
| 1565 | 12/14/76 | 19.35.16 | 30.0 | 132.4 | 5.3 | 0 | SE OF SHIKOKU, JAPAN | 237 |
| 1566 | 12/14/76 | 20.22.21 | 55.1 | 159.0 | 6.0 | 0 | KAMCHATKA | 217 |
| 1567 | 12/19/76 | 11.43.45 | 50.7 | 153.4 | 4.8 | 0 | KURILE ISLANDS REG. | 222 |
| 1568 | 12/20/76 | 18.30.10 | 51.2 | 158.0 | 5.1 | 0 | NEC KAMCHATKA | 218 |
| 1569 | 11/ 6/76 | 23.18.53 | 28.2 | 57.1 | 4.8 | 0 | SOUTHERN IRAN | 353 |
| 1570 | 11/ 7/76 | 1.57.43 | 27.5 | 101.1 | 5.1 | 0 | SZECHWAN PROV. CHINA | 307 |
| 1571 | 11/ 7/76 | 11. 7.57 | 33.2 | 48.0 | 5.5 | 0 | WESTERN IRAN | 347 |
| 1572 | 11/ 9/76 | 17.59.54 | 33.8 | 59.2 | 5.1 | 0 | IRAN | 348 |
| 1573 | 11/10/76 | 10.45.58 | 38.8 | 75.0 | 4.6 | 0 | S. SINKIANG PROV. | 321 |
| 1574 | 11/11/76 | 2.20. 8 | 39.4 | 73.8 | 5.3 | 0 | TADZHIK-SINKIANG BOR | 719 |
| 1575 | 11/12/76 | 5. 6. 2 | 44.8 | 149.3 | 5.2 | 0 | KURILE ISLANDS | 221 |
| 1576 | 11/12/76 | 21.27.14 | 27.6 | 101.2 | 4.8 | 0 | SZECHWAN PROV. CHINA | 307 |

## TABLE A-1

## DATA BASE

(PAGE 15 OF 16)

| EVNO | DATE | TIME | LAT. | LONG. | MB | Q | LOCATION | SUBREG |
|---|---|---|---|---|---|---|---|---|
| 1577 | 11/14/76 | 17.10.39 | 37.1 | 141.5 | 5.1 | 0 | EC HONSHU, JAPAN | 228 |
| 1578 | 11/15/76 | 12.50.16 | 42.5 | 72.4 | 4.8 | 0 | KIRGIZ SSR | 716 |
| 1579 | 11/15/76 | 14.14.18 | 45.2 | 148.4 | 5.1 | 0 | KURILE ISLANDS | 221 |
| 1580 | 11/16/76 | 11.10.21 | 27.4 | 101.1 | 4.3 | 0 | SZECHWAN PROV. CHINA | 307 |
| 1581 | 11/17/76 | 5.33.35 | 51.0 | 156.2 | 5.5 | 0 | KURILE ISLANDS | 221 |
| 1582 | 11/19/76 | 15.14. 1 | 36.1 | 141.7 | 5.2 | 0 | EC HONSHU, JAPAN | 228 |
| 1583 | 11/20/76 | 4.19.36 | 36.3 | 69.2 | 4.8 | 0 | HINDU KUSH REGION | 718 |
| 1584 | 11/22/76 | 2.32.20 | 23.9 | 122.4 | 4.8 | 0 | TAIWAN REGION | 243 |
| 1585 | 11/24/76 | 12.22.19 | 39.1 | 44.0 | 6.1 | 0 | NW IRAN-USSR BOR. | 344 |
| 1586 | 11/24/76 | 12.30.41 | 39.1 | 43.9 | 5.0 | 0 | TURKEY | 366 |
| 1587 | 11/24/76 | 12.36.46 | 39.2 | 44.3 | 5.5 | 0 | NW IRAN-USSR BOR. | 344 |
| 1588 | 11/24/76 | 13.18. 7 | 39.1 | 43.7 | 4.8 | 0 | TURKEY | 366 |
| 1589 | 11/24/76 | 15. 4. 4 | 39.2 | 43.7 | 4.9 | 0 | TURKEY | 366 |
| 1590 | 11/24/76 | 15.11. 5 | 39.0 | 44.2 | 5.0 | 0 | NW IRAN-USSR BOR. | 344 |
| 1591 | 11/24/76 | 20.46. 6 | 39.1 | 44.0 | 4.8 | 0 | NW IRAN-USSR BOR. | 344 |
| 1592 | 11/27/76 | 6.17.41 | 36.8 | 138.2 | 4.8 | 0 | HONSHU, JAPAN | 227 |
| 1593 | 11/27/76 | 15.12.10 | 36.2 | 71.4 | 4.9 | 0 | AFGHANISTAN-USSR BOR | 717 |
| 1594 | 11/27/76 | 21.42.12 | 36.5 | 71.0 | 6.1 | 0 | AFGHANISTAN-USSR BOR | 717 |
| 1595 | 11/28/76 | 12.53.24 | 41.1 | 140.7 | 5.2 | 0 | HOKKAIDO, JAPAN REG. | 224 |
| 1596 | 11/28/76 | 20.39.39 | 40.2 | 63.8 | 4.6 | 0 | UZBEK SSR | 339 |
| 1597 | 11/29/76 | 8.16. 2 | 42.0 | 142.5 | 5.1 | 0 | HOKKAIDO, JAPAN REG. | 224 |
| 1598 | 11/29/76 | 19.44.39 | 51.2 | 159.5 | 4.6 | 0 | EC KAMCHATKA | 219 |
| 1599 | 12/ 1/76 | 9. 1.47 | 39.5 | 73.1 | 4.9 | 0 | TADZHIK-SINKIANG BOR | 719 |
| 1600 | 12/ 1/76 | 11.59.35 | 27.0 | 54.9 | 4.7 | 0 | SOUTHERN IRAN | 353 |
| 1601 | 12/ 2/76 | 0.42.58 | 39.7 | 117.5 | 4.9 | 0 | NORTHEASTERN CHINA | 658 |
| 1602 | 12/ 2/76 | 1.19.29 | 31.0 | 139.5 | 5.6 | 0 | S. OF HONSHU, JAPAN | 211 |
| 1603 | 12/ 2/76 | 11.22.54 | 31.0 | 139.2 | 4.7 | 0 | S. OF HONSHU, JAPAN | 211 |
| 1604 | 12/ 2/76 | 17.19.44 | 39.7 | 78.0 | 4.9 | 0 | S. SINKIANG PROV. | 321 |
| 1605 | 12/ 3/76 | 5. 6.25 | 31.1 | 139.1 | 4.7 | 0 | S. OF HONSHU, JAPAN | 211 |
| 1606 | 12/ 3/76 | 20.34.30 | 39.1 | 44.1 | 4.0 | 0 | NW IRAN-USSR BOR. | 344 |
| 1607 | 12/ 4/76 | 4.10.33 | 39.3 | 43.6 | 4.8 | 0 | TURKEY | 366 |
| 1608 | 12/ 4/76 | 21.12.55 | 39.6 | 73.4 | 4.9 | 0 | TADZHIK-SINKIANG BOR | 719 |
| 1609 | 12/ 5/76 | 19.14.54 | 39.0 | 43.8 | 4.2 | 0 | TURKEY | 366 |
| 1610 | 12/ 6/76 | 3.58. 4 | 39.0 | 44.4 | 4.4 | 0 | NW IRAN-USSR BOR. | 344 |
| 1611 | 12/ 6/76 | 4. 6. 5 | 38.9 | 44.4 | 4.4 | 0 | TURKEY-IRAN BORDER | 343 |
| 1612 | 12/ 6/76 | 16.13.12 | 24.2 | 94.6 | 4.7 | 0 | BURMA-INDIA BORDER | 294 |
| 1613 | 12/ 8/76 | 7.49.32 | 24.6 | 99.0 | 4.5 | 0 | YUNNAN PROV. CHINA | 318 |
| 1614 | 12/ 9/76 | 15.37.41 | 44.5 | 147.8 | 5.2 | 0 | KURILE ISLANDS | 221 |
| 1615 | 12/ 9/76 | 15.59.21 | 51.4 | 159.4 | 4.7 | 0 | EC KAMCHATKA | 219 |
| 1616 | 12/ 9/76 | 20. 2.26 | 27.6 | 56.2 | 4.6 | 0 | SOUTHERN IRAN | 353 |

### TABLE A-1

### DATA BASE
(PAGE 16 OF 16)

| EVNO | DATE | TIME | LAT. | LONG. | MB | Q | LOCATION | SUBREG |
|---|---|---|---|---|---|---|---|---|
| 1617 | 12/10/76 | 17.56.49 | 38.1 | 73.8 | 4.9 | 0 | TADZHIK-SINKIANG BOR | 719 |
| 1618 | 12/11/76 | 0.35.44 | 45.1 | 150.4 | 4.8 | 0 | KURILZ ISLANDS | 221 |
| 1619 | 12/12/76 | 10.39.39 | 39.7 | 74.1 | 5.1 | 0 | S. SINKIANG PROV. | 321 |
| 1620 | 12/13/76 | 2.55.59 | 36.7 | 140.7 | 4.5 | 0 | EC HONSHU, JAPAN | 228 |
| 1621 | 12/13/76 | 6.36.58 | 27.4 | 101.1 | 5.4 | 0 | SZECHWAN PROV. CHINA | 307 |
| 1622 | 12/13/76 | 7.23.47 | 27.3 | 101.1 | 4.5 | 0 | SZECHWAN PROV. CHINA | 307 |
| 1623 | 12/13/76 | 23. 1.32 | 31.1 | 142.2 | 5.4 | 0 | S. OF HONSHU, JAPAN | 211 |
| 1624 | 12/15/76 | 0.27.26 | 48.6 | 85.0 | 4.9 | 0 | EASTERN KAZAKH SSR | 329 |
| 1625 | 12/17/76 | 13. 2.11 | 33.3 | 93.9 | 5.1 | 0 | TSINGHAI PROV. CHINA | 325 |
| 1626 | 12/18/76 | 3. 5.56 | 38.3 | 142.0 | 4.8 | 0 | EC HONSHU, JAPAN | 228 |
| 1627 | 12/19/76 | 0.45.30 | 37.4 | 72.3 | 4.7 | 0 | TADZHIK SSR | 715 |
| 1628 | 12/19/76 | 18.37.53 | 46.6 | 151.6 | 5.3 | 0 | KURILE ISLANDS | 221 |
| 1629 | 12/20/75 | 15.22.25 | 41.9 | 142.2 | 4.8 | 0 | HOKKAIDO, JAPAN | 228 |